Hydrocarbon molecules databases for waste treatment applications

Xianwu Jiang

université
PARIS-SACLAY

Hydrocarbon molecules databases for waste treatment applications

Thèse de doctorat de l'Université Paris-Saclay

École doctorale n° 573, Approches interdisciplinaires: fondements, applications et innovation (INTERFACES)
Spécialité de doctorat: Physique
Unité de recherche: Université Paris-Saclay, CentraleSupélec, CNRS, Laboratoire SPMS, 91190, Gif-sur-Yvette, France
Référent: : CentraleSupélec

Thèse présentée et soutenue à Gif-sur-Yvette, le 17 novembre, par

Xianwu JIANG

Composition du jury:

Khaled HASSOUNI Professeur, université Paris 13	Président
Ioan SCHNEIDER Professeur, Université du Havre	Rapporteur & Examinateur
Dahbia TALBI Directrice de recherche, Laboratoire Univers et Particules de Montpellier	Rapporteur & Examinatrice
Hichem DAMMAK Professeur, Université Paris Saclay	Examinateur
Nicolas DOUGUET Maître de Conférences, Kennesaw State University	Examinateur
Pietro CORTONA Professeur, Université Paris Saclay	Directeur
Mehdi AYOUZ Maître de Conférences, Université Paris Saclay	Codirecteur
Viatcheslav KOKOOULINE Professeur, Université de Floride Centrale	Codirecteur
Samantha Fonseca dos SANTOS Maître de Conférences, Rollins College	Invitée

Thèse de doctorat

NNT: 2020UPAST039

HYDROCARBON MOLECULES DATABASES FOR WASTE TREATMENT APPLICATIONS

by

XIANWU JIANG

A thesis submitted in partial fulfilment of the requirements
for the degree of Doctor of Philosophy
in the Laboratory of Structures, Propriétés et Modélisation des Solides (SPMS)
in CentraleSupélec
at Université Paris-Saclay

Fall Term
2020

ABSTRACT

In this thesis, we investigate the vibronic (de-) excitation and dissociative recombination of CH^+ by low-energy electron impact.

We first develop a theoretical approach for the electron-impact vibronic (de-) excitation of CH^+. In this approach, the fixed-nuclear R-matrix method is employed to compute electron-ion scattering matrices in the Born-Oppenheimer approximation. A vibronic frame transformation and the closed-channel elimination procedure in a spirit of molecular quantum defect theory are employed to construct an energy-dependent scattering matrix describing interactions between vibronic channels of the target ion induced by the incident electron. The obtained scattering matrix accounts for Rydberg series of vibronic resonances in the collisional spectrum. Cross sections for vibronic excitation for different combinations of initial and final vibronic states are computed. A good agreement between electronic-excitation cross sections, obtained using the quantum defect theory and in a direct R-matrix calculation, demonstrates that the present approach provides a reliable tool for determination of vibronic (de-) excitation cross sections for targets with low-energy electronic resonances. Such targets were difficult to treat theoretically using earlier methods.

Within the same framework applied for the vibronic (de-) excitation, we further compute the cross sections for low-energy dissociative recombination of CH^+ by coupling the outgoing-wave basis function defined by complex absorbing potential. The contribution of the three lowest $X^1\Sigma^+$, $a^3\Pi$ and $A^1\Pi$ ionic states and the Rydberg series converging to those states are taken into account. The obtained DR cross sections are quantitatively in good agreement with the experimental measurements and exhibit a resonance feature analogous to the experimental cross-section curve. The origination of the prominent resonances in the computed results are analyzed through computing the DR probabilities for the partial waves of the incident electron. The d-type

partial waves including $d\sigma$, $d\pi$ and $d\delta$ are found considerably contributing to the DR of the ground-state CH^+. This may explain the discrepancies observed between theory and experiment in the preceding studies.

ACKNOWLEDGMENTS

I would like to first thank my supervisors Prof. Pietro Cortona and Dr. Mehdi Ayouz for accepting me as their PhD student in a top university in the world. Much appreciated for the unfailing support from Prof. Pietro Cortona and his patience and time answering any questions and requests throughout the course of the PhD. I felt really nice working with him. I'm also grateful for the dedicated guidances and helpful advices, especially on coding, from Dr. Mehdi Ayouz during the past three years. He provides me the chances working in a international research team and as a short-term scholar to the USA. My horizon was broadened and my dreams of watching a NBA game and having a look at Liberty Status were achieved during the visiting. This thesis would not exist without his persistent help, enthusiasm and encouragement.

Very special gratitude goes to Prof. Viatcheslav Kokoouline at University of Central Florida for his very critical suggestions and insights in all my projects. He is our intimate collaborator who is working like a co-supervisor to me. It is him introducing me into the world of electron-molecular ions scattering where I saw the beauty of multi-channel quantum defect theory. With his ideas and inspirations, it became possible for me to carry out research work at the frontier of scattering physics. I would also thank Dr. Chi Hong Yuen at University of Central Florida for his very useful discussions and friendship during my PhD and the time during my visiting to Rollins College of the USA. Whenever I met problems from my projects or I was puzzled by physical theories, he is available to give me a hand. I was inspired and learned a lot from the talks with him.

I'm really happy that I had a four-month visiting at Rollins College where I worked with Dr. Samantha Fonseca and Dr. Nicolas Douguet. I want to first appreciate for their hospitality and very helpful discussions for my second project during my visiting. They provide me a very comfortable working conditions. The most excited parts are the lunch time at the canteen and the gym of Rollins

College, and the NCAA men's basketball game after work. There were also many famous resorts we went and delicious food we tried with Dr. Chi Hong Yuen and his girlfriend.

I would also give my gratitude to SPMS lab where I had enjoyed a comfortable working environment and met my colleagues who offered me many helps and treated me kindly and friendly. And thanks are also given to all new friends I met in the USA for their friendship and caring. Apologize for not giving the long list of their names here, but it's really grateful meeting you guys.

I must give my deepest gratitude with all my heart to my parents and my big brother for all their endless love, support, and encouragement. I have been in a boarding school since I was twelve. I feel really regret for always being miles away from them and missing thousands of important moments in their lives. I was absent for the past eighteen birthdays of my parents and I lost the time to stay with my big brother growing up together. They are the best ones in my heart. I wish them good health and I hope I could have time to make up for the lack of companionship after my graduation. And I need express my love and very special thanks to my girlfriend LIU Hainan. She is also my family who gave me endless love, support and caring. She gave me this chance to study in France, so that we could experience an exotic culture and drop a visit to the whole Europe. She is always believing in me and her encouragement and company help me through all the difficulties whatever in daily life or from the research work during my PhD. I owned her a lot. I love her and looking forward to lifelong journey with her!

I gratefully acknowledge the funding from Chinese Scholarship Council that made my PhD work possible. This dissertation is also supported by the Thomas Jefferson Fund of the Office for Science and Technology of the Embassy of France in the United States and the National Science Foundation, Grant No. PHY-1806915. It has also received funding from the program "Accueil des chercheurs étrangers" of CentraleSupélec and "Séjour à l'étranger 2019" of L'école doctorale INTERFACES of Université Paris-Saclay.

TABLE OF CONTENTS

LIST OF FIGURES

LIST OF TABLES

CHAPTER 1: Introduction

The title of the thesis "Hydrocarbon molecule (C_xH_y) databases for waste treatment applications" could be ambiguous at one's first glance. To be exact, we theoretically study on the low-energy electron collisions with hydrocarbon molecules (molecular ions) to produce key data, including cross sections [1] and rate coefficients [2], which will be used as databases for the plasma waste treatment modeling. We first discuss the questions that why the electron collisional processes need to be investigated and why the cross section and rate coefficients of the collisions with hydrocarbon molecules (molecular ions) are needed in the plasma waste treatment modeling.

Low-energy [3] electron collisions with molecules (molecular ions) are of great interest from a pure quantum mechanical perspective. They are fundamental processes taking place in chemical processing, discharge and plasma. In the natural world, they occur in the (planetary) ionosphere [1] and atmosphere of earth through aurora [2] and lightning [3]. In the space, vast tracks of the interstellar medium, including interstellar clouds and planetary nebulae, are weakly ionized cold plasma where the electron-molecule (molecular ion) collisions predominates their chemistry [4]. In the daily life, it is now widely accepted that the processes are mainly responsible for radiation damage in living system (which arise primarily from the interaction of low energy secondary electrons through dissociative interaction with components of DNA or the water around them) [5]. The processes also initiate spark plug [6], lasers [7] and technological plasma used for waste treatment, etching, cleaning, coating [8] and deposition [9–11]. The importance of low-energy electron-molecules (molecular ions) collisions thus stimulates significant work both experimentally and theoretically.

[1] A function of (electron) scattering energy which specifies a measure of probability that a specific process will take place in a collision of two particles, and its unit is m^2 in SI.

[2] Dependents on temperature which quantifies the rate of the specific process taking place and its unit is m^3/s in SI.

[3] Defined as the incident electron energy is below the ionization of the target molecule's ionization threshold

Plasma applied for the waste treatment, as compared with traditional landfills, ocean dumpsites and incineration, has over the past decades been a prominent technology due to its increased process controllability, small installation size, near zero-emission and generation of salable co-product [12]. The waste feedstock to be treated, such as municipal solid waste (MSW), hazardous materials, health care waste and organic liquid waste, is mainly consisting of carbonaceous (hydrocarbon and halogenated hydrocarbon) materials [13–15]. The hydrocarbons to be destroyed are injected into the chamber of plasma reactor and flow through the plasma torch with temperature up to 20000 $^{\circ}$C ($\sim$ 2 eV) [16], which resulting in decomposition through bonds breaking induced by electron collisions [13]. A detailed understanding of the physics and the resulted chemistry underlying the electron-hydrocarbons (hydrocarbon ions) collision becomes essential to describe the plasma dynamic and improve sophistication and effectiveness of plasma process modeling in process control. Additional processes such as low-energy ($<$ 2 eV) ro-vibrational excitation (RE, VE), dissociative excitation (DE) and dissociative recombination (DR) drive the charged particles kinetics in low-temperature plasma, as well as the production of reactive atomic and molecular species. The cross sections and rate constants for such processes offer detailed information about the distribution of each rotational, vibrational and electronic excited state that affect thermodynamics, transport coefficients and kinetics of the plasma. The data are thus very critical in the so-called state-to-state plasma modeling [17] where each excited state is considered as an independent chemical species.

Besides in the plasma for waste treatment, the hydrocarbon molecular ions are major constituents in other cold ionized environments, such as diffuse interstellar clouds [18] and technological plasma [19, 20]. To start our research work, we choose CH^+, which is the simplest one among the family of the hydrocarbon molecular ions ($C_xH_y^+$), as the object of study. Collisions of the CH^+ ion with electrons have been studied theoretically since, at least, 1951 [21–24]. The interest was motivated by the detection of the ion in diffuse interstellar clouds, made initially by Douglas and Herzberg [25] in 1941 through performing the laboratory analysis of three previously observed

interstellar lines as $R(0)$ lines in the $A^1\Pi$-$X^1\Sigma^+$ transition spectra. These and later detections by Adams [26] confirm that CH^+ is ubiquitous as a major constituent of interstellar clouds. The ion is also an important intermediate in combustion and in the formation of large hydrocarbons in the interstellar medium (ISM). Reactive collisions of CH^+ with a low-energy electron determine the energy balance and evolution of low-temperature hydrocarbon plasmas such as in the ISM. The theoretical study of the e^--CH^+ collision system is thus of a considerable astrophysical interest. Processes taking place in e^--CH^+ collisions are also of interest for technological plasmas: For example, they play an important role in plasma processing of diamond films [19] and at the edge plasma of fusion reactors [27], where graphite is used as plasma facing material.

In this thesis, we'll focus on the vibrational (de-) excitation (see Eq. (2.58)) and dissociative recombination processes (see Eq. (2.82)) of CH^+. Rotational structures are not included here but within our future plan. As we mentioned above, the time-resolved vibrational distribution function (VDF) determines the vibrational-state population of the ions in the state-to-state approach of plasma modeling. The VDF is thus very critical in the kinetic evolution of the plasma. It relies on the rate constants of vibrational excitations and expressed by

$$\frac{\partial n_v}{\partial t} = n_e \sum_{v'} (k_{v',v} n_{v'} - k_{v,v'} n_v) \tag{1.1}$$

where n_e is the electron density and $k_{v',v}$ specifies the rate constant for the v to v' vibrational transition. Only one estimation of cross sections for vibronic excitations was recently calculated by multiplying the Franck-Condon factors between vibronic states with the electronic excitation cross sections obtained at equilibrium [18]. The approximated results need to be improved and we will discuss it in section 3.6. In the state-to-state modeling method, ions in each different state are viewed as an independent species. To compute the abundance of each species, one commonly solves time-dependent chemical rate equation as shown in Eq. (42) of Ref. [28], where rate constants for

vibrationally resolved dissociative recombination are needed. The first quantitatively computation of the DR cross sections of CH^+ were carried out by Takagi in 1991 [29] using a multichannel quantum defect theory (MQDT) treatment. The obtained results agree well with the experimental measurements. However, the electron scattering energy is limited below 0.3 eV and only the ground ionic state is considered. In 2000, Carata *et al* [30] performed an elaborate MQDT method to compute the cross sections for low-energy dissociative recombination of CH^+. The Rydberg manifolds converging to the $X^1\Sigma^+$ ground electronic state and the next two $a^3\Pi$ and $A^1\Pi$ excited states of the ion core are included in the treatment. They successfully reproduced the prominent structure at low collisional energy (< 4eV), whereas the absolute value of the cross section is not reproduced. Chakrabarti *et al.* [18] performed a similar MQDT calculation where the second-order solution of the Lippmann-Schwinger equation was adopted. They obtained quantitatively accurate DR cross section compared with the storage ring data, while the shape is not comparable.

Rydberg state CH appear in the eigenphase spectra (see section 2.3.1) in the form of abundant Rydberg resonances as seen in Figs. 3.4 and 3.5 due to the low-lying bound excited electronic states of CH^+. This kind of resonance could be also found in many other diatomics with low-lying bound excited electronic states [18, 31, 32]. To our best knowledge, the above mentioned MQDT method based on earlier theory suggested by Lee [33] and Giusti [34] is the only one theoretical approach able to treat vibrational excitation and dissociative recombination for such molecular ions. In the method, the R-dependent quantum defects for considered Rydberg series must be explicitly derived and used to account for non-adiabatic couplings. In the case where core-excited Rydberg states are included, the quantum defects are used to scale the Rydberg-Rydberg coupling, see Eq. (5) of Ref. [30] or Eq. (2) of Ref. [31]. The adiabatic potential curves of neutral dissociative states produce numerous avoided crossings. The quantum defects of Rydberg states corresponding to these potentials will show their adiabatic character by large variations near the avoided crossing points. Rydberg states need to be treated in a quasi-diabatic representation, such

that the appropriate Rydberg-Rydberg coupling around the avoided crossings could be obtained. However, the step transforming the adiabatic Rydberg state potential to quasi-diabatic potentials through diabatization of the coupled Rydberg states (see Fig. 1 in Ref. [31]) actually turns up to be very complicated since numerous of Rydberg states are involved. Therefore, we aim to develop a general theoretical approach in this thesis for computation of cross section for vibrational excitation and dissociative recombination of CH^+ where scattering matrices are used. In the approach, the scattering matrices are obtained from the fixed-nuclear R-matrix method and will be combined to vibronic frame transformation and MQDT close-channel elimination procedure.

The thesis is organized as follows. Chapter 2 give theories and methods used in the electronic structure and scattering calculations. The theoretical approaches for vibronic (de-) excitations and dissociative recombination are outlined based on the those given theories and methods and also included in this chapter. It serves as a tool box to follow the work of this thesis. Chapter 3 is devoted to the detailed description of the theoretical approach used for the computation of cross sections and rate constants for vibronic (de-) excitations of CH^+. The electronic structure of CH^+ is computed using the tools from chapter 2. Based on the approach developed in chapter 3, we demonstrate the theoretical study of the dissociative recombination of CH^+ by coupling the complex absorbing potentials formalism in chapter 4. The conclusion and perspective of the these research works are given in chapter 5.

CHAPTER 2: Theoretical background

In this chapter, we will briefly review the theoretical tools and methods involved in the study of vibronic (de-) excitation and dissociative recombination of CH^+ by low-energy electron impact.

A good knowledge of the electronic structure of a molecular ion is the preliminary step. Therefore, we first recall the electronic structure theory in section 2.1, where the potential energy curves (PECs) [1] are computed. Within the obtained PECs, we perform the nuclear dynamics calculating using a discrete variable representation (DVR) method in the following section to compute the vibrational wavefunctions. Coupling the DVR method with complex absorbing potential formalism, the outgoing-wave basis function is derived.

After the determination of the vibrational states, we turn to the scattering calculation part. We developed a theoretical approach that combines the fixed-nuclei R-matrix method, vibronic frame transformation and multi-channel quantum defect theory (MQDT) to compute the cross section for electron-induced vibronic (de-) excitation of CH^+. The fixed-nuclei R-matrix method introduced in section 2.3 is used to model the e^--CH^+ collisional process and evaluate the scattering matrix. A vibronic frame transformation is given in section 2.4 to compute the vibronic transition amplitudes using the obtained vibrational states and scattering matrices. Multi-channel quantum defect theory given in section 2.5 is used to determine the cross section including Rydberg series of resonances. Dissociative recombination (DR) competes with vibronic transitions. An estimation of its cross section is of great importance for a complete treatment. For this purpose, we combine our vibronic theoretical model to the complex absorbing potential (CAP) formalism in section 2.6 to obtain cross sections for DR of CH^+.

[1] In general, it is a surface for multidimensional potential

2.1 Electronic structure theory

2.1.1 Diatomic molecular spectral terms

Let's first recall the way to label the molecular electronic states. These states are classified through the value of quantum numbers associated with total orbital and spin angular momenta and the information is condensed in the corresponding molecular term symbol [35].

In diatomic molecules, Oz with respect to the internuclear axis is a symmetry axis. Therefore, the Hamiltonian commutes with the operator corresponding to the quantum number

$$\Lambda = \sum_i \lambda_i, \tag{2.1}$$

the sum over all Oz projection λ of Molecular orbitals' (MOs) angular momentum l. Capital greek letters $(\Sigma, \Pi, \Delta, \Phi, ...)$ are used for classification of molecular terms depending on the value assumed by Λ in the sequence (0, 1, 2 , 3, . . .). Moreover, each electronic term is characterized by the total spin

$$S = \sum_j^N s_j \tag{2.2}$$

where s is the spin of an electron and N is the number of electrons. The multiplicity $(2S+1)$ originates singlet $(2S+1=1)$, doublet $(2S+1=2)$, triplets $(2S+1=3)$, etc., as seen for atoms. The general term symbol assumes the form

$$^{2S+1}\Lambda \tag{2.3}$$

In the case of diatomic molecules, the term symbol also retains information about the parity of the electronic wavefunction with respect to some symmetry operations. In particular, the reflection

about a plane containing the internuclear Oz returns a state with the same energy but with opposite sign of the projection of the orbital angular momentum, thus leading to the conclusion that all terms with $\Lambda \neq 0$ are doubly degenerate. However for Σ state $(\Lambda = 0)$, which are nondegenerate, the parity is usually specified adding the sign plus or minus as superscript to the term symbol for even or odd states, i.e.

$$^{2S+1}\Lambda^{+/-} \tag{2.4}$$

In the case of homonuclear diatomic molecules, a new symmetry arises due to the inversion center bisecting the internuclear axis. In such situation, the subscripts g and u are used as $^{2S+1}\Lambda_{g/u}$ for even (gerade) and odd (ungerade) states, respectively. "X" is conventionally used to precede before the term of a ground electronic state. For the excited states which has an identical spin with the ground state, we put capital "A,B,. . . " before the corresponding term, while use "a,b,. . . " for the states with a different spin.

2.1.2 Symmetry point group

We introduce point group theory for a time-saving purpose in the electronic structure calculations. The electronic states could be classified according to its symmetry by the theory. This theory is originally used to classify molecule with different symmetry elements (point, axis, and surface) and operations (identity $\widehat{E}$, rotation $\widehat{C}_n$, reflection $\widehat{\sigma}$, inversion $\widehat{I}$, and improper rotation $\widehat{S}_n$). Groups of molecular physics are related to invariance of the molecular Hamiltonian with respect to symmetry transformations, i.e. operations of a symmetry group commute with the molecular Hamiltonian. And the wavefunction of a given system is the basis of the system's symmetry point group. More details on the group theory could be seen in Ref. [36]. Here, we shall only introduce the symmetry point group of a heteronuclear diatomic molecule for CH^+.

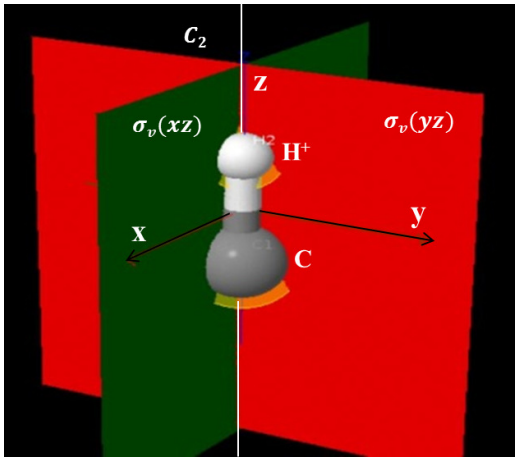

Figure 2.1: Schematic of C_{2v} symmetry point group for diatomic molecule CH^+.

The natural symmetry point group of CH^+ is $C_{\infty v}$ [2]. However, an quantum chemistry software only uses Abelian subgroups since the symmetry operators of such a group commute with each other. This property greatly reduces computational cost in an electronic structure calculation since we don't need to compute electronic wavefunctions for a large number of symmetries. Hence, $C_{\infty v}$ is reduced to C_{2v} point group for CH^+ in the calculations. Here the linear structure for CH^+ in C_{2v} group symmetry is given in Fig. 2.1. There are only 4 symmetry operations: the permutations of identical particles E, the π rotation C_2 [3], and the mirror reflection upon xz and yz faces ($\sigma_v(xz)$ and $\sigma_v(yz)$). Four irreducible representations, $\Gamma = A_1, A_2, B_1, B_2$, are used to represent 4 different symmetries of the electronic states. Here, we take C_{2v} symmetry point group as an example to explain the interpretation of its character table shown in Table 2.1. To know more character tables for other symmetry point groups, one can refer to Ref. [37].

A and B are used to refer to non-degenerate symmetries which are respectively symmetric and antisymmetric when the rotation operation C_2 around the Oz axis is applied. The subscript "1"

[2]Characterized with infinity of reflection symmetries (σ_v) upon the mirror plane that contains the Oz axis and two rotation symmetries along the Oz axis with arbitrary angle ($2C_\infty$) are included.

[3]The subscript designates the rotation of $2\pi/n$

Table 2.1: Character table for C_{2v} symmetry point group.

C_{2v}	E	C_2	$\sigma_v(xz)$	$\sigma_v(yz)$
A_1	+1	+1	+1	+1
A_2	+1	+1	-1	-1
B_1	+1	-1	+1	-1
B_2	+1	-1	-1	+1

or "2" are used for A and B depending on whether the irreducible representation is symmetric or antisymmetric with respect to a C_2 operation perpendicular to the Oz axis. Otherwise, we designate "1" or "2" according to the symmetry or inverse symmetry of reflection upon the σ_v. "+1" and "-1" in the table are the characters of irreducible representations Γ for the symmetry operations. "+1" means unchanged, while "-1" inversed. It could be interpreted as the eigenvalue of the symmetry operations on the the electronic wavefunction with a certain symmetry, for example,

$$\widehat{C}_2 \varphi^{B_1} = -1 \varphi^{B_1}. \tag{2.5}$$

Real spherical harmonics are used in all primitive basis functions (see below section introducing basis set). They are then symmetry-adapted for the C_{2v} symmetry point group used in the calculation. However, the complex spherical harmonics are used as the basis in the channel function definition due to the involved azimuth (see Eq. (A3) of Ref. [38]) in the further rotation study. This is different to the case of only vibration considered. On the other hand, complex spherical harmonics are the basis for the rotation symmetry operation of natural symmetry point group of CH^+ ($C_{\infty v}$). The transformation from the C_{2v} to $C_{\infty v}$ point group is achieved by the transformation of the real spherical harmonics to complex ones. The real harmonics denoted by $Y_{l,\pm\lambda}$, are simply

related to the complex harmonics, denoted by $Y_l^{\pm\lambda}$, by an unitary transformation

$$\begin{pmatrix} Y_{l,+\lambda} \\ Y_{l,-\lambda} \end{pmatrix} = U \begin{pmatrix} Y_l^{+\lambda} \\ Y_l^{-\lambda} \end{pmatrix} = \frac{1}{\sqrt{2}} \begin{pmatrix} 1 & (-1)^{\lambda} \\ -i & i(-1)^{\lambda} \end{pmatrix} \begin{pmatrix} Y_l^{+\lambda} \\ Y_l^{-\lambda} \end{pmatrix} \tag{2.6}$$

where the transformation matrix is denoted by U. The transformation of the scattering matrix from the C_{2v} to $C_{\infty v}$ is through

$$S_{C_{\infty v}} = U^{total} S_{C_{2v}} U^{\dagger total} \tag{2.7}$$

The scattering matrix describes the total symmetry of the collisional system (see section 3.3.2). Therefore, one needs to note that the total transformation matrix should be

$$U^{total}_{l'\lambda' i', l\lambda i} = U^{electron}_{l'\lambda', l\lambda} U^{target}_{i',i} \tag{2.8}$$

where $l\lambda$ is the partial wave of the scattering electron and i numerates the symmetry of the target states. This means the transformation is imposed to the target states by U^{target} and the partial wave of the scattering electron by $U^{electron}$. According to the Eq. (2.6), we can have the transformation matrix element

$$U^{electron}_{l'\lambda', l\lambda} = \begin{cases} 1 & \text{for } \lambda' = \lambda = 0 \\ 0 & \text{for } |\lambda'| \neq |\lambda| \\ \frac{(-1)^m}{\sqrt{2}} & \text{for } \lambda' > 0 \text{ and } \lambda = \lambda' \\ \frac{1}{\sqrt{2}} & \text{for } \lambda' > 0 \text{ and } \lambda = -\lambda' \\ \frac{i}{\sqrt{2}} & \text{for } \lambda' < 0 \text{ and } \lambda = \lambda' \\ \frac{-i(-1)^m}{\sqrt{2}} & \text{for } \lambda' < 0 \text{ and } \lambda = -\lambda' \end{cases} \tag{2.9}$$

for the transformation of the symmetry of the scattering electron from the C_{2v} to $C_{\infty v}$ [39]. In

practice, we only consider the three lowest electronic states in the case of CH^+ (which will be discussed in chapter 3)). But this part is not finished and will be continued in the further study of the rotational excitation of CH^+. For convenience of referring, we give here the the partial correlations of these two symmetry point group in Table 2.2.

Table 2.2: Partial correlation table between $C_{\infty v}$ and C_{2v}.

Λ	$C_{\infty v}$	C_{2v}
0	$A_1 = \Sigma^+$	A_1
0	$A_2 = \Sigma^-$	A_2
± 1	$E_1 = \Pi$	$B_1 \oplus B_2$
± 2	$E_2 = \Delta$	$A_1 \oplus A_2$

With the above table, we also describe that how the symmetry of the scattering electron and the target state constitute the total symmetry of the scattering matrix as seen in Table 2.3.

Table 2.3: Constitution of the total symmetry of the scattering matrix in $C_{\infty v}$ and C_{2v}.

$(l\lambda)^{electron}$	$\Gamma^{electron}_{C_{\infty v}}$	$\Gamma^{electron}_{C_{2v}}$	$\Gamma^{target}_{C_{\infty v}}$	$\Gamma^{target}_{C_{2v}}$	$\Gamma^{total}_{C_{\infty v}}$	$\Gamma^{total}_{C_{2v}}$
00,10,20,30,40,22,32,42,44	σ, δ	a_1	$^1\Sigma^+$	A_1	$^2\Sigma^+, ^2\Delta$	$^2A_1$
11,21,31,41,33,43	π	b_1	$^1\Sigma^+$	A_1	$^2\Pi, ^2\Phi$	$^2B_1$
1-1,2-1,3-1,4-1,3-3,4-3	π	b_2	$^1\Sigma^+$	A_1	$^2\Pi, ^2\Phi$	$^2B_2$
2-2,3-2,4-2,4-4	δ	a_2	$^1\Sigma^+$	A_1	$^2\Delta, ^2\Sigma^-$	$^2A_2$
00,10,20,30,40,22,32,42,44	σ, δ	a_1	Π	$B_1 \oplus B_2$	$^2\Pi, ^2\Phi$	$^2B_1 \oplus ^2B_2$
11,21,31,41,33,43	π	b_1	Π	$B_1 \oplus B_2$	$^2\Delta, ^2\Sigma^+, ^2\Sigma^-$	$^2A_1 \oplus ^2A_2$
1-1,2-1,3-1,4-1,3-3,4-3	π	b_2	Π	$B_1 \oplus B_2$	$^2\Delta, ^2\Sigma^+, ^2\Sigma^-$	$^2A_1 \oplus ^2A_2$
2-2,3-2,4-2,4-4	δ	a_2	Π	$B_1 \oplus B_2$	$^2\Pi, ^2\Phi$	$^2B_1 \oplus ^2B_2$
$\vdots$	$\vdots$	$\vdots$	$\vdots$	$\vdots$	$\vdots$	

2.1.3 Basis sets

To obtain the electronic wavefunction in Eq. (2.5), we need molecular orbitals (MOs), which are constructed through the linear combination of atomic orbitals (LCAOs)

$$\omega_i = \sum_u c_{ui} f_u \tag{2.10}$$

where f_u is atomic orbital type functions, c_{ui} is the combination coefficient of ith MO that is need to be determined by variational method. The set of atomic orbital functions employed in the calculation is referred as the basis set.

Two general classes of atomic orbital functions are typically employed in molecular orbital calculations, Slater Type Orbitals (STOs) and Gaussian Type Orbitals (GTOs). STOs are solutions of the Schrödinger equation of hydrogen-like atoms, and decay exponentially far away from the nucleus. Functional form of STOs depending on spherical coordinates,

$$s(r) = N r^{n-1} e^{-\varsigma r} Y_{l\lambda}(\theta, \varphi) \tag{2.11}$$

where N is a normalization constant, ς is called orbital exponent, which governs the size of the orbital. The r, θ, φ are spherical coordinates of electrons, and $Y_{l\lambda}(\theta, \varphi)$ is real spherical harmonics used as the angular wavefunction that describes the shape of orbitals. The n, l, λ are respectively principal, angular momentum, and magnetic quantum numbers (coming from hydrogen-like atom model). However, hydrogen-like atoms lack many-electron interactions, thus the orbitals do not accurately describe electron state correlations [4]. And functions of this kind are not suitable for fast calculations of two-electron integrals. The integral computations could be greatly simplified by

[4]It is usually the Coulomb interactions between electrons in the electronic structure of a quantum system.

using GTOs basis functions with the functional form

$$g(r) = Nx^a y^b z^c e^{-\varsigma r^2} \tag{2.12}$$

where

$$r^2 = x^2 + y^2 + z^2 \tag{2.13}$$

x, y and z are Cartesian coordinate of electrons. a, b and c are not quantum number, but simply the integral exponents. The sum of the exponents

$$l = a + b + c \tag{2.14}$$

is used analogously to the angular momentum quantum number for atoms, to distinguish functions as s-type $(l = 0)$, p-type $(l = 1)$, d-type $(l = 2)$, f-type $(l = 3)$, etc. In particular, for a p_x-type orbital, we would set $a = 1, b = c = 0$. While for d_{xy}-type orbital, we would have $a = b = 1, c = 0$.

Unfortunately Gaussian functions do not match the shape of an atomic orbital very well, especially at large r. Gaussian functions are suitable for numerical calculations especially for evaluating two-electron integral (see next section). Whereas, Slater's functions describe the features of MOs better than Gaussian functions. To make a best compromise between the calculation time consuming and a good representation of the MO asymptotic wave, we use contracted GTOs (CGTOs): a fixed linear combination of n primitive GTO [5] with different exponential parameters ζ_i

$$G(r) = \sum_i^n d_i g_i(r) \tag{2.15}$$

to approximate a STO. d_i is the fixed combination coefficient. CGTOs are therefore equipped with good convergence and MO approximation. They will be used in Eq. (2.10) to construct the MOs.

[5] In the jargon of chemistry a single Gaussian function is called a primitive Gaussian function, or primitive GTO.

Beyond the specific functional form used as the basis sets, different types of basis sets had been developed, such as People-style basis sets [6], and Dunning's correlation-consistent basis sets. Pople basis sets are somewhat outdated, as correlation-consistent basis sets typically yield better results with similar resources. This is attributed that the (Dunning's) correlation-consistent basis sets better represent the correlation and polarization effects. While the two effects play important roles in the electronic structure calculation of CH^+. We therefore selected the Dunning's correlation-consistent basis sets to compute the potential energy curves of CH^+ in this thesis. The basis sets are built up by adding shells of functions to a core set of atomic Hartree-Fock functions (see in the next section). They are usually denoted by the general nomenclature `cc-pVNZ`, which means correlation-consistent polarized valence N zeta basis set. N is the number of functions used to describe a valence orbital, N=D,T,Q,5,6,... (D=double-zeta, T=triple-zeta, etc.). For the 1^{st} and 2^{nd} row atoms, the `cc-pVDZ` basis set adds $1s$, $1p$, and $1d$ function. The `cc-pVTZ` set adds another s, p, d, and an f function, etc.

Table 2.4: Basis sets used for CH^+ in this thesis.

Quality	C	H^+
DZP (Dunning-Hey)	$9s5p1d \rightarrow 4s2p1d$	$4s1p \rightarrow 2s1p$
cc-pVDZ	$9s4p1d \rightarrow 3s2p1d$	$4s1p \rightarrow 2s1p$
cc-pVTZ	$10s5p2d1f \rightarrow 4s3p2d1f$	$5s2p1d \rightarrow 3s2p1d$
cc-pVQZ	$12s6p3d2f1g \rightarrow 5s4p3d2f1g$	$6s3p2d1f \rightarrow 4s3p2d1f$
cc-pV5Z	$14s8p4d3f2g1h \rightarrow 6s5p4d3f2g1h$	$8s4p3d2f1g \rightarrow 5s4p3d2f1g$

The basis sets (in MOLPRO style) for C and H^+ atoms used in this thesis are listed in Table 2.4. "$10s5p2d1f \rightarrow 4s3p2d1f$" means 10 s-type, 5 p-type, 2 d-type and 1 f-type Gaussian functions are contracted to 4 s-type, 3 p-type and 2 d-type, and 1 f-type CGTOs, respectively. We take `cc-pVTZ` basis set as an example shown in Fig. 2.2 to describe its details. The basis set file is taken

[6]The general nomenclature is $N-M1G$ or $N-M11G$, where N and M are the numbers of Gaussian primitives used for each MO.

from Ref. [40]. The essential input data for a basis set is exponents and contraction coefficients. Below the general information of the basis set, we see its main body starting with "basis set=". For Carbon atom, $10s5p2d1f$ is contracted to $4s3p2d1f$ [7]. The "s" in the next line is type of AO. The followings are "C" Carbon and the exponents of the Gaussian functions. The three lines below have the similar structure, where "c" is Carbon. The "1.10" next to it means the first to the 10th s-type Gaussian function are involved in the contraction. The 10 corresponding coefficients are the followed. The next parts of the basis are in the similar form.

```
!----------------------------------------------------------------------
! Basis Set Exchange
! Version v0.8.11
! https://www.basissetexchange.org
!----------------------------------------------------------------------
!   Basis set: cc-pVTZ
! Description: cc-pVTZ
!        Role: orbital
!     Version: 1  (Data from ccRepo/Grant Hill)
!----------------------------------------------------------------------


basis={
!
! carbon              (10s,5p,2d,1f) -> [4s,3p,2d,1f]
s, C , 8.236000E+03, 1.235000E+03, 2.808000E+02, 7.927000E+01, 2.559000E+01, 8.997000E+00, 3.319000E+00, 9.059000E-01, 3.643000E-01, 1.285000E-01
c, 1.10, 5.310000E-04, 4.108000E-03, 2.108700E-02, 8.185300E-02, 2.348170E-01, 4.344010E-01, 3.461290E-01, 3.937800E-02, -8.983000E-03, 2.385000E-03
c, 1.10, -1.130000E-04, -8.780000E-04, -4.540000E-03, -1.813300E-02, -5.576000E-02, -1.268950E-01, -1.703520E-01, 1.403820E-01, 5.986840E-01, 3.953890E-01
c, 8.8, 1.000000E+00
c, 10.10, 1.000000E+00
p, C , 1.871000E+01, 4.133000E+00, 1.200000E+00, 3.827000E-01, 1.209000E-01
c, 1.5, 1.403100E-02, 8.686600E-02, 2.902160E-01, 5.010080E-01, 3.434060E-01
c, 4.4, 1.000000E+00
c, 5.5, 1.000000E+00
d, C , 1.097000E+00, 3.180000E-01
c, 1.1, 1.000000E+00
c, 2.2, 1.000000E+00
f, C , 7.610000E-01
c, 1.1, 1.0000000
}
```

Figure 2.2: `cc-pVTZ` basis set in Molpro form.

[7] The contracted orbitals are actually AOs: $(1S)(2S2P)(3S3P3D)(4S4P4D4F)$ of Carbon

2.1.4 Calculation methods

Once the MOs are constructed by a basis set, we now need to seek computation methods to approximate the electronic wavefunction of CH^+ using these MOs. Hartree-Fock (HF) method provides a starting point in the electronic structure calculation and a foundation for more elaborate theoretical methods. It is based on the very known Born-Oppenheimer (BO) approximation where the electronic and nuclear wavefunctions are separately treated because mass of electron is much smaller than that of the nuclei. In this method, the total electronic wavefunction φ of an N-electron system is approximated by a Slater determinant

$$\varphi_{HF}(x_1, x_2, ..., x_N) = \frac{1}{\sqrt{N!}} \begin{vmatrix} \chi_1(x_1) & \chi_2(x_1) & \cdots & \chi_N(x_1) \\ \chi_1(x_2) & \chi_2(x_2) & \cdots & \chi_N(x_2) \\ \vdots & \vdots & \ddots & \vdots \\ \chi_1(x_N) & \chi_2(x_N) & \cdots & \chi_N(x_N) \end{vmatrix} \tag{2.16}$$

where N is total number of electrons. Space-spin molecular orbital $\chi(x)$ is used. It is expressed by

$$\chi = \omega\gamma \tag{2.17}$$

product of a spatial MO ω (see Eq. (2.10)) and a spin function γ (either α with spin quanta $s_z = 1/2$, or β with $s_z = -1/2$). $x = \{r, s_z\}$ is the set of space-spin coordinates of electrons. An interesting consequence of this functional form is that the electrons are all indistinguishable, each electron is associated with every orbital. The permutation of any two electrons corresponds to permutation of two rows of the determinant in the above equation, which leads to the sign reversal of the electronic wavefunction. This satisfies the antisymmetry requirement. Besides, a pair of electrons must occupy the same spatial with different spins. This is consistent with Pauli exclusion principle. For simplification, the determinant could be written as shorthand expression $|\, \chi_1\chi_2\cdots\chi_N >$ if we know

the list of the occupied spin orbitals $\{\chi_1\chi_2\cdots\chi_N\}$. The normalization constant is implied by noting the subscript number N. The molecular orbitals are optimized by HF equation

$$f(x_1)\chi_i(x_1) = \varepsilon_i\chi_i(x_1) \tag{2.18}$$

where ε_i is the eigenenergy [8] of the fock operator $f(x_1)$. The operator consists of one-electron operator $h_i(x_1)$, Coulomb operator $J_j(x_1)$ and exchange operator $K_j(x_1)$ as

$$f(x_1) = h_i(x_1) + \sum_{j\neq i} J_j(x_1) - \sum_{j\neq i} K_j(x_1) \tag{2.19}$$

As we introduced before, basis set will be used to construct the initial space-spin MOs χ in Eq. (2.18) with combination coefficients c_{ui}. Variational method is then employed to optimize these molecular orbitals iteratively. For this reason, HF method is also called a self-consistent-field (SCF) approach. Better approximate wavefunction is thus obtained by varying c_{ui} until we minimize the energy ε within the given functional space. However, HF method is not flexible enough to account for electron correlation since only the ground electronic configuration is taken into account. Meanwhile, the instantaneous interaction between electrons is ignored due to the mean field approximation [9].

Multiconfigurational self-consistent field method (MCSCF), a post-Hartree-Fock method, is thus needed to generate more qualitatively correct reference states of molecules as the next step. Those optimized molecular orbitals could be used in this method. The method is actually a Configuration Interaction (CI) method that treats non-dynamic electronic correlations. A particularly important MCSCF approach is the complete active space SCF method (CASSCF), where the entire possible configuration state functions (CSFs) that arise from a particular number of electrons in a complete

[8] It can be also interpreted as the energy of a MOs at HF level.

[9] An electron is assumed moving in an averaged multi-electron electronic field.

active space (CAS) are included in a linear combination form. CSF is a symmetry-adapted linear combination of Slater determinants and denoted by ψ. The electronic configuration for CH^+ is shown in Fig. 2.3, the inner orbital is called core orbital. The unoccupied orbitals are called virtual orbitals, plus the remaining two occupied orbitals construct the CAS where 4 electrons could freely distribute.

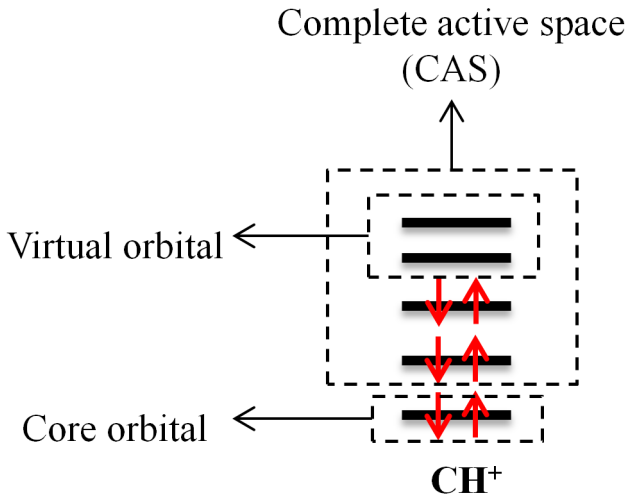

Figure 2.3: Ground electronic configuration of CH^+.

Besides the ground state configuration, singlet, doublet and multi-excitation configuration ψ_k^g, ψ_k^s, ψ_k^d, etc., are constructed by the corresponding determinants and finally combined represent the trial total electronic wavefunction in the form

$$\varphi_{CI} = \sum_k b_k \psi_k = b_0^g \psi_0^g + b_1^s \psi_1^s + b_2^d \psi_2^d + \cdots \tag{2.20}$$

where b_k is expansion coefficient. In an MCSCF calculation, the set of coefficients of both the CSFs and the molecular orbitals in LCAOs are varied by variational method to obtain the total electronic wavefunction with the lowest possible energy. To be exact, the coefficient b_k is first optimized with the given c_{ui} obtained from HF method. The coefficient c_{ui} is then optimized with the obtained b_k.

The optimization of c_{ui} and b_k proceeds to convergence in a self-consistent field (SCF).

There are two types of correlation in an electronic system: static correlation and dynamical correlation. The first type rises from fixing an electron in a given orbital and the later one is caused by the assumption of the averaged field of the other electrons. In reality, the motion of the electrons depends on the instantaneous positions of all the other electrons. CASSCF method is a single-reference method where the multi configurations are constructed referring to the MOs orbitals optimized by HF method. The dynamical electron correlation is not considered in this method. But it is included in the multi-reference CI (MRCI) method. The optimized multi configurations in CASSCF method is used in MRCI method as multi reference spaces. The additional electronic configurations created by the multiple excitations from the multi references [10] are also taken into account in MRCI method. The resulted CSFs denoted by $\psi_I^{s,d}$ are included in Eq. (2.20)

$$\varphi_{MRCI} = b_0^g \psi_0^g + b_1^s \psi_1^s + b_2^d \psi_2^d + \sum_I c_I \psi_I^{s,d} \cdots \tag{2.21}$$

where I numerates the reference configuration and c_I is the expansion coefficients. s and d are single and double excitations from the reference configuration, i.e. only one and two excited electrons are considered. The truncation of the number of excited electrons is usually mandated due to the very steep increase in the number of CSFs, and the consequent computational effort. The expansion coefficients b_i and c_I in the above equation will be optimized by the variational method. The potential energy curves denoted by $V(R)$ of the electronic states of CH^+ are finally determined by this method.

[10] Besides the ground configuration, the configurations of excited states obtained by CASSCF method are now used as references.

2.2 Vibrational wavefunctions

2.2.1 Discrete variable representation method for bound vibrational states

According to BO approximation, the nuclei vibrate within the electronic potential energy. For CH^+, the nuclear motion (rotation is ignored here) is described by the Schrödinger equation

$$[-\frac{\hbar^2}{2m}\nabla^2 + V(R)]\phi_v(R) = E_v\phi_v(R) \tag{2.22}$$

where ϕ_v and E_v are the vibrational wavefunction and vibrational energy. The subscript v is a vibrational quantum. m is the reduced mass of CH^+. As we mentioned in the above section, $V(R)$ is the electronic potential energy computed in the electronic structure calculation. The kinetic energy is best represented in the momentum representation $|k\rangle$, while the potential is best treated in the internuclear coordinate representation $|R\rangle$

$$-\nabla^2|k\rangle = k^2|k\rangle \ [11], \hat{V}(R)|R\rangle = V(R)|R\rangle \tag{2.23}$$

To solve this problem, we employ discrete variable representation (DVR) method [41–43] to solve the Eq. (2.22). To be exact, Fourier Grid Hamiltonian (FGH) methods [44] is used here. The method is a special case of DVR method with the advantage of simplicity since plane wave basis is used.

Assuming the vibration of nuclei is within the range of L, which is separated by N uniform spacing

[11] $\hat{P}^2 = -\hbar^2\nabla^2$

between the grid points of ΔR value ($L = N\Delta R$). The bond length R varies within L as

$$R_j = j\Delta R \tag{2.24}$$

where $j \in [1, N]$. The wavefunction is expanded in the discrete basis by

$$\langle R_j | \phi_v \rangle = \phi_v(R_j) \tag{2.25}$$

The grid size and spacing chosen in coordinate space determines the reciprocal grid size in momentum space. The total length $N\Delta R$ determines the longest wavelength and therefore the smallest frequency in the momentum space is

$$\Delta k = \frac{2\pi}{N\Delta R} \tag{2.26}$$

which is defined as the uniform grid in momentum space.

Fourier transforms emerge naturally as the transformation between these two representations. The transformation matrix elements between the coordinate and momentum representations is

$$\langle k_i | R_j \rangle = \frac{1}{\sqrt{2\pi}} e^{-ik_i R_j} \tag{2.27}$$

The Hamiltonian operator matrix elements in the coordinate representation are

$$H_{ij} = \langle R_i | \hat{T} + \hat{V} | R_j \rangle = \sum_j^N \langle R_i | k_j \rangle \frac{k_j^2}{2m} \langle k_j | R_j \rangle \Delta k + V(R_j)\delta_{ij}\Delta R \tag{2.28}$$

Combining with Eqs. (2.26) and (2.27), we could now obtained the matrix elements

$$H_{ij} = \begin{cases} \frac{\pi^2}{mL^2}\frac{N^2+2}{6} + V(R_i) & \text{for } i = j, \\ (-1)^{i-j}\frac{\pi^2}{mL^2}\frac{1}{sin^2[(i-j)\pi/N]} & \text{for } i \neq j, \end{cases} \tag{2.29}$$

where N is either an odd or even number.

The expectation value of the energy E_v corresponding to the bound vibrational state function ϕ_v is

$$\frac{\sum_{ij}\phi_v^*(R_i)\Delta R H_{ij}\Delta R\phi_v(R_j)}{\Delta R\sum_j\left|\phi_v(R_j)\right|^2} \tag{2.30}$$

The eigenvectors of (2.29) are the bound vibrational wavefunctions $\phi_v(R)$. They give directly the approximate values evaluated at the grid points. We will use this method to compute the bound vibrational wavefunctions $\phi_v(R)$ of the lowest three $X^1\Sigma^+$, $a^3\Pi$ and $A^1\Pi$ electronic states of CH^+. These states are used in the calculation of cross section for vibronic excitation after normalization by

$$\sum_j^N |\phi_v(R_j)|^2\Delta R = 1 \tag{2.31}$$

2.2.2 Outgoing-wave basis functions defined by the complex absorbing potential

In our theoretical approach for dissociation recombination (DR), the vibrational continua states needs to be included. They could be discretized by the outgoing-wave basis functions defined by a complex absorbing potential (CAP). Similar to the technique of Siegert pseudostates [45], the CAP is actually a boundary condition as seen Eq. (1) of Ref. [46]. The artificial CAP is placed at the end of the internuclear distance grid (see Eq. (2.24)) and is purely imaginary and added to the adiabatic potentials $V(R)$, which makes the Hamiltonian in Eq. (2.22) non-Hermitian

$$\widehat{H} = -\frac{\hbar^2}{2m}\nabla^2 + V(R) - i\eta W(R) \tag{2.32}$$

where η denotes the CAP strength and $W(R)$ a potential function. Exponential CAP in the form [47]

$$W(R) = \begin{cases} Nexp(-\frac{2L}{R-R_0}) & \text{for } R > R_0, \\ 0 & \text{for } R < R_0. \end{cases} \tag{2.33}$$

is used in the present study, where N is a constant with value of 13.22 from Ref. [47]. As introduced in the section 2.2.1, L specifies the grid length of the adiabatic potentials of the $X^1\Sigma^+$, $a^3\Pi$ and $A^1\Pi$ electronic states. R_0 is the starting point of a CAP on the potential. The complex eigenenergies and vibrational basis of the Hamiltonian in Eq. (2.32) are obtained by the DVR method introduced in the above section. But the form of the eigenenergies turns to be complex

$$E_{vi} = E'_{vi} - i\frac{\Gamma}{2} \tag{2.34}$$

where E'_{vi} and Γ are the position and width of the resonance. i stands for the ion electronic state and v for the vibrational quantum in the ionic potential. They would keep constant if the parameters, i.e. length $(L-R_0)$ and the strength η, of the CAP are appropriately chosen. The set of obtained vibrational wavefunctions $\phi_{vi}(R)$ are the called CAP basis and obey orthonormality relationship

$$\delta_{v'i',vi} = \int dR \phi_{v'i'}(R)\phi_{vi}(R) \tag{2.35}$$

where neither the bra nor ket is complex conjugated. The form in Eq. (2.35) is usually called as c-product and could be found in Eq. (2.1) of Ref. [48]. The vibrational continua wavefunctions obtained by the CAP correspond to c-normalized function (see Eq. (2.7) of Ref. [48]), which satisfy the orthonormality relationship of the above equation.

2.3 Fixed-nuclei R-matrix method

2.3.1 Principle of the method

Once the potential energy curves and vibrational states are determined, we turn to the scattering calculation part where fixed-nuclear R-matrix method is used. Before the introduction of this method, we first describe the e^--CH^+ scattering process as shown in Fig. 2.4. In order to formulate the this scattering process in the fixed-nuclear approximation, we adopt a frame of reference (Body-frame reference, see subsection 2.4), where the center of the mass of the target is taken as the origin O of the coordinate and the z-axis is conventionally chosen to lie along the internuclear axis. The incident electron with partial wave $l_i\lambda_i$ (the angular quantum number and its Oz projection, see section 2.4) associated with channel i [12] approaches the CH^+ ion core with a sphere of $r_0 = a$. The value of the radius a is chosen to enclose the entire electronic density of the target states of interest. We use $F_i(r)$ to represent the radial wavefunction of this incident electron, in which r denotes the radial coordinate of the scattering electron. The angular wavefunctions are also represented by real spherical harmonics (see section 2.1.3). When the electron penetrates the sphere of the ion core, $u_{ij}(\Omega, r)$ is used here to specify the extra continuum orbitals introduced by the scattering electron. Ω is the angular part of the scattering electron. They are described by a set of GTOs (see section 2.1.3) centered on the center of mass of the collisional system. The generated extra continuum orbitals need to satisfy the orthogonalization to the target states. Then the electron is scattering away with partial wave $l_j\lambda_j$ associated with channel j. Note that $F_{ij}(r)$ is used to represent the radial wavefunction of the electron incident in channel i while leaving the core after collision by channel j. This is sometimes hard for a beginner in this field to understand the subscripts of these functions.

[12] A combination of target's electronic state φ_i (see Eq. (2.41)) and partial wave $l_i\lambda_i$ of the scattering electron.

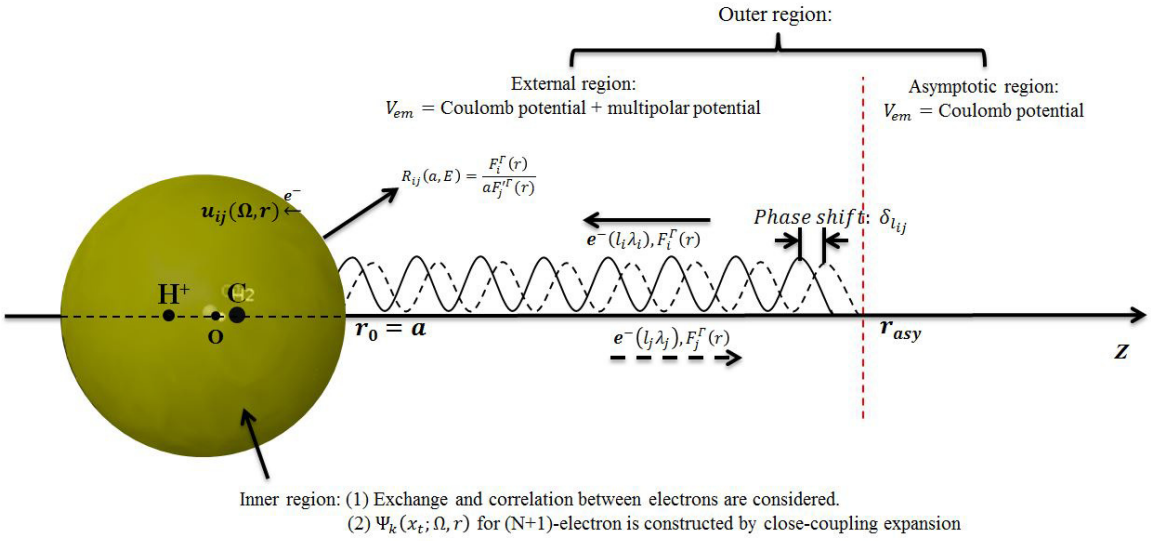

Figure 2.4: Schematic of the e^--CH^+ collisional process modeled by R-matrix method. a is chosen as 13 a_0 in the e^--CH^+ scattering calculation. It is tuneable in the R-matrix calculation. r_{asy} is usually taken as 70 a_0.

Consider the e^--CH^+ scatteing process represented by

$$\mathbf{CH}^+(i) + e^-(l_i\lambda_i) \rightarrow \mathbf{CH}^+(j) + e^-(l_j\lambda_j) \tag{2.36}$$

where $CH^+(i)$ and $CH^+(j)$ represent CH^+ in the initial φ_i and final φ_j electronic states, respectively. We assume the target has N electrons. We reserve discussions of the vibrational excitation and dissociative recombination processes to the section 2.5 and 2.6. The Schrödinger equation of this process is

$$\widehat{H}_{N+1}\Phi(x_t;\Omega,r) = E\Phi(x_t;\Omega,r) \tag{2.37}$$

where Φ is the total wavefunction of the collisional system and E is the total energy of the scattering system. x_t represents the collective coordinate of the fixed-nuclear target ion. The Hamiltonian

$\widehat{H}_{N+1}$ is

$$\widehat{H}_{N+1} = \widehat{H}_t + V_{et} - \frac{\hbar^2}{2m_e}\nabla_r^2 \tag{2.38}$$

where $\widehat{H}_t$ is the electronic Hamiltonian of the target ion, V_{et} is the electrostatic interaction potential between the scattering electron and the target molecular, and the third term $-\frac{\hbar^2}{2m_e}\nabla_r^2$ represents the kinetic energy of the scattering electron. The task of the scattering calculation is actually solving the Schrödinger equation (2.37). Well, there are a variety of theoretical procedures developed for treating the low-energy (below molecular ionization energy with a magnitude of 10 eV) electron-ion scattering, such as complex Kohn variational method [49] and Schwinger multichannel method [50]. The former one is based Kohn variational principle [51], where the T-matrix is chosen as the variational quantities instead of the K-matrix [50, 52]. Some recent application of this method could be found in Refs. [53, 54]. The later one is based on Schwinger variational principle for the scattering amplitude [55]. Details of this approach can be found in Ref. [56] and references therein. Both the methods are variational approaches, while R-matrix method is a bound state approach [57, 58]. Compared with those two methods, R-matrix method has a major advantage that the inner region problem is solved independently of the scattering energy denoted by $E_{\rm el}$. The dependence on the scattering energy needs only to be considered in the outer region where obtaining solutions is relatively quick and simple. It becomes particularly appropriate for studying systems with complicated energy dependence of the scattering observables such as problems with many resonances. R-matrix method is thus particularly appropriate for treating electron collisions with cations since they have compact target wavefunctions and usually display complicated resonance structures.

Now, let's recall the principle of R-matrix method which is used to model the e^--CH^+ collisional process of Eq. (2.36) in the present thesis. This method was originally proposed by Wigner in the 1940s [59, 60] for nuclear scattering processes. In the 1970s the R-matrix method was developed as electron-atom collisional treatment [61–63] and electron-diatomic molecule scattering [64–67]

technique. However, it was not until the 1990s that polyatomic codes were developed for general electron-molecule scattering [68–72]. Nowadays, R-matrix is a generally used treatment of the low-energy electron collision processes. The formalism for the this method has been described in detailed by Ref. [57, 58, 68, 69, 73]. We therefore omit a detailed discussion about it, but give a outline of the method for completeness below.

First, the configuration space is divided into two distinguishable regions: the inner region with a sphere of $a = 13$ bohrs and the the outer region which is the space outside of the sphere. Within the inner region, the scattering electron is considered to be indistinguishable from the electrons of CH^+, hence correlation and exchange effects (as introduced in sections 2.1.3 and 2.1.4) must be taken into consideration and $(N+1)$-electron collision complex behaves in a similar way to a bound state. The Schrödinger equation of inner region is

$$(\widehat{H}_{N+1} + \hat{L}_{N+1})\Psi_k(x_t;\Omega,r) = E_k\Psi_k(x_t;\Omega,r) \tag{2.39}$$

where $\hat{L}_{N+1}$ is Bloch operator, see Eq. (7) of Ref. [73]. It is used to keep the hermicity of $\widehat{H}_{N+1}$ which is broken by inserting the boundary r_0 in the coordinate space. Ψ_k is used as the inner part electronic wavefunction for $(N+1)$-electron system. k (note k here is a number) is determined by the number of eigenchannel defined by the target state i and the partial wave $l_i\lambda_i$ of the scattering electron. The total wavefunction expands in the inner region by

$$\Phi(x_t;\Omega,r) = \sum_k A_k(E)\Psi_k(x_t;\Omega,r) \tag{2.40}$$

where $A_k(E)$ is the expansion coefficient. The wavefunction Ψ_k is constructed by close-coupling expansion

$$\Psi_k(x_t,r) = \hat{A}\sum_{ij} a_{ijk}\varphi_i(x_t)u_{ij}(\Omega,r) + \sum_i b_{ik}\psi_{ik}(x_t;\Omega,r) \tag{2.41}$$

where $\hat{A}$ is the anti-symmetrized operator, $\varphi_i(x_t)$ is the ith target state wavefunctions. $\psi_i(x_t;\Omega,r)$ is the CSFs (see section 2.1.3) for $(N+1)$-electron when the penetrated electron occupied the virtual orbital of the target ion and takes into account the polarization of the N-electron target wavefunction in presence of the projectile electron. a_{ijk} and b_{ik} are the coefficient expansions and are found by diagonalizing the total Hamiltonian operator in the basis $\Psi_k(x_t;\Omega,r)$. The inner region calculation is complicated but solvable. Combining Eqs. (2.39) and (2.41) and then projecting the equation onto the channel functions φ_i to obtain an expression of the radial wavefunction $F(r)$. Evaluating it on the boundary of the inner region by inserting $r=a$, we obtain

$$F_i(a) = \frac{1}{a}\sum_k \frac{\rho_{ik}\rho_{jk}}{E-E_k}\frac{F_i}{rF_j'} \tag{2.42}$$

where a is the radius of the inner region. The R-matrix at the boundary of radius is defined by

$$R_{ij}(a,E) = \frac{1}{a}\sum_k \frac{\rho_{ik}\rho_{jk}}{E-E_k} \tag{2.43}$$

where ρ_{ik} are the surface amplitudes, given by

$$\rho_{ik} = \sum_j u_{ij}a_{ijk} \tag{2.44}$$

where u_{ij} is referred as the continuum orbital of the scattering electron (see the beginning of this part) and a_{ijk} is the expansion coefficient of Eq. (2.41). For more details see Ref. [57].

Beyond the radius r_0 in the outer region, the electron is treated as being distinct. This region could be again divided into two subregions: external region where e^--CH^+ interpotential includes Coulomb potential and multipolar potential (mainly dipolar potential) and asymptotic region located at r_{asy}=70 bohrs [13] where only Coulomb potential left. The total wavefunction in the external region

[13]The obtained R-matrix in the inner region is propagated to that far to match the asymptotic radial wavefunction of

is expanded in the form

$$\Phi(x_t;\Omega,r) = \sum_i \varphi_i(x_t) F_i(r) Y(\Omega) \tag{2.45}$$

where $Y(\Omega)$ is the angular function of the scattering electron. We now no longer include the antisymmetrization operator, since the scattered electron and the target electrons occupy different regions of space. Substituting the above equation into Eq. (2.37) and projecting onto the target state $\varphi_i(x_t)$ (electronic channel i) yields the following equation

$$[-\frac{\hbar^2}{2m_e}\nabla^2 + \frac{l_i(l_i+1)}{r^2} - k_i^2]F_i(r) = 2\sum_j^n V_{ij}F_j(r) \tag{2.46}$$

In this equation, the wave number of the incident electron associated with channel i is

$$k_i^2 = 2(E - E_i) \tag{2.47}$$

where E_i is the energy of channel i. A channel is said to be open if $k_i^2 \geq 0$ since it can be reached asymptotically and closed if $k_i^2 \leq 0$ (see section 2.5). The potential matrix element in Eq. (2.46) is defined as

$$V_{ij} = \sum_{n=0} \frac{\alpha_{ij}^n}{r^{n+1}} \tag{2.48}$$

where α provides coupling between the channels in the outer region, for instance Coulomb potential ($n = 0$) and dipoles ($n = 1$). One could refers Eq. (20) and (21) of Ref. [57]) for more details. The set of equation given in Eq. (2.46) could be solved at the boundary between the external and asymptotic region by a number of methods available for obtaining asymptotic solutions [74–77]. The most commonly used procedure is based on the use of an asymptotic expansion introduced by

---

the scattering electron.

Gailitis [77]. The resulted reduced radial wavefunction that satisfy the boundary condition is

$$F_{ij}(r \to \infty) \approx \begin{cases} \frac{1}{\sqrt{k_i}}(sin\theta_i + cos\theta_i K_{ij}) & \text{for open channel,} \\ 0 & \text{for closed channel.} \end{cases} \tag{2.49}$$

where K_{ij} is the reactance matrix, called as K-matrix. θ is a diagonal matrix with elements expressed by

$$\theta_i = k_i r - \frac{1}{2} l_i \pi - \frac{Z-N}{k_i} ln(2k_i r) + \sigma_i \tag{2.50}$$

and note that the Coulomb phase shift σ_i for an electron-ion collisional process is

$$\sigma_i = \arg\Gamma\left(l_i + 1 + i\frac{Z-N}{k_i}\right) \tag{2.51}$$

where Z is the charge of nuclei and Γ here is Euler Gamma function. Note that the asymptotic channel i is defined by an electronic state of the separated target state and a partial wave $l_i\lambda_i$ of the scattering electron. To obtain the K-matrix (K_{ij} in Eq. (2.49)), we first propagate the R-matrix in Eq. (2.44) from the boundary r_0 to the asymptotic radius r_{asy} [78, 79]. Combining Eqs. (2.42), (2.44) and (2.49), we could finally have the $N_o \times N_o$ dimensional K-matrix $K_{l_j\lambda_j,l_i\lambda_i}(E,R)$ determined where N_o is number of open channels (see subsection 2.5). All the scattering observables can be extracted from this matrix. Scattering matrix $S_{l_j\lambda_j,l_i\lambda_i}(E,R)$ are then computed through the transformation

$$\hat{S} = \frac{1+i\hat{K}}{1-i\hat{K}} \tag{2.52}$$

This matrix will be used in the cross section calculations for vibronic excitations and dissociative recombination of CH^+ (see section 2.5 and 2.6). For the partial wave of the scattering electron, $l \leq 4$ is defaulted in the R-matrix calculation. Considering λ could be the value of from $-l$ to l, we will have 25 possible combination of $l\lambda$, i.e. 25 partial waves. These partial waves belong to

four categories of symmetries: a_1, a_2, b_1 and b_2 as seen in Table. 2.3.

As we see in Fig. 2.4, the phase shift between the incident and the outgoing electron is defined as eigenphase $\delta_{l_{ij}}$. i and j are used as the subscript to specify the incoming wave in channel i, which then outgoes in channel j. The eigenphase sum (over all channels in the same symmetry) is obtained from the sum of the eigenvalue of the K-matrix as

$$\delta(E,R) = \sum_i arctan(K^D_{l_i\lambda_i,l_i\lambda_i}(E,R)) \tag{2.53}$$

where $K^D_{l_i\lambda_i,l_i\lambda_i}$ is the diagonal elements of the K-matrix. Note that we use $il_i\lambda_i$ and $jl_j\lambda_j$ to numerate the incident (initial) and outgoing (final) channel in this section for keeping consistent with the description of the R-matrix in Ref. [57]. In the following parts of the thesis, we'd use $il\lambda$ and $i'l'\lambda'$ as usually seen in literatures.

2.3.2 Brief introduction of Resonances

The eigenphase sum obtained from Eq. (2.53) for e^--CH^+ is featured of resonances (see Fig. 3.19 shown in section 3.2). A resonance is known as a transient state when the target molecule captures the incident electron. Treatment of the resonances is very important because the cross sections for a electron collisional process including the vibronic excitation and dissociative recombination may be increased by the presence of resonances.

There are different type of resonances. The simplest resonance is called shape resonance [80]. It occurs when an electron becomes trapped behind a centrifugal barrier in the electron-molecule potential; as the barrier depends on l, s-wave scattering cannot lead to shape resonances. From a chemical perspective, a shape resonance is a situation in which the scattering electron occupies the lowest unoccupied molecular orbital. Shape resonances are often short lived and usually appear as

broad peaks in the eigenphase sum as a function of energy.

Feshbach resonances [81, 82] occur when the scattering electron also excites the target molecule leading to a double excitation of the target molecule. The resonances in the e^--CH^+ collisional spectrum are most of this kind (see also Fig. 3.19 in section 3.2). The target molecule is excited into a configuration which is not its ground state, known as the parent state, and the scattering electron is temporarily captured into an unoccupied virtual orbital. At the end of the resonance's lifetime the state decays to the parent state. Feshbach resonances are prevalent in ionic targets and generally take the form of Rydberg states. There are also valence states embedded in the continuum which appear as Feshbach resonances. Capturing into such a resonance state may lead to direct dissociative recombination if the state is repulsive state (see section 2.6). Nuclear-excited Feshbach resonances [83] can only occur in molecules when there is a weakly bound state just below the ionization threshold of the molecule. The collision by an electron excites the molecule to a high vibrational level in the weakly bound state. Resonances of this type are responsible for the indirect process in dissociative recombination. This is particular important for CH^+ due to its low-lying excited electronic states (see section 2.6).

The position E^r and width Γ [14] of a resonance could be generally determined by two approaches: the CAP method (see section 2.2.2) and the eigenphase method. Through fitting the derivative of the eigenphase sum δ over the total energy of the collisional system E in the Breit-Wigner form,

$$\frac{d\delta}{dE} = \frac{\Gamma/2}{(E-E^r)^2 + (\Gamma/2)^2} \tag{2.54}$$

For convenience to locate the positions of the resonances, we can also use derivative of the eigenphase sum over total energy ($\frac{d\delta}{dE}$). This method is used in this thesis as P. G. Burke pointed out that it often provides an accurate procedure for analyzing the positions and widths of the

[14] Determines the lifetime of a resonant state [84]

resonances [58]. On the other hand, the Rydberg resonances (Feshbach resonances) are taken into account in our proposed approach through the energy-independent scattering matrix combined with the quantum defect theory (QDT) (see section 2.5). We use the positions and widths of the resonances to compare with that obtained directly from the R-matrix method. However, they are not the necessary input data in the cross section (for vibronic excitations and dissociative recombination of CH^+, see section 2.5 and 2.6) calculations. This differs from the theoretical methods in Refs. [31, 34] where the positions and widths of the resonance are needed to be explicitly included to account for the electronic coupling for the study of, for instance, dissociative recombination.

2.4 Vibronic frame transformation

We've already discussed how to model a fixed-nuclei electron-ion collision through the R-matrix method. Here we will address the question that how we should take the effects of the nuclei into accounts. In order to simplify the discussion, we only consider electronic capture by vibrational level of the target. Chang and Fano pointed out that the interaction between the electron and the molecule exhibits qualitatively different physical features when their distance coordinate lies in different regions, as illustrated in Fig. 1 of Ref. [85]. The dominant terms in the Hamiltonian of the collisional system determines which physical observables are approximately conserved. The salient point is the relative importance of the nuclear kinetic-energy operator and the electron-ion interaction potential which depends on the proximity of the scattering electron to the target. As shown below in Fig. 2.5 (a), for simplicity, we accordingly divided the space into a Λ and M region [86, 87]. The radius $r_0(=a)$ is the boundary of the inner region in the R-matrix method (see Fig. 2.4). r_v is determined by kinetic energy of the scattering energy associated with v vibrational

state of the target [15].

In the Λ region, a Body-frame of reference is more appropriate since a strong electron-molecule interaction, rather like a strong axially symmetric electric field, is more suitably accounted for in this reference frame. A schematic of the Body-frame coordinate system is given in Fig. 2.5 (b). The projections μ and λ of the angular momentum j and l of the target molecular ion and the scattering electron in the Body-frame correspondingly are conserved, as well as $\Lambda = \lambda + \mu$. In this representation that the orientation of the internuclear axis is fixed, channels with different values of Λ (or we can say different symmetries) are not coupled. In practice, the Body-frame reactance matrix is thus calculated separately for each Λ. The S-matrix or K-matrix obtained in section 2.3.1 will be block-diagonal, where each block corresponds to a given projection Λ of the electron-ion collisional system (see Table 2.3). In the outer part of this region within r_v in the Fig. 2.5 (a), the effects of the nuclear vibrational Hamiltonian on the wavefunction of the scattering electron should be explicitly taken into account. The total wavefunction of the ionization channels in this part could be written as

$$\Phi_v^{\Lambda}(R,r) = \phi_v^{N+1}(R)\varphi(R)[f_l(\nu,r) - tan(\delta_l(R))g_l(\nu,r)] \tag{2.55}$$

where $\phi_v^{N+1}(R)$ is the wavefunction of v vibrational state of the electron-ion system, $\varphi(R)$ is the electronic wavefunction of the ion core. $f_l(\nu,r)$ and $g_l(\nu,r)$ are respectively the regular and irregular Coulomb functions for a partial wave l of the scattering electron. ν is a effective quantum number defined by $\nu = 1/\sqrt{-2E}$ $(E < 0)$. $\delta_l(R)$ is a eigenphase evaluated by the R-matrix method at R.

In the M region at a large distance, a Laboratory-frame of reference is more justified since the coupling of the electron angular momentum to the molecular axis is no longer strong. A schematic

[15] It is "r_2" in Fig.1 of Ref. [85]

of the Laboratory-frame reference system is given in Fig. 2.5 (c). It is advantageous to couple the angular momentum j and l in such a formulation, since the resultant total angular momentum $J = l + j$ and its projections $M = m_l + m_j$ along the lab polar axis are constants of the motion [88]. In this region, vibronic couplings vanish so that the channel wavefunction is well separated in an electronic and vibrational part. The total wavefunction for the collisional system expressed by

$$\Phi_v^M(R,r) = \sum_{v'} \phi_{v'}(R)\varphi(R)[f_l(\nu',r)\delta_{v',v} - K_{v',v}g_l(\nu',r)] \tag{2.56}$$

where $\delta_{v',v}$ is a Kronecker delta and ν' corresponds to $1/\sqrt{2(E-E_{v'})}$. The $K_{v',v}(R)$ is the matrix describing the vibrational transitions from v to v'. Note that in this thesis, the rotational structure is neglected and will be considered in a future study.

The low-energy incident electron is generally captured in vibrational state of a high Rydberg state within $[r_0, r_v]$. Such a Rydberg state is an adiabatic potential energy curve of a neutral molecule (electron-ion system) that is close to its parent state. Accordingly, it looks very similar to its parent ionic potential curve. Hence, we could consider the vibrational wavefunctions of such a Rydberg state is in a good accordance with the corresponded ionic ones $\phi_v^{N+1}(R) \approx \phi_v(R)$. We can now relate the wavefunctions in the two regions by expanding the wavefunction Φ_v^M of Eq. (2.55) over Φ_v^Λ of Eq. (2.56) on the boundary with the help of a unitary transformation

$$\Phi_v^M = \sum_{v'} a_{v'}\Phi_{v'}^\Lambda \tag{2.57}$$

Assuming the regular Coulomb functions on both sides of the above equation are nearly identical for different channels, which means that $f_l(\nu,r) \approx f_l(\nu',r)$. It is straightforward to show that $a_{v'} = \delta_{v',v}$. Considering now the coefficient of the irregular Coulomb function on both sides, we obtain

$$K_{v',v}\phi_{v'}(R) = tan(\delta_l(R))\phi_v(R) \tag{2.58}$$

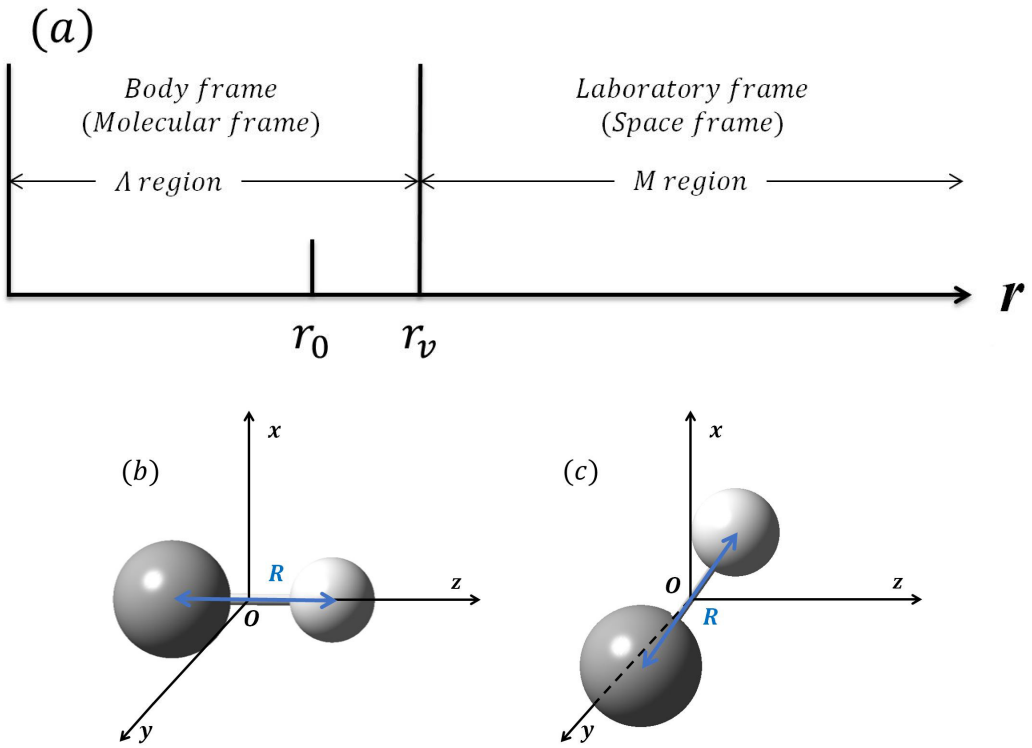

Figure 2.5: (a) Partitioning of configuration space for frame transformation, (b) the Body-frame representation used in Λ region, where the internuclear axis is taken as the z axis, and (c) the Laboratory-frame representation used in M region, where the z axis fix along the initial momentum vector of the incident electron.

By multiplying both sides of the equation by $\phi^*_{v'}(R)$ and integrating over R, we finally arrive at the desired result that

$$K_{v',v} = \int \phi^*_{v'}(R) tan(\delta_l(R)) \phi_v(R) dR \tag{2.59}$$

Considering Eq. (2.52), we could also couple the vibrational motion to the S-matrix. This mechanism is called the frame transformation procedure of Chang and Fano [85] that transforms the Body-frame fixed-nuclear scattering function into the Lab reference frame at the boundary radius. In the thesis, the additional two $a^3\Pi$ and $A^1\Pi$ excited states of CH^+ are also considered.

Thus, we used a vibronic frame transformation in the form

$$S_{l'\lambda'v'i',l\lambda vi}(E) = \int \phi^*_{v'i'} S_{l'\lambda'i',l\lambda i}(E,R)\phi_{vi}dR \tag{2.60}$$

to compute the vibronic (de-)excitation amplitudes for the process represented by

$$\mathrm{CH}^+(vi) + e(l\lambda) \rightarrow \mathrm{CH}^+(v'i') + e(l'\lambda') \tag{2.61}$$

ϕ_{vi} and $\phi_{v'i'}$ numerate the initial and final vibronic state. $l\lambda$ and $l'\lambda'$ numerate the initial and final angular momenta and their projection in the Body-frame.

But one should notice that, first, the rotational frame transformation is very different. One could refer to Ref. [38, 89] for more details. Second, we used an assumption (of $f_l(\nu,r) \approx f_l(\nu',r)$) that the regular Coulomb functions are energy-independent within the space of vibrational level. This actually means that the effective quantum number $\nu \approx \nu'$. In such a condition, the scattering matrix ($S = exp(2i\pi\mu)$, μ is quantum defect as seen in the next section) should be energy-independent, i. e. smooth with regards to E in the space of vibrational levels, considering the relationship between the ν and K-matrix (considering Eqs. (2.52), (2.53), (2.63), and (2.65)). Therefore, one has to note that adoption of the standard vibrational frame transformation of Chang and Fano [85] requires energy-independent S-matrices. The total energy E is defined by

$$E = E_{\mathrm{el}} + E_{00} \tag{2.62}$$

where E_{el} is the electron scattering energy. E_{00} is vibrational energy level of the ground-state CH^+. It is the zero energy level in this thesis. Thus, we have $E = E_{\mathrm{el}}$ and we will use E_{el} in the rest parts of this thesis.

2.5 Multi-channel Quantum Defect Theory

2.5.1 Rydberg states

As we introduced in the preceding section the way to compute the vibronic amplitudes, here we will discuss how to take into account the Rydberg resonances. A molecular Rydberg state is an electronic state where the incident electron is captured into an excited orbital far from the molecular ion core. The electron moves in this state is called a Rydberg electron. It is like a hydrogenic electron, but the difference is that nuclei of the molecular ion are clamped by electrons. Hence, we describe the Rydberg state by an effective quantum number $v_{n,l}$, computed by

$$v_{n,l} = n - \mu_{n,l}(R) \tag{2.63}$$

where $\mu_{n,l}(R)$ is a $R-$dependence quantum defect of the Rydberg state. n and l numerate the principle and angular quantum number. Then the potential energy curve of a Rydberg state is given by

$$E_{n,l}(R) = E_{ion}(R) - \frac{1}{2(n-\mu_{n,l}(R))^2} \tag{2.64}$$

When the electron bounded in the Rydberg state close nearly to the threshold, which means n goes to infinity, the quantum defect of the Rydberg electron converges and connects with the phase shift $\delta_l(R)$ of radial wavefunction for the scattering electron by

$$\lim_{n\to\infty} \mu_{n,l}(R) = \mu_l(R) = \frac{\delta_l(R)}{\pi} \tag{2.65}$$

This is firrst introduced in 1966 [90] by Seaton in his communication on Quantum Defect Theory (QDT). We surprisingly find the connection between the scattering theory for electron-ion collisional system and the QDT, that short-range scattering electron (within r_v in Fig. 2.5) could be

viewed as a Rydberg electron in the compound system. The electronic state of the collisional system generated by the electron-ion interaction is a Rydberg state with $\mu_l(R)$.

Therefore, one can actually extract the scattering phase shift from the quantum defect. This is the most important foundation of the widely used QDT in the scattering problems. As we introduced in subsection 2.3.1, that phase shift $\delta_l(R)$ could be obtained through an *ab initio* scattering calculation using, for instance the fixed-nuclear R-matrix method. The quantum defects represented the electronic state of any highly excited Rydberg states, as well as low energy electron continuum states could be sorted out by QDT. However, as we discussed in section 2.3.2, we don't need to extract the quantum defects (or the eigenphase) to account for the non-adiabatic couplings, such as couplings between the Rydberg states. The couplings are included by using an energy-independent scattering matrix coupling with the MQDT elimination procedure (see the next two sections).

2.5.2 The multi-channel approach

We now describe in more detail QDT from one-channel approach. The asymptotic radial wavefunction of a Rydberg electron is a linear superposition of regular and irregular Coulomb wavefunction (f,g) [91]

$$F(r) = N_l[f_l(\nu,r)cos\pi\mu_l - g_l(\nu,r)sin\pi\mu_l] \tag{2.66}$$

where N_l is a normalization constant. The remaining electrons and nuclei are supposed staying within $r_0(=a)$. Inserting the expressions of Coulomb wavefunctions (see Eq. (3) of Ref. [91]) to obtain

$$F(r) = \sqrt{\frac{1}{\pi k}}(sin(\beta+\pi\mu_l)D^{-1}r^{-\nu}e^{kr} - cos(\beta+\pi\mu_l)Dr^{\nu}e^{-kr}) \tag{2.67}$$

where the coefficients β is effective quantum number related parameter defined as

$$\beta = \pi\nu \tag{2.68}$$

D are constants depending on l and total energy E of the system. We define $k = (-2E)^{1/2} = \frac{1}{\nu}$. The bound state solution is exponentially decreasing as $r \to \infty$, the constraint obtained for integer l is

$$sin\pi(\nu + \mu_l) = 0 \tag{2.69}$$

We could thus arrive Eq. (2.64) which is used to compute the bound states energies.

Consider a general case, i.e. a multi-channel case, where there are multiple electronic channels which are described by a discrete set of functions $\varphi_i(x)$. x specifies the collected ionic coordinates as well as the angular momentum of the scattering electron. The index i numerates N electronic channels (states). The asymptotic solution of the Schrödinger equation for the collisional system could be written as

$$\Phi_i(x,r) = \sum_{i'=1}^{N} \varphi_i(x)\phi_\nu(R)[f_{i'}(k_{i'}r)\delta_{i'i} - K_{i'i}(R)g_{i'}(k_{i'}r)] \tag{2.70}$$

where $K_{i'i}(R)$ is the the reaction matrix and $k_{i'} = \frac{1}{\sqrt{E-E_{i'}}}$. It is in a similar form with Eq. (2.56) but with a multi electronic channel cases. The incoming electron (wavefunction) in i electronic channel is randomly scattered to outgoing i' channel. Therefore, $K_{i'i}$ represents $N \times N$ independent solutions for N-channel problem. This matrix could be evaluated by the fixed-nuclear R-matrix method (see section 2.3.1). More detailed description and explanation could be found in Refs. [58, 86, 90–93].

2.5.3 Closed-channel elimination procedure

So far, we didn't discuss about the physical significance of the solutions. We define an open or closed channel on the basis that whether the total energy E is higher or lower than the corresponding channel's energy. E is the total energy of the electron-ion collisional system obtained by Eq. (2.62). It is a sum of scattering energy $E_{\rm el}$ and the zero piont energy of the initial state of the target. We use N_o and N_c to denote the number of open and closed channels $(N = N_o + N_c)$. The index "o" and "c" represent "open" and "closed", respectively. The obtained transformed scattering matrix by Eq. (2.60) in section 2.4 could both be partitioned in four sub-matrices

$$S(E_{\rm el}) = \begin{pmatrix} S^{oo} & S^{oc} \\ S^{co} & S^{cc} \end{pmatrix} \tag{2.71}$$

To be physically acceptable, the solutions corresponding to closed channels have to vanish asymptotically as seen by Eq. (2.49) in section 2.3.1. Thus, the Schrödinger equation has only N_o independent solutions. In order to express the physical solutions in the open channels, we need to eliminate the divergent solutions (combining Eqs. (2.47) and (2.67)) in the asymptotic region, i.e. solutions of the closed channels. The form of the physical scattering matrix is given by

$$S^{phys}(E_{\rm el}) = S^{oo} - S^{oc}\left[S^{cc} - e^{-2i\beta(E_{\rm el})}\right]^{-1} S^{co} \tag{2.72}$$

where $\beta(E_{\rm el})$ is diagonal matrix representing the effective quantum numbers (mentioned in section 2.4) in terms of energies of a channel

$$\beta(E_{\rm el}) = \frac{\pi}{\sqrt{2(E_{vi} - E)}} \tag{2.73}$$

E_{vi} is the energy of the v vibrational state of the i ionic state. This quantity is also found in Eq. (2.67) in section 2.5.1.

The above equation is used to account for the Rydberg states caused by the closed ionization channel defined as a vibrational level. This is different in the electronic excitation study, where the ionization channels are defined by the electronic states of the target. Therefore, one doesn't need to implement the vibronic frame transformation by Eq. (2.60). The scattering matrices $S_{l'\lambda'i',l\lambda i}(E,R)$ obtained directly from the R-matrix method are partitioned into four submatrices through Eq. (2.71). To account for the electronic Rydberg resonances, we apply the electronic closed-channel elimination procedure by Eq. (2.72). The difference is that the vibronic channel's threshold E_{vi} in Eq. (2.73) is replaced by electronic state energy $E_i(R)$.

Physical understanding of the elimination procedure is given here. The scattering process in the short range of $r < r_v$ could be viewed as a Rydberg electron interacts with the target ion core. When the Rydberg electron approaches to a closed channel, which means the total energy becomes closed to a threshold of a given ionic channel, infinite Rydberg states attached to the given closed channel could be "seen" by this Rydberg electron. Transient neutral compound will be formed as the Rydberg electron moves in these Rydberg states. As a consequence, infinite resonances will be seen in the collisional spectrum (see, for example, Fig. 3.5 in section 3.3). These physical resonances caused by the closed channel could be recovered by the elimination procedure with the quantum defect parameters (included in the quantity β of Eq. (2.73)).

Since we've had the physical S-matrix for the vibronic excitation in Eq. (2.72), the cross section for this process is expressed as

$$\sigma_{v'i',vi}(E_{\mathrm{el}}) = \frac{\pi\hbar^2}{2m_e E_{\mathrm{el}}} \sum_{l'\lambda',l\lambda} \left| S^{phys}_{l'\lambda'v'i',l\lambda vi}(E_{\mathrm{el}}) - \delta_{l'\lambda'v'i',l\lambda vi} \right|^2 \tag{2.74}$$

where m_e is the mass of an electron. For the cross section of electronic excitation, the $S^{phys}_{l'\lambda'v'i',l\lambda vi}(E_{\rm el})$ is replaced by $S^{phys}_{l'\lambda'i',l\lambda i}(E_{\rm el},R)$.

The corresponding thermally averaged rate coefficients for vibronic excitations are computed by

$$\alpha_{v'i',vi}(T) = \frac{8\pi}{(2\pi k_{\rm b}T)^{3/2}} \int_0^\infty \sigma_{v'i',vi}(E_{\rm el}) e^{\frac{-E_{\rm el}}{k_{\rm b}T}} E_{\rm el} dE_{\rm el}, \tag{2.75}$$

where $k_{\rm b}$ is the Boltzmann constant and T is the temperature. Similarly, for the rate coefficient electronic excitation, the $\sigma_{v'i',vi}(E_{\rm el})$ is replaced by $\sigma_{i',i}(E_{\rm el},R)$.

Rydberg resonances contribute a lot to the dissociative recombination (DR) cross section for electron-ion collisions. Therefore, closed-channel elimination procedure is also a very critical MQDT tool for the modeling of a DR process. See Refs [34, 94, 95] and therein for more details. We'll describe the theoretical approach based on the MQDT method to compute the DR cross section for this process in the next section.

2.6 Dissociative recombination

2.6.1 Direct DR mechanism

In a collision process, the incoming electron could be captured by the molecular ions. A doubly excited dissociative state is formed when the electron collision energy $E_{\rm el}$ is not transferred directly into the kinetic motion of the nuclei, but rather to the electronic ionic clouds. One of the bound electrons is excited by the scattering electron. This state is situated in the ionization-continuum. The potential curve of a neutral dissociative state is repulsive and intersects, or approaches very closely, the potential curve of the ion at a nuclear separation within the extent of the vibrational motion of the ion. The electron-electron interactions in the dissociative state give rise to the mixing of its

configuration with the configurations where only one electron is excited. The excited electron in the latter configuration has sufficient energy to escape from the molecule. It is therefore an unstable state against autoionization, i.e. re-emitting the electron leading to vibronic excitations. This state with a certain width given by the autoionization width is also called a resonance state. However, if the dissociative process happens fast enough so that the products of dissociation are already at a large distance from each other after a time equivalent to the order of the autoionizing lifetime, most of the collisional energy is already converted into nuclei kinetic energy and autoionization becomes impossible. In such a case, the system will irreversibly breakdown in one of the dissociative channels. This is so-called *direct dissociative recombination* (DDR) process proposed by Bates in 1950 [96].

In this case, the rate coefficient is approaximately proportional to the square of a matrix element between the vibrational wavefunctions for the ion and neutral states

$$\left\langle \Psi_{N+1}(r,R)\phi_v(R)|\hat{H}_{N+1}(R)|\Psi_d(r,R)\phi_d(R)\right\rangle \tag{2.76}$$

Here, $\hat{H}_{N+1}(R)$ is the (N+1)-electronic Hamiltonian, r and R denote the electron coordinate and internuclear distance. Ψ_{N+1} is the electronic wavefunction for the $(N+1)$-electron, $\Psi_d(r,R)$ is the neutral dissociative state wavefunction. $\phi_v(R)$ specifies the bound vibrational wavefunction of the ion core. $\phi_d(R)$ is the continuum vibrational wavefunction in the neutral dissociative state. We can know from the above equation that a high vibrational wavefunction overlap requires the neutral dissociative state crosses the ion curve between the turning points of the ion vibrational level, leads to a high direct DR rate coefficient. The cross section of the DDR is written by O'Malley [97] and Bardsley [98]

$$\sigma^{DDR}(E_{\rm el}) = \sigma_{capture}(E_{\rm el})\tau(E_{\rm el}) \tag{2.77}$$

where $\sigma_{capture}(E_{\rm el})$ is the cross section for formation of the neutral dissociative state and $\tau(E_{\rm el})$ is the

survival factor representing that this state will decay by dissociation rather than by autoionization. Considering Eq. (2.76), the capture cross section is also expressed by

$$\sigma_{capture}(E_{\mathrm{el}}) = \frac{\pi^2}{m_e E_{\mathrm{el}}} \frac{z}{2} \frac{\Gamma_c}{U_d'(R_{\mathrm{c}})} |\phi_v(R_{\mathrm{c}})|^2 \tag{2.78}$$

where z represents the ratio of the multiplicity of the intermediate state to the initial state of ionic core. R_c is the internuclear distance where the electron scattering energy E_{el} is the difference between the initial ionic state and the neutral dissociative state. U_d' is the slope of the PEC of the dissociative state and Γ_c is the width of the neutral dissociative (resonance) state at R_{c}. We usually regard the $\frac{|\phi_v(R_{\mathrm{c}})|^2}{U_d'(R_{\mathrm{c}})}$ as the Frankon-Condon factor.

2.6.2 Indirect DR mechanism

It may happen that the resonant (dissociative) state is situated far away from the ionic ground state, either above or below it. This is often seen in a closed shell ions, such as HeH^+ [99, 100]. In this case, a direct capture of a low energetic electron into the neutral resonant state is unlikely. An *indirect DR (IDR)* mechanism was therefore predicted by Bardsley in 1968 [101]. This indirect process can be considered as the result of two non-radiation transitions. In contrary to the direct process, the kinetic energy of the electron was transferred to the motion of the molecular nuclei. The incident electron then moves in a hydrogenic-like orbital with high principle quantum number (see Eq. (2.64)). A ro-vibrationally (but rotational structure is neglected in the this DR study) excited Rydberg state is formed. The second transition is predissociation of the state by the resonance (repulsive) state of the direct DR mechanism. Capture occurs by a BO approximation breakdown mechanism. The appropriate matrix element for the capture is analogous to Eq. (2.76) but with a

Rydberg state substituting the dissociative state

$$\left\langle \Psi_{N+1}(r,R)\phi_v(R)|\hat{T}_n(R)|\Psi_{Ryd}(r,R)\phi_{v'}(R)\right\rangle \tag{2.79}$$

where $\hat{T}_n(R)$ is the nuclear kinetic energy operator. Alternatively, the matrix element in the above equation can be evaluated by the quantum defects. Once capture occurs, the Rydberg electron may autoionize or predissociate via electronic coupling in Eq. (2.76) with $\Psi_{Ryd}(r,R)$ replacing $\Psi_{N+1}(r,R)$ on the left side of the matrix element.

In the indirect recombination mechanism of the molecular ions with low-energy electron, the Rydberg states are the source of structure in the DR cross section. According to Eq. (2.64) in subsection 2.5.1, Rydberg energies are actually close to each other. Their separations become ultimately much smaller than the separation of vibrational energies of the ion. Indeed, this is a case of breakdown of the Born-Oppenheimer approximation. The interactions between the vibrational motion and the electronic motion can be non-negligible. Therefore, an electron in the continuum is able to exchange its energy with the vibrational motion of the ion and consequently be captured in one of the Rydberg state. Then, the electron can be represented as descending in cascade from orbitals to orbitals, exchanging energy with the ionic core until it reaches a path for dissociation.

In the above discussion, only the Rydberg states attached to the ground ionic state is considered. However, there are other Rydberg states that having excited ionic states as the core can also play an important role. Rydberg states with an excited core can affect the DR of the vibrational levels of the ground ionic state for ions with low-lying ($<$ 4.0 eV) excited electronic states [102–105]. The Rydberg states are formed by a double excitation from the ground state ion and the scattering electron. The coulpling matrix elements for the captures are

$$\left\langle \Psi_{N+1}(r,R)\phi_v(R)|\hat{H}_{N+1}(R)|\Psi_{Ryd}^{excited\ core}(r,R)\phi_{v'}(R)\right\rangle \tag{2.80}$$

These Rydberg states have already been included in MQDT cross section calculations [18, 102, 102–105]. The treatment of the IDR is very different from that of DDR. It is usually treated by normal resonance theory developed for atomic and nuclear systems. The cross section is given in form similar to the Breit-Wigner formula (see Eq. (2.54))

$$\sigma^{IDR}(E_{\rm el}) = \sum_i \frac{\pi\hbar}{2m_e E_{\rm el}} \frac{z}{2} \frac{\Gamma_{ia}\Gamma_{id}}{(E_{\rm el}-E_i)^2 - \frac{1}{4}\Gamma_i^2} \tag{2.81}$$

where i denotes the resonances and Γ is the width of the resonance. z represents the ratio of the multiplicity of the intermediate state to the initial state of ionic core. Γ_{ia} and Γ_{id} are the width for the autoionization and predissociation of the ith resonance. The computation of these two parameters could be found by Eqs. (3) and (6) of Ref. [106]. This indirect DR process usually plays a exclusively constructive role, in opposition with the numerous cases where it has destructive role. The total process is well taken into account by Eq. (2.85) expressing a quantum interference, which can be constructive or destructive, according to the relative importance of the predissociation versus the vibrational autoionization.

2.6.3 Theoretical approach for DR of CH^+

Through the preceding two parts, we are aware of the fundamentals of DR process for a diatomic molecular ion. MQDT treatment for the cross section calculations has been proven to be the most successful theoretical method. In this thesis, we will also employ the MQDT treatment for the low-energy DR of CH^+. The process is represented by

$$CH^+(vi) + e(l\lambda) \rightarrow C + H \tag{2.82}$$

It is a competition process to the vibronic transitions of Eq. (2.61). A detailed DDR and IDR processes are given and discussed in section 4.2. Computation of this process is in the similar framework of MQDT but coupled with additional CAP formalism as we introduced in section 2.2.2. The dissociation proceeds through a number of excited Rydberg states, which are bound with respect to dissociation. MQDT treats such a system as a coupled vibrational states. To describe the dissociation, the vibrational continua states of the considered PECs (the three lowest electronic states) of CH^+ should be included in the model. The states are discretized through a CAP formalism that obey outgoing-wave boundary conditions. They are introduced as the closed ionization channel by vibrational frame transformation [107]. The vibrational continua states of the neutral Rydberg states attached to these outgoing-wave basis could be taken account for through MQDT closed-channel elimination procedure. The the dissociative flux of the neutral molecule is thus simulated to escape on the boundary.

As we introduced in section 2.4, the scattering matrix describing the vibrational excitation of fully relaxed (ground-state) CH^+ is computed by Eq. (2.60), but the used CAP basis $\phi_{v'i'}$ of CH^+ in the equation is not conjugated. The equation is thus expressed by

$$S_{l'\lambda'v'i',l\lambda vi}(E_{\mathrm{el}}) = \int \phi_{v'i'} S_{l'\lambda'i',l\lambda i}(E_{\mathrm{el}},R)\phi_{vi}dR \tag{2.83}$$

The ionization channels are now a set of CAP basis for ionic PECs. Each of the channels associated with the threshold energy of a vibrational level of the ionic electronic states. In the MQDT closed-channel elimination procedure as shown in Eqs. (2.72) and (2.73), we need to use the threshold energy E_{vi}. As seen in Eq. (2.34), the eigenenergy of the CAP vibrational basis is a complex. In the practical treatment, we sorted successively the vibrational level's energy E_{vi} from lower to higher energy values according to the real part of the eigenenergies. These ranked eigenenergies are used to represent the threshold of the ionization channels. Again, we neglect any rotational structure

here (but will include it in the further study). The total energy E of the e^--CH^+ system divides all channels as energetically open when it situated above the corresponding ionization threshold or otherwise closed (as mentioned in section 2.5.3). The transformed scattering matrix is thus written as submatrices of Eq. (2.71).

The physical scattering matrix $S^{phys}(E_{\rm el})$ restricted to open channels is obtained using MQDT close-channel elimination procedure by Eq. (2.72). But the quantity $\beta(\mathrm{E}_{el})$ of Eq. (2.73) becomes complex because the higher ionization thresholds are represented by the CAP vibrational basis with complex eigenenergies (as seen in Eq. (2.34)). This fact makes the $S^{phys}(E_{\rm el})$ sub-unitary. Physically, the lost flux is associated with an electronically closed channel attached to a vibrational wavefunction described by a dissociative CAP basis.

To calculate the total cross section (including DDR and IDR), we also need the conjugated scattering matrix. To be precise, we need $S^{\dagger phys}_{l'\lambda'v'i',l\lambda vi}(E_{\rm el})$. We first compute the fram-transformed scattering matrix by Eq. (2.83) with the complex-conjugate scattering matrix $S^{\dagger}(E_{\rm el},R)$

$$S^{\dagger}_{l'\lambda'v'i',l\lambda vi}(E_{\rm el}) = \int \phi_{v'i'} S^{\dagger}_{l'\lambda'i',l\lambda i}(E_{\rm el},R)\phi_{vi}dR. \tag{2.84}$$

We then use MQDT elimination procedure of Eq. (2.72) to compute the conjugated physical scattering matrix

$$S^{\dagger phys}(E_{\rm el}) = S^{\dagger oo} - S^{\dagger oc}\left[S^{\dagger cc} - e^{2i\beta(E_{\rm el})}\right]^{-1} S^{\dagger co} \tag{2.85}$$

where conjugated submatrices of $S^{\dagger}(E_{\rm el},R)$ are used. One needs to notice that β in $e^{2i\beta(E_{\rm el})}$ is not complex conjugated. The obtained $S^{\dagger phys}(E_{\rm el})$ is not a simply Hermitian conjugate of the $S^{phys}(E_{\rm el})$, i.e. $S^{\dagger phys}(E_{\rm el})$ could not be computed by complex conjugation of $S^{phys}(E_{\rm el})$. The essential reason is that the CAP vibrational basis is used in the DR case.

Once the scattering matrices $S^{phys}(E_{\rm el})$ and $S^{\dagger phys}(E_{\rm el})$ are determined, the DR cross section for a

specific partial wave is extracted from the unitarity defect of the scattering matrix

$$\sigma_{l\lambda vi}(E_{\rm el}) = \frac{\pi\hbar^2}{2m_e E_{\rm el}} \left[1 - \sum_{l'\lambda' v' i'} S^{phys}_{l'\lambda' v' i', l\lambda vi}(E_{\rm el}) S^{\dagger phys}_{l\lambda vi, l'\lambda' v' i'}(E_{\rm el}) \right] \tag{2.86}$$

where the CH^+ is initially in ground state where $vi = 00$ representing the ground vibrational state of $X^1\Sigma^+$ ground electronic state. The total cross section for the ground-state CH^+ is computed by

$$\sigma_{total}(E_{\rm el}) = \sum_{l\lambda} \sigma_{l\lambda 00}(E_{\rm el}) \tag{2.87}$$

So far, we reviewed the electronic structure theory for computation of the potential energy curves and the fixed-nuclear R-matrix method used for the scattering calculations. Based on these fundamentals, we described the MQDT treatment using vibronic frame transformation and closed-channel elimination procedure for the vibronic (de-)excitation of CH^+ by low-energy electron impact. We will show more calculation details about this method in chapter 3. We also introduced an theoretical approach in a similar framework coupled with additional CAP vibrational basis to treat the low-energy DR of CH^+. A detailed description of this approach is found in chapter 4.

CHAPTER 3: Vibronic (de-) excitation of CH^+ by electron impact

3.1 Introduction

As stated in chapter 2, low-energy electron-impact vibronic excitation of CH^+ of Eq. (2.61) competes with the dissociative recombination represented by Eq. (2.82). Both processes will be treated in the MQDT framework. In this chapter, we will benefit from the theoretical tools introduced in chapter 2 to describe the details about the treatment vibronic excitation processes induced by electron-impact.

In many fields of research and applications, it is essential to have accurate cross sections for different processes taking place in collisions between molecular ions and electrons. Among such processes are electron-impact rotational (RE), vibrational (VE), or electronic (EE) excitation of the ions, dissociative recombination (DR), photoionization and its inverse process, radiative recombination. Some cross sections could be obtained in experiments. However, for many processes, especially, for the processes involving excited-state ions (ions here and below are assumed to be molecular ions, not atomic) or such ions as radicals, which are unstable in collisions with other species present nearby, an experimental approach is difficult or impossible. Even for stable ions in their ground quantum state, an experimental approach is often very expensive.

On the other hand, for theoretical approaches a significant complication in computation of the cross sections is the presence of vibrational and rotational degrees of freedom that have to be accounted for an accurate description of the processes. Electronic excitation and ionization of molecules can be treated theoretically, at least, to some extent in the Born-Oppenheimer approximation or taking into account the Franck-Condon factor. For other processes, such as rovibrational excitation or dissociative recombination, non-Born-Oppenheimer effects should be accounted for explicitly.

With modern development of electron-scattering methods and abundant computational resources, it became possible to compute, with an acceptable uncertainty, cross sections for many processes in electron-ion collisions. Significant progress was made for processes in diatomic ions formed by light elements: H_2^+ [108], HeH^+ [108], BeH^+ [109], BF^+ [110], CH^+ [18,30,111,112], SH^+ [113], N_2^+ [31,114,115], O_2^+ [116] with a few other diatomic ions, and the simplest triatomic ion H_3^+ with its isotopologues [117–121], where non-Born-Oppenheimer effects in electron-ion collisions were accurately accounted for, typically using a quantum-defect approach combined with rotational and vibrational frame transformations. With some additional simplifications, such processes as rovibrational excitation and dissociative recombination were also successfully described theoretically for larger molecular ions: CH_3^+ [122], H_3O^+ [122,123], NH_4^+ [124], HCO^+ [125–131], BF_2^+ [132], N_2H^+ [131], $HCNH^+$ [53,133–135], $CH_2NH_2^+$ [136], and NH_2CHOH^+ [137].

Theoretically, non-Born-Oppenheimer couplings in electron-ion collisions are treated differently for the ions with low-energy electronic resonances appearing for geometries near the equilibrium of the target ion (in a fixed-nuclei picture) and for the ions without such low-energy electronic resonances. In the former case, usually, the potential energy surface (PES) of the doubly-excited neutral molecule cross the ionic PES near the equilibrium geometry; in the later case, there is no such a resonance PES. The ions of the first type usually (not always) have the first excited electronic state at a relatively low energy, below 5 eV; the ions of the second type have the first excited electronic state at a higher energy.

The presence of low-energy electronic resonances in the first type of the ions increases significantly, compared to the ions of the second type, the DR, EE, VE, RE cross sections at low collision energies. Due to the significant difference in the physics of couplings in electron-ion collisions in the two types of the ions, one developed two types of approaches. The first approach, developed for DR, VE, and RE processes and originated from studies by O'Malley [97] and Bardsley [22,101,138], takes into account explicitly the PES crossing. The second approach, based mainly on studies by

Lee [33], Jungen *et al.* [139, 140], and Giusti [141] and employed when there is no PES crossing, accounts for the coupling between the incident electron and the rovibronic Rydberg resonances of the neutral molecule. In an absence of a PES crossing, such resonances are responsible for the major contribution to the DR cross section at low energies [117, 141, 142]. This is especially important for polyatomic ions, listed above. All these ions have a closed electronic shell, the first excited electronic state at a high energy, and no PES crossing near the equilibrium geometry of the ions.

There are situations, where there is a PES crossing near the ion equilibrium geometry and, in addition, there is one or several low-energy electronic resonances in the collisional spectrum. Many open-shell ions are of this type, for example. The two approaches mentioned above are not able to describe satisfactory the DR and excitation processes. On the basis of an earlier theory suggested by Giusti [34, 141], Jungen, Mezei, and Schneider have developed an efficient approach that can deal with such a situation. The approach was applied to several diatomic ions for which the dissociative electronic PES of the neutral molecule crosses the ionic PES near the ion equilibrium [18, 143–145]. The approach is based on the quantum-defect theory (QDT), where, in addition to one or several electronic states of the ion, the dissociative state is explicitly included into the coupling scheme [34, 141]. Couplings between different electronic states of the target ion are derived from *ab initio* calculations of electronic (Rydberg) bound states of the neutral molecule. Couplings between the ionic and dissociative states are obtained from the autoionization widths of dissociative states of the neutral molecule (where autoionization is allowed). The widths are typically obtained in electron-scattering calculations.

The above theoretical approach is the only one able to describe non-Born-Oppenheimer effects on electron-ion collisions in a presence of coupled electronic channels of the target. One significant limitation of the approach is the difficulty in obtaining couplings between the electronic states. The procedure of diabatization of coupled Rydberg states obtained in *ab initio* calculations, used in the

approach, is laborious, not unique and sometimes not accurate. It becomes even more ambiguous and very complicated for polyatomic ions, such that an extension of the approach to polyatomic ions becomes non-practical.

Here, we propose another approach which combines some of the original ideas from the molecular quantum defect theory [139, 141, 146], more recent DR and VE studies in polyatomic ions [118, 125, 129, 131, 142], and recent progress in electron-scattering calculations. The approach can be applied to determine EE, VE, RE, and DR cross sections for a wide range of small polyatomic ions, including the ions with one or several low-energy excited ionic and/or resonant states of the system. In this chapter, we focus on the VE process of CH^+. However, the treatment can easily be applied to small polyatomic ions and, with some additions similar to Refs. [34, 141], for the DR process.

3.2 Calculation of the electronic structure, vibrational dynamics and the scattering process

3.2.1 Potential energy curves calculated by Gaussian and Molpro

In this section, we provide details about *ab initio* calculations of the bound electronic states of CH^+. This ion is formed through a covalence bound between C atom $(1s^2 2s^2 2p^2)$ and H^+. The configuration of the ground electronic state is $1\sigma^2 2\sigma^2 3\sigma^2$. Therefore, the spectral term of the ground electronic state is $X^1\Sigma^+$. We label the first and second excited states by $a^3\Pi$ and $A^1\Pi$ due to their electronic configurations $1\sigma^2 2\sigma^2 3\sigma 1\pi$ with total spin singlet $(2S+1=1)$ and triplet $(2S+1=3)$, respectively.

We first made use of Gaussian [147] to compute the potential energy curves and the results are shown in Fig. 3.1. The upper panel displays the ground electronic state. The red and blue curves were obtained with `cc-pVTZ` in QCISD method and `6-311`* in CISD method, respectively. The $X^1\Sigma^+$ ground and $A^1\pi$ excited electronic states are both picked up from the work of Biglari *et*

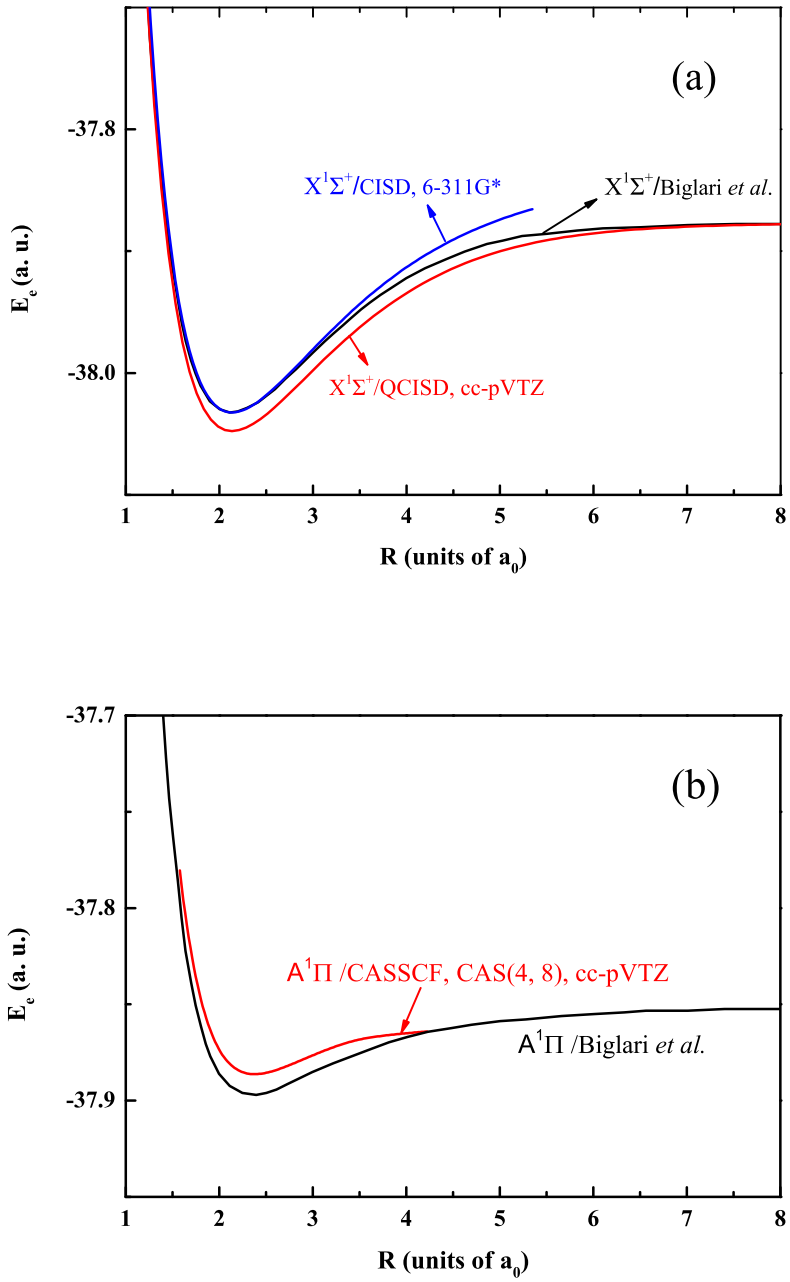

Figure 3.1: The ground $X^1\Sigma^+$ electronic state (upper panel) and the excited $A^1\Pi$ electronic state obtained using CASSCF method with `cc-pVTZ` and CAS(4,8) (lower panel) by Gaussian

al. [148] in 2014 as the standard theoretical results, which is obtained by ORCA suite (MRCI method with `cc-pV5Z` basis set and CAS(4, 14), see Ref. [148]). The red curve matches with the standard one of Ref. [148] at the large nuclear distance, while it mismatches in the main well of the potential curve. On the contrary, the blue curve shows a good agreement in the main well but has a higher dissociative limit compared with the black curve. In practice, we performed various calculations including different methods and basis sets but failed to find a potential curve showing good agreement with the standard one. We also tried to reproduce the potential curve of the excited $A^1\Pi$ electronic state in the work of Biglari *et al.* [148]. As shown in the lower panel, the red curve is obtained using CASSCF method with `cc-pVTZ` basis set and CAS(4, 8), where 4 electrons distribute in a CAS with 8 active orbitals (see introduction of the CAS in section 2.1.4). Discrepancy is shown between the computed red curve and the black curve. We tried to use different basis and method to eliminate the discrepancy but all failed.

Then we turned to Molpro [149] and successfully obtain accurate results for the scattering calculation. Molpro is a professional multi-reference calculation software package designed by Peter Knowles and Hans-Joachim Werner [149]. Quadratically convergent MCSCF method and internally contracted MRCI program are adopted for faster convergence, reduction of computational cost and highly accurate computations of electronic states. Gaussian is a general purpose computational chemistry software package released by John Pople [150], in which only HF and MCSCF methods (or we can say only single-reference methods) are included for electronic structure calculation. One can find that they release the same results in the HF calculation and MCSCF method, but Molpro works with higher efficiency on the electronic state calculation, especially for the excited states, due to the adopted high-level (multi-reference) MRCI method where static and dynamical electron correlations (see section 2.1.4) are extensively taken into account. Accurate treatments of excited states therefore became possible. There are also differences in some details. For instance, Gaussian uses Cartesian coordinate based function (see "Running Gaussian" of Quick Start tutorial

for Gaussian), while Molpro uses spherical harmonics (see section 11.2 of the manual for Molpro). And, the core orbitals are defaulted closed for MCSCF method in Gaussian, however in Molpro, these orbitals could be manually set to be open, closed or frozen.

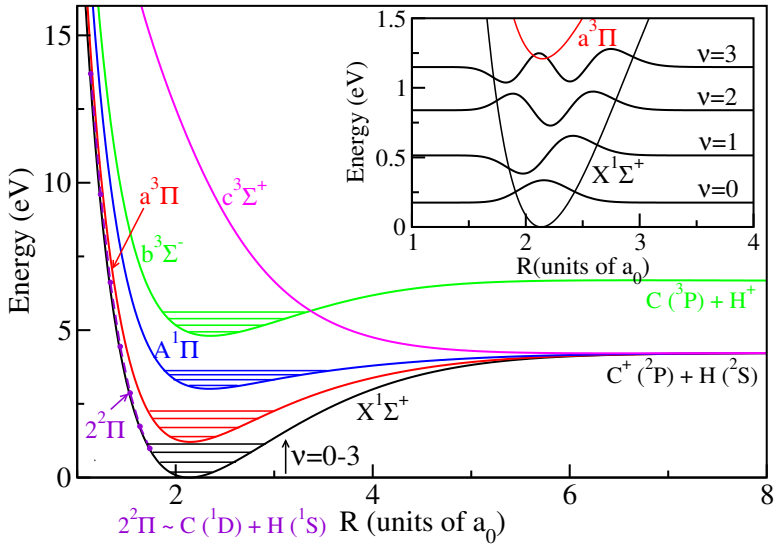

Figure 3.2: Potential energy curves for the $X^1\Sigma^+$ (the black curve), $a^3\Pi$ (the red curve), $A^1\Pi$ (the blue curve), $b^3\Sigma^-$ (the green curve) and $c^3\Sigma^+$ (the purple curve) electronic states of CH^+. Four lowest vibrational levels for the four lowest electronic states are shown by horizontal thin lines in potential wells of the states. The inset displays the four vibrational states $v = 0$, 1, 2, 3 of the $X^1\Sigma^+$ state. The $2^2\Pi$ resonance state for e^--CH^+ collision system is plotted as dotted line using resonance positions with respect to internuclear distance R. The resonance positions are obtained from fixed-nuclei R-matrix calculations at R from 1.137 bohrs to 1.737 bohrs with an interval of 0.1 bohrs. The dissociation limits are also given in the figure.

The potential energy curves $V(R)$ of CH^+ shown in Fig. 3.2 were calculated using the C_{2v} symmetry point group with a multi-reference configuration interaction (MRCI) method and the `cc-pV5Z` basis set (see table 2.4). To be exact, the calculation is carried out in three steps. First we use a HF method (see the Eq. (2.18) in section 2.1.4) to obtained a set of optimized MOs, i.e. the coefficients c_{ui} in Eq. (2.10) of MOs are optimized by variational method iteratively to convergence. These ground configuration constructed by these MOs will be used in the CASSCF method (see Eq. (2.20) in

section 2.1.4). We kept the 1σ orbital of carbon doubly occupied and we allow the 4 remaining electrons to be freely distributed in 14 orbitals, i.e. 2σ-7σ, 1π-3π and 1δ in the complete active space (CAS). The coefficients c_{ui} of the MOs and the expansion coefficients b_k of Eq. (2.20) will be optimized and used in the MRCI method (see Eq. (2.19)). The configurations included in MRCI method are constructed by the multireference obtained in the CASSCF method using the same CAS. The calculated potential energy curves of the $X^1\Sigma^+$, $a^3\Pi$, $A^1\Pi$, $b^3\Sigma^-$ and $c^3\Sigma^+$ electronic states are shown in Fig. 3.2. The $X^1\Sigma^+$, $a^3\Pi$, $A^1\Pi$, and $c^3\Sigma^+$ curves correlate with the $C^+(^2P)$ + $H(^2S)$ dissociation limit at large internuclear distances.

3.2.2 Vibrational states obtained by DVR method

As we discussed in section 2.2.1, in order to describe the vibronic excitation process of Eq. (2.61), we determined the vibrational energies E_v and the corresponding vibrational wavefunctions $\phi_v(R)$ within these electronic states of CH^+, we solved the Schrödinger equation of Eq. (2.22) for vibrational motion along R using the DVR method [43]. The lowest 4 vibrational energy levels $v = 0, 1, 2, 3$ in the $X^1\Sigma^+$ state are listed in Table 3.1.

Table 3.1: Comparison of the 4 lowest vibrational energy levels (in eV) of the $X^1\Sigma^+$ state obtained in this study with the calculations by Biglari *et al.*

Ref.	$v = 0$	$v = 1$	$v = 2$	$v = 3$
Biglari *et al.* [148]	0.175218	0.514360	0.838974	1.149288
This work	0.175189	0.514102	0.838515	1.148720
Relative error	0.017%	0.050%	0.055%	0.054%

As one can see, the present computed energies agree well with the theoretical calculations by Biglari *et al.* [148]. The corresponding 4 vibrational waves of the ground $X^1\Sigma^+$ electronic state are displayed in Figure 3.3 and one also in the inset of the Fig. 3.2.

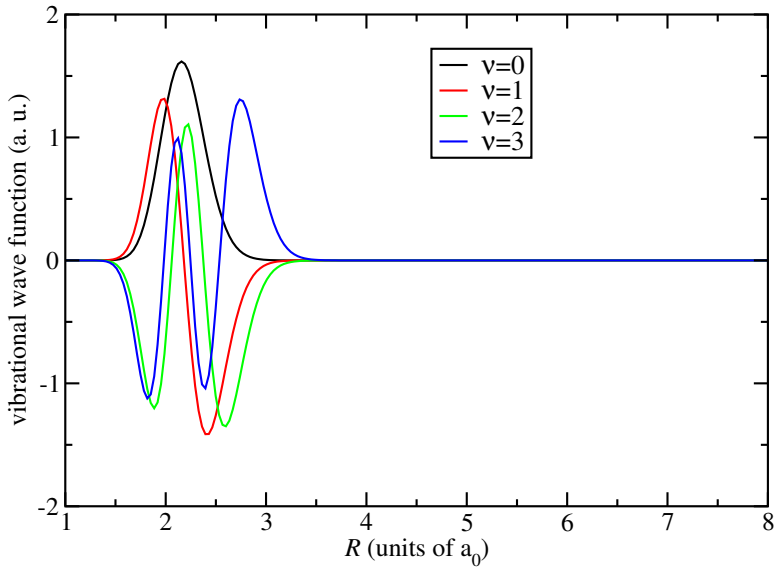

Figure 3.3: The four vibrational states $v = 0$, 1, 2, 3 of the ground $X^1\Sigma^+$ electronic state.

3.2.3 Scattering calculations for e^--CH^+ collision.

In order to describe transition between a vibronic level to another one of the target, we carried out the e^--CH^+ scattering calculations using R-matrix method [57] (see section 2.3.1) through the Quantemol-N interface [151] which provides an expert interface for driving the highly sophisticated UK molecular R-matrix code [152]. The CAS configuration interaction (CI) method in the C_{2v} abelian subgroup were used in the calculations. The inner orbital $1a_1^2$ of CH^+ was frozen, and 4 external electrons were distributed in the space of the $[2a_1, 3a_1, 4a_1, 5a_1, 6a_1, 7a_1, 8a_1, 1b_1, 2b_1, 3b_1, 1b_2, 2b_2, 3b_2, 1a_2]$ orbitals $(2\sigma, 3\sigma, 4\sigma, 5\sigma, 6\sigma, 7\sigma, 1\pi, 2\pi, 3\pi, 1\delta$ in $C_{\infty v}$ symmetry group). We chose a R-matrix sphere of radius $r_0 = 13$ bohrs (see Fig. 2.4) and continuum Gaussian-type orbitals with partial waves $l \leq 4$. As we mentioned in section 2.3.1, this means we will have 25 partial waves, i.e. 25 possible $l\lambda$ values. The two different R-matrix calculations described in the following section 3.3; closed-coupling expansions with 3 and 14 lowest electronic states of CH^+ were used for constructing the total wavefunctions for the e^--CH^+ system (see Eq. (2.41)). In the

vibrational frame transformation of Eq. (2.60), the electron scattering calculations were performed in the interval between 1.537 and 3.937 bohrs with a step of 0.1 bohrs along the internuclear coordinate R. Note that the center-of-mass frame are adopted in the R-matrix calculation. Namely, the origin of the input coordinate of the target molecular ion should locate at the center of mass of the target. To make sure that the origin is put at the center of mass, we just need to click the button "move to the center of mass" in the input interface of Quantemol. While for Molpro, it doesn't matter since the origin will be automatically moved to the center of mass. The obtained potential energies are the same and only behaviour as a function of internuclear distance R.

3.3 Theoretical approach

3.3.1 QDT description of electronic resonances

In the theoretical method employed in the present study, one needs scattering matrices obtained numerically for fixed geometries of the target ion. The scattering matrices are obtained using the UK R-matrix code [57] as described in the above section, where we outlined the details of the numerical calculations using the R-matrix code for e^--CH^+ collisions.

A theoretical description of low-energy e^--CH^+ collisions is complicated due to the presence of a low energy electronic $2^2\Pi$ resonance (detailed discussion about this state could be seen in chapter 4) and several low-energy excited electronic states of CH^+ [24, 29, 30] (see Fig. 3.2). The excited ionic states produce series of Rydberg resonances (see section 2.5.1) that influence all collisional processes. In this situation, the standard vibrational-frame-transformation approach by Chang and Fano [85], used in many theoretical studies on electron-molecule collisions [91, 146], is not well adapted: The approach requires that the scattering matrix or, alternatively, the matrix of quantum defects, obtained for fixed inter-nuclear positions (in the Born-Oppenheimer approximation), to

be a smooth function of the collision energy – ideally, to be energy independent. However, the presence of the $2^2\Pi$ resonance and the low-energy excited electronic states makes the fixed-nuclei scattering matrix to be strongly energy dependent. This is demonstrated in Figure 3.4 showing the eigenphase sums of the three symmetries $^2\Sigma^+$, $^2\Pi$ and $^2\Sigma^-$ of the e^--CH^+ system computed at the equilibrium R_e = 2.137 bohrs. Several series of Rydberg resonances (see section 2.5.1) converge to the electronic states $a^3\Pi$ and $A^1\Pi$ as marked by the blue vertical lines in Fig. 3.4.

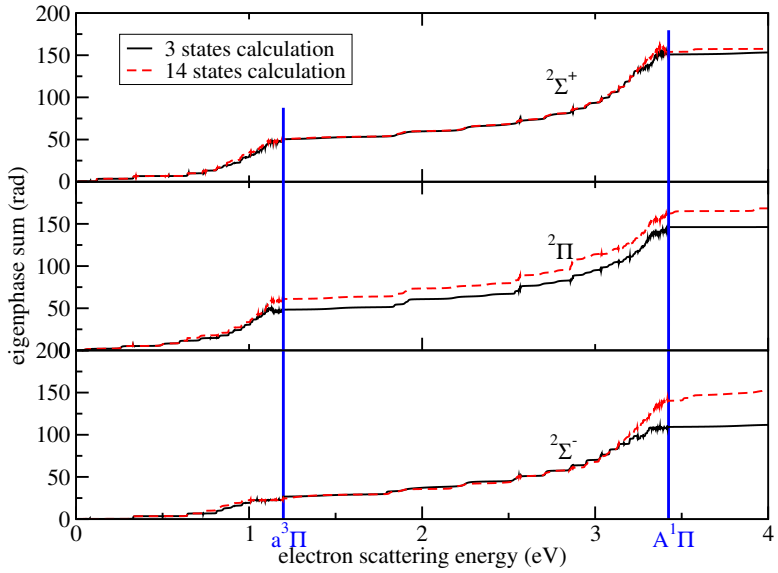

Figure 3.4: The eigenphase sum for three symmetries $^2\Sigma^+$, $^2\Pi$ and $^2\Sigma^-$ of the e^--CH^+ obtained for the equilibrium internuclear distance R_e = 2.137 bohrs in two different calculations: Black solid curves show the results obtained taking into account only three lowest electronic states of CH^+ while red dashed curves are obtained with 14 states.

To describe low-energy electronic resonances, in different e^--CH^+ scattering processes, we use the MQDT approach and need an energy-independent scattering matrix. This matrix includes not only the ground electronic state of CH^+ but also a few more states because of the low-lying excited electronic states within the energy range of interest (up to 4 eV discussed in the introduction section). These states can produce resonances at scattering energies of the interest. In the e^--CH^+ case

low-energy resonances are well reproduced if one takes into account only three electronic states of the ion. Figure 3.4 shows the eigenphase sums of three symmetries $^2\Sigma^+$, $^2\Pi$ and $^2\Sigma^-$ of the e^--CH^+ obtained at equilibrium in 3 states (black solid curve) and 14 states (red dashed curve) calculations (described in section 3.2.3). In one calculation (black solid curves), only the three lowest $X^1\Sigma^+$, $a^3\Pi$ and $A^1\Pi$ states are included. In the other calculation (red dashed lines) 14 lowest states were included. Numerous of low-energy resonances are on the curves in the two calculations. Below the threshold of the $A^1\Pi$ state marked by bold blue curve, generally good agreement between the two calculations could be observed. Above that threshold, the eigenphase sum in 14 states calculations shows slight fluctuation, whereas a plateau for that in 3 states calculations.

To clearly compare the resonance structures, we make the derivatives of the eigenphase sums of those two calculations shown in Fig. 3.4 and exhibit the derivatives in Fig. 3.5 (see section 2.3 with discussion of definition of eigenphase sum and the way of deriving the resonances used in this thesis). As one can see, at low energies, below the $A^1\Pi$ ionization limit, the two calculations agree quite well with each other. In the second calculation with a larger number of ionic states, there are a few narrow resonances at low scattering energies that are not reproduced in the first, smaller calculation. These resonances are attached to very excited electronic states of the ion and do not influence significantly the low-energy spectrum.

Therefore, the electronic scattering matrix at low energies could be well represented by the three states $X^1\Sigma^+$, $a^3\Pi$ and $A^1\Pi$ of the ion. With this set of electronic states, the above-mentioned $2^2\Pi$ resonance is included in the scattering model. Note that the negative derivatives of the eigenphase are eliminated. Fig. 3.6 shows the eigenphase of $^2\Pi$ symmetry at the equilibrium in the upper panel and derivative of the eigenphase of $^2\Pi$ symmetry in the lower one. One can see the negative derivative values using the straightforward derivative $\frac{d\sigma}{dE}$ (the black curve). In our treatment, we added π to ensure the continuity of the derivative of $\delta(E_{\text{el}})$.

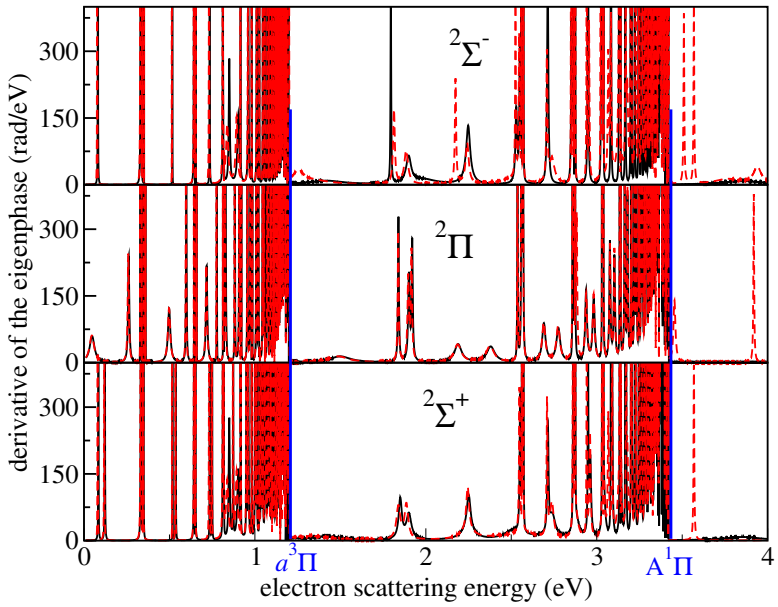

Figure 3.5: Derivatives of the eigenphase sum shown in Fig. 3.4. Black solid curves show the results obtained taking into account only three lowest electronic states of CH^+. Red dashed curves are obtained with 14 states.

In order to account for vibrational and rotational excitation (for further work) of the target, the standard MQDT approach is to use vibrational and rotational frame transformations [85, 139]. The approach is applicable only if the electronic scattering matrix, obtained for a number of different geometries of the ion, is energy independent. As Fig. 3.5 demonstrates, the e^-–CH^+ scattering matrix depends strongly on energy below the $A^1\Pi$ ionization limit and its dimension changes from 1×1 to 3×3 (above the $A^1\pi$ state). Namely, the scattering matrix cannot be immediately used in the frame transformation. A possible solution is to take the (almost) energy-independent scattering matrix, obtained at an energy above the $A^1\Pi$ ionization limit, and use it at energies below the limit. Therefore, the vibrational (and rotational) frame transformation is performed on a 3×3 electronic scattering matrix (the $X^1\Sigma^+$, $a^3\Pi$, and $A^1\Pi$ three electronic states), which produces a $N \times N$ matrix with N vibronic (rovibronic) channels. Technically, N should be 25 partial waves (as stated in section 2.3.1) multiplying 3 electronic states. Such a rovibronic scattering matrix is

essentially energy-independent and a QDT closed-channel elimination procedure [93, 94] should be performed to obtain the physical energy-dependent matrix, used to compute cross sections for various processes.

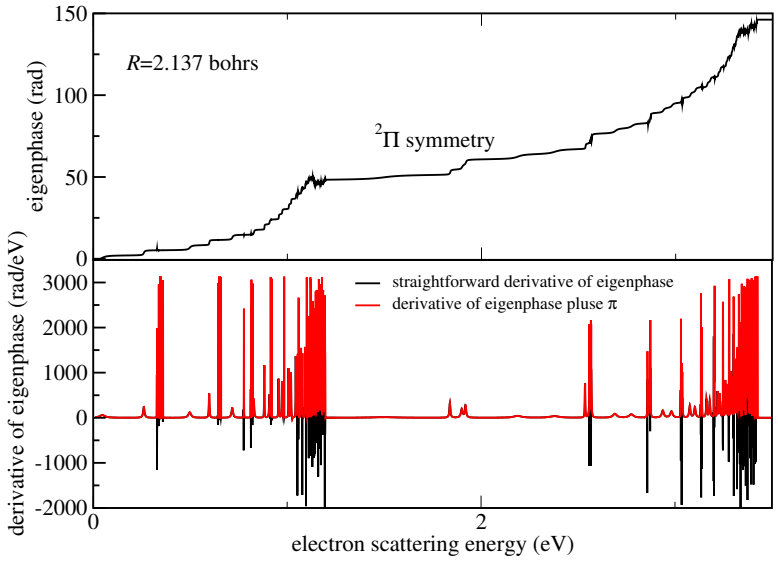

Figure 3.6: The upper panel shows the eigenphase sum for $^2\Pi$ symmetry of three states calculation at R_e = 2.137 bohrs. The bottom panel shows its derivative: Black solid curves show the results obtained using the finite difference approximation for a derivative $(\frac{d\sigma}{dE})$. Red dashed curves are obtained by adding π to the eigenphase where the derivative is negative.

3.3.2 Electronic excitation of CH^+

Before discussing the vibronic frame transformation applied to the e^--CH^+ collisions, we compare the fixed-nuclei electronic scattering matrices obtained (1) using the elimination procedure of the closed electronic states and by (2) a direct scattering R-matrix calculation at the same internuclear distance.

The elimination of closed electronic channels at a geometry R is given by Eq. (2.72) [93, 94]. In that equation, E_{el} is the scattering energy and S^{oo}, S^{oc}, S^{cc}, and S^{co} are submatrices of the

weakly-dependent electronic scattering matrix $S(E_{\rm el}, R_{\rm e})$ (3×3 in the present case of the e^-–CH^+ system). $E_{\rm el}$ is used here to represent the electron scattering energy. As shown in Eq. (2.62), the total energy of the collisional system E is the sum of the $E_{\rm el}$ and initial ground-state E_{00} (which are set as the zero point energy). In the case of electronic excitation, we assume energy $E_{i=0}(R_{\rm e})$ of the ground electronic state at $R_{\rm e}$ as the zero point energy. Thus we have $E = E_{\rm el}$ and we will still use $E_{\rm el}$ in the following parts of the thesis. The matrix elements are partitioned according to Eq. (2.71) in the "o"- and "c"- parts on the basis whether the corresponding channel are open or closed for excitation for the particular scattering energy $E_{\rm el}$. The quantity of $\beta\,(E_{\rm el})$ in Eq. (2.72) is a diagonal $N_c \times N_c$ matrix and expressed by Eq. (2.73). But the E_{vi} is substituted by $E_i(R_{\rm e})$ which denotes the energy values of the ith electronic states at internuclear distance $R_{\rm e}$.

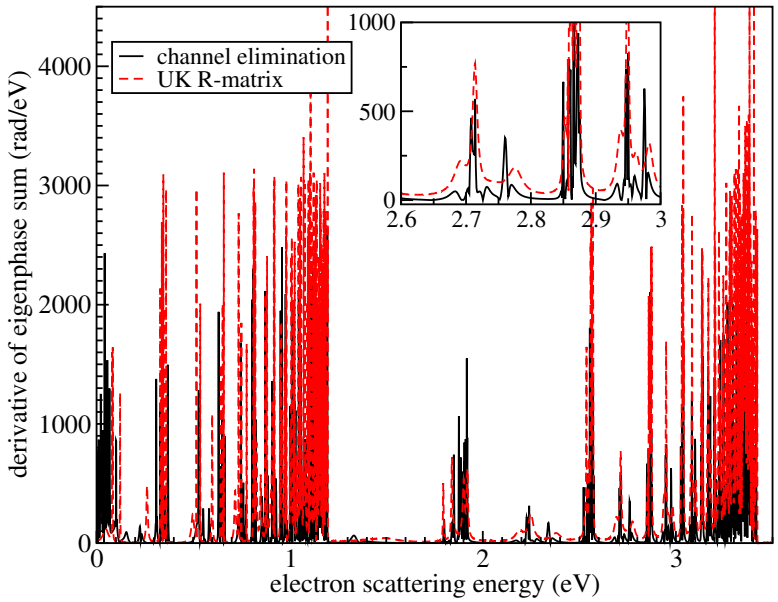

Figure 3.7: Comparison of eigenphase-sum derivatives below the $A^1\Pi$ state obtained at a fixed CH^+ geometry in (1) the direct R-matrix calculations (red dashed curve) and using (2) the energy-independent 3×3 scattering matrix and the procedure of elimination of closed electronic channels (black solid curve). The inset shows an enlarged view for the 2.6–3.0 eV interval of energies.

Figure 3.7 shows derivatives of eigenphase sums obtained from the scattering matrices computed

at the equilibrium distance R_e. The red dashed curve is the result from the R-matrix calculation while the black solid curve is channel elimination method using using the energy-independent 3×3 electronic scattering matrix. Overall, positions of the resonances in the two calculations are the same but widths in the R-matrix calculation are wider as seen in the inset of Fig. 3.7. This means that diagonal elements of the scattering matrices in the two calculations are very similar but the non-diagonal elements, responsible for channel couplings and widths of the resonances, are slightly different, suggesting that highly-excited electronic states, neglected in the 3×3 channel elimination procedure, have non-negligible contributions to the coupling between the lowest channels. Note that π was added to ensure the continuity of the derivative of the eigenphase.

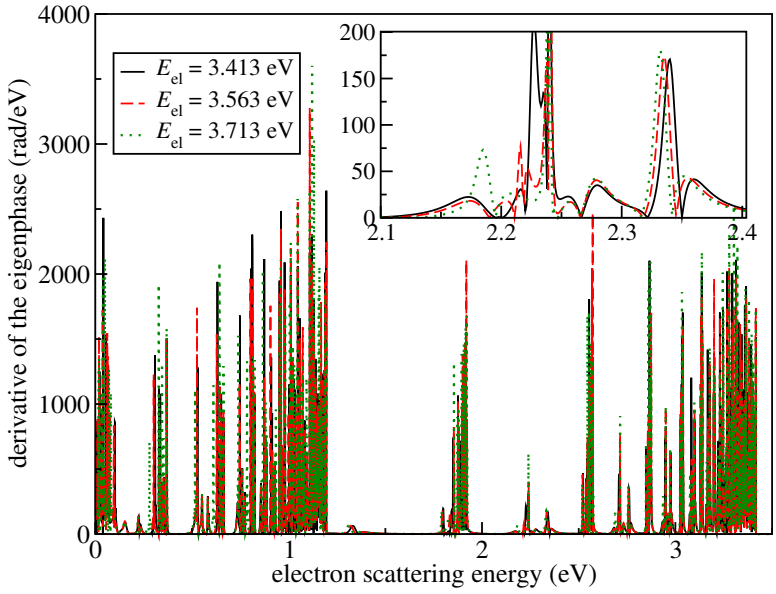

Figure 3.8: Comparison of eigenphase-sum derivatives computed for a fixed CH^+ geometry using three different energy-independent 3×3 scattering matrices and the procedure of elimination of closed electronic channels. The three matrices are taken at energies 3.413 eV (black solid curve), 3.563 eV (red dashed curve) and 3.713 eV (green dotted curve). The inset shows an enlarged view for 2.1–2.4 eV energies.

The choice of the 3×3 scattering matrix used in the channel-elimination procedure is not unique, because the matrix depends on energy, even above the $A^1\Pi$ electronic state. To assess the result

of uncertainty in the choice of the energy at which the 3×3 scattering matrix is taken, we plot in Fig. 3.8 eigenphase-sum derivatives obtained for 3×3 scattering matrices taken at three different energies above the $A^1\Pi$ state: at 3.413, 3.563, and 3.713 eV. Positions and the widths of the resonances are nearly the same in the three calculations.

An important conclusion from the results discussed above is that the $e^- - CH^+$ scattering physics below the $A^1\Pi$ state can be represented using an energy independent multichannel scattering matrix evaluated at a higher energy, above the $A^1\Pi$ ionization limit in a combination with the closed-channel elimination.

A rough idea about the magnitude of cross sections for electron-impact electronic excitation of a molecule is obtained from a fixed-geometry calculation. Here, for a comparison between the MQDT and direct R-matrix approaches, we present such excitation cross sections. The vibrational dynamics during the process is discussed in the next section.

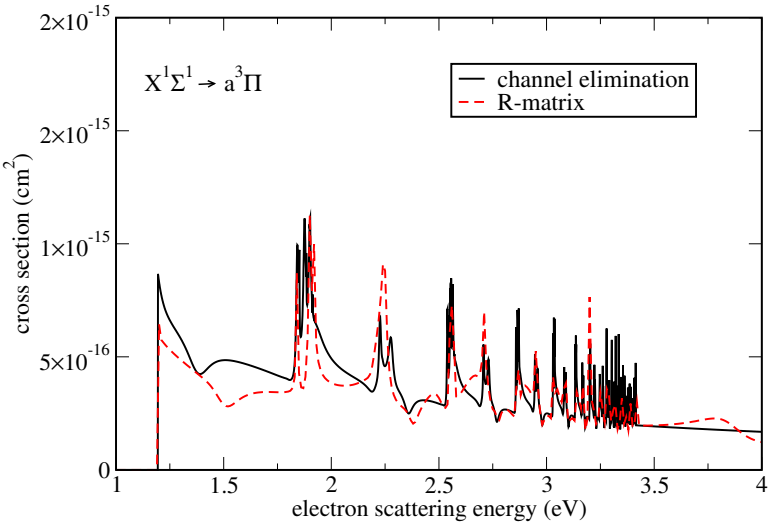

Figure 3.9: Cross sections for the $X^1\Sigma^+ \rightarrow a^3\Pi$ electronic excitation of CH^+ at a fixed geometry R_e obtained in the direct R-matrix calculations (red dashed curve) and using the QDT channel elimination procedure (black solid curve).

Using the physical scattering matrix $S^{phys}(E_{\rm el}, R_{\rm e})$ of Eq. (2.72) describing electronic transitions at the equilibrium geometry $R_{\rm e}$ of CH^+, cross sections $\sigma_{i',i}$ of the electronic excitation from the $X^1\Sigma^+$ state to the $a^3\Pi$ state can be evaluated in the QDT approach as Eq. (2.74) [118]. In that expression, element of the scattering matrix $S^{phys}_{l'\lambda'\nu'i',l\lambda\nu i}(E_{\rm el})$ is replaced by $S^{phys}_{l'\lambda'i',l\lambda i}(E_{\rm el}, R_{\rm e})$ where i and i' refer to the initial ($X^1\Sigma^+$ in this case) and final ($a^3\Pi$ here) electronic states. The indexes $l\lambda$ and $l'\lambda'$ numerate initial and final angular momenta and their projections in the molecular reference frame (where *ab initio* calculations are performed). The cross section in the R-matrix approach is obtained by the same formula, except that the scattering matrix in the above equation is replaced with the one obtained directly in the R-matrix calculations at the corresponding energy $E_{\rm el}$.

Figure 3.9 compares the cross sections for the $X^1\Sigma^+ \rightarrow a^3\Pi$ transition obtained in the two approaches. The general agreement between the two curves is good, even for the widths of the resonances. One noticeable difference is in the position of the minimum near 1.5 eV: In the QDT calculations it is shifted slightly to the left. The agreement is better at energies approaching the $A^1\Pi$ ionization limit.

Another difference is seen at scattering energy of ~ 2.25 eV that our computed cross section shows double resonances. The selected $S(E_{\rm el}, R_{\rm e})$ describing the collisional system is in four symmetries, including $^2\Sigma^+$ ($^2A_1$), $^2\Pi$ ($^2B_1/^2B_2$) and $^2\Sigma^-$ ($^2A_2$) of the e^--CH^+ system. Its symmetry is identified by the symmetry of target state denoted by i and the partial wave represented by $l\lambda$ of the scattering electron. For example, when the symmetry of target state is B_1 and scattering electron is a_1, then the scattering matrix will be in in B_1 symmetry. This is also found in Table 2.3. To locate the origin of the double resonances, we computed the electronic excitation cross section using the selected scattering matrix elements $S_{l'\lambda'i',l\lambda i}(E_{\rm el}, R_{\rm e})$ for separate symmetries of the collisional system. The computed results are shown in Fig. 3.10. The double-resonance part in the dashed cyan box was enlarged in the inset. As we can clearly see the double resonances are from $^2\Sigma^+$ ($^2A_1$) symmetry.

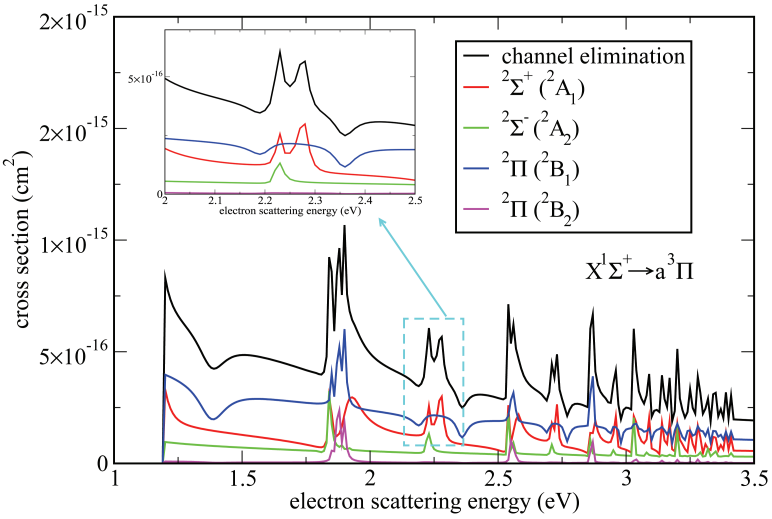

Figure 3.10: Cross sections for the $X^1\Sigma^+ \rightarrow a^3\Pi$ electronic excitation of CH^+ at a fixed geometry R_e obtained by QDT channel elimination procedure (black solid curve) using the selected S-matrix in four different symmetries of the collisional system. Inset shows the enlarged view of the double resonances within 2-2.5 eV interval.

Table 3.2: Symmetries of the the involved lowest $X^1\Sigma^+$, $a^3\Pi$ and $A^1\Pi$ three electronic states of CH^+ and the scattering electron in C_{2v} point group. One may have a better understanding combining Table 2.3

Symmetry of the target $\Gamma^{target}_{C_{2v}}$		Symmetry of the scattering electron $\Gamma^{el}_{C_{2v}}$			
$X^1\Sigma^+$	A_1	a_1	a_2	b_1	b_2
$a^3\Pi$	B_1	b_1	b_2	a_1	a_2
	B_2	b_2	b_1	a_2	a_1
$A^1\Pi$	B_2	b_2	b_1	a_2	a_1
	B_1	b_1	b_2	a_1	a_2
Total symmetry: $\Gamma^{total}_{C_{2v}} = \Gamma^{target}_{C_{2v}} \otimes \Gamma^{el}_{C_{2v}}$		$^2A_1$	$^2A_2$	$^2B_1$	$^2B_2$

As we described above, the $S(E_{el}, R_e)$ is selected above the $A^1\Pi$ state at the equilibrium. Thus, the lowest $X^1\Sigma^+$ $(i = 0)$, $a^3\Pi$ $(i = 1)$ and $A^1\Pi$ $(i = 2)$ three electronic states of the target are referred as the electronic channels and included in the selected S-matrix. Here we give symmetries of the involved target states and the scattering electron in C_{2v} point group as shown in Table 3.2. The symmetries of the $X^1\Sigma^+$, $a^3\Pi$ and $A^1\Pi$ target states corresponds respectively to A_1, B_1/B_2

and B_1/B_2. Coupling with the symmetries of the scattering electron, the total symmetries of the collisional system are shown in the bottom line of the table: $^2A_1$, $^2A_2$, $^2B_1$ and $^2B_2$. As we see from Fig. 3.10, the double resonances are from the cross section computed by the S-matrix elements of $^2A_1$ total symmetry. And one can see that the position of the double resonances is above the threshold of the first excited $a^3\Pi$ electronic state but below the threshold of the second excited $A^1\Pi$ electronic state of CH^+. This suggests that the double resonances are recovered by the closed $A^1\Pi$ electronic channel. We thus guess that there are differences in the S-matrix elements describing the electron-induced coupling of the $X^1\Sigma^+$ ground state and the degenerate states of the $A^1\Pi$.

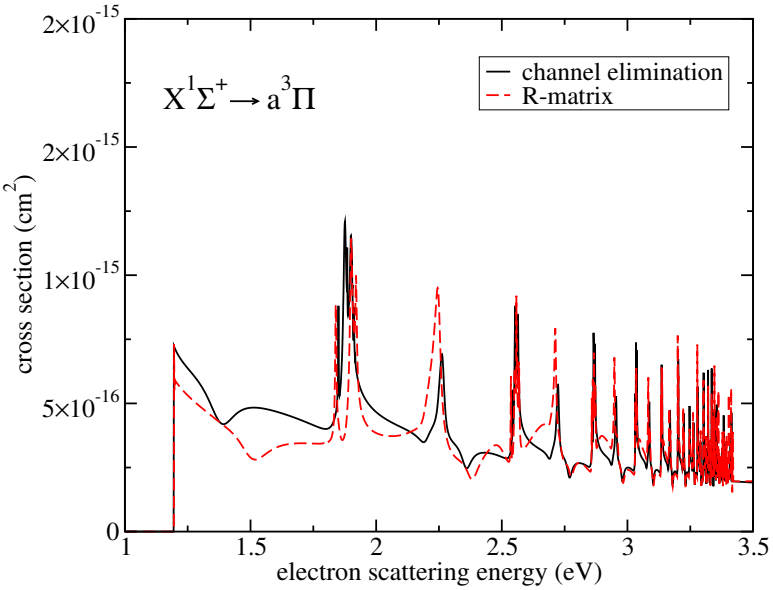

Figure 3.11: Cross sections for the $X^1\Sigma^+ \rightarrow a^3\Pi$ electronic excitation of CH^+ at a fixed geometry R_e obtained in the direct R-matrix calculations (red dashed curve) and the QDT channel elimination procedure (black solid curve). The selected S-matrix elements describing the electron collision with degenerate states of the $A^1\Pi$ are averaged over real and imaginary parts, respectively.

To fix the problem, we made an average over the selected S-matrix elements describing the electron

collision with degenerate states of the $A^1\Pi$ using

$$\overline{S}_{b_1B_1,a_1A_1} = \overline{S}_{b_2B_2,a_1A_1} = (S_{b_1B_1,a_1A_1} + S_{b_2B_2,a_1A_1})/2 \tag{3.1}$$

where the subscript is the symmetry of the electron $\Gamma^{electron}_{C_{2v}}$ and the target $\Gamma^{target}_{C_{2v}}$ (see Table 2.3). One has to note that the average is performed over the real and imaginary parts, respectively. Then we tried to compute the cross section using the averaged S-matrix. Figure 3.11 compares the cross sections for the $X^1\Sigma^+ \rightarrow a^3\Pi$ transition obtained in the two approaches. As one can see that the double resonances are eliminated successfully. However, we didn't use this average operation in the calculation of the cross section for vibronic excitation because the resulted rate constants are slightly affected. On the other hand, the average of the scattering matrix is not a robust solution which may influence the unitarity of the transformed scattering matrix.

Differences observed in the cross sections obtained by the two methods (R-matrix and QDT elimination procedure) are smeared out in the thermally-averaged rate coefficient $\alpha_{i',i}(T,R_e)$ using Eq. (2.75) computed from the cross sections $\sigma_{i',i}(E_{el},R_e)$. The obtained rate coefficients, shown in Fig. 3.12, are matching with each other. This confirms that major couplings between electronic channels are accurately represented in the QDT approach and validates the approach.

3.4 Cross sections and rate coefficients for vibronic excitation

Once the method validated with the R-matrix calculations, we performed scattering calculations for different geometries of the CH^+ target. The energy-dependent physical scattering matrix for vibronic transitions is obtained in two steps. First, one computes the energy-independent vibronic scattering matrix assuming that all vibronic channels are open. On the second step, an elimination of closed vibronic channels is applied to produce the required energy-dependent vibronic scattering

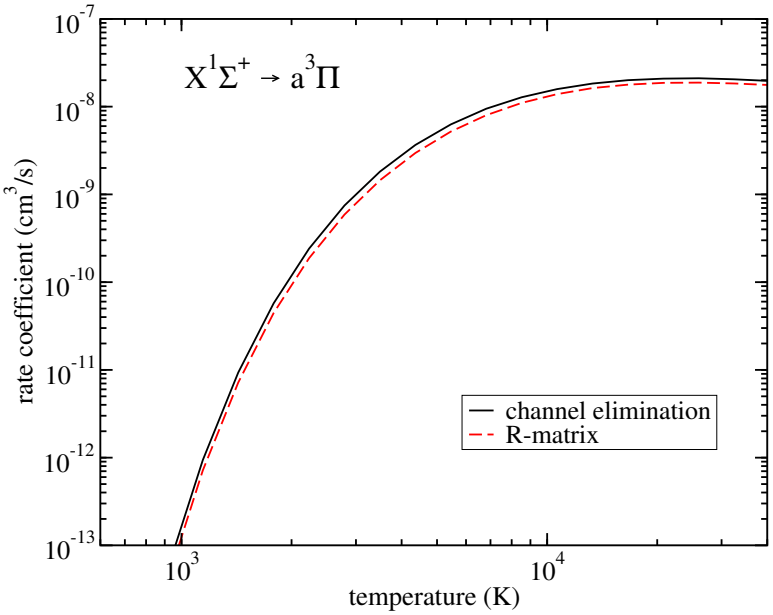

Figure 3.12: The rate coefficients for the $X^1\Sigma^+ \rightarrow a^3\Pi$ electronic excitation of CH^+ at R_e obtained in the direct R-matrix calculations (red dashed curve) and the QDT channel elimination procedure (black solid curve).

matrix.

The first step is performed by the vibronic frame transformation using Eq. (2.74). An integration runs over the vibrational coordinate R. On the second step, the energy-dependent physical scattering matrix $S^{phys}(E_{el})$ is obtained by the QDT vibronic closed-channel elimination procedure, described by Eqs. (2.72) and (2.73). The cross sections $\sigma_{v'i',vi}(E_{el})$ for vibronic (de-) excitation of CH^+ are computed using Eq. (2.74).

Figure 3.13 illustrates cross sections obtained for different combinations of initial and final vibronic states. Panel (a) shows results for pure vibrational excitations between levels of the ground electronic state $X^1\Sigma^+$. As expected, the cross section for the transition with $\Delta v = 1$ is the largest one between inelastic processes. Panel (b) gives cross sections from the ground vibronic state $X^1\Sigma^+, v = 0$ to several vibrational levels of the $a^3\Pi$ state. Since the potential curves of the $X^1\Sigma^+$ and $a^3\Pi$ states

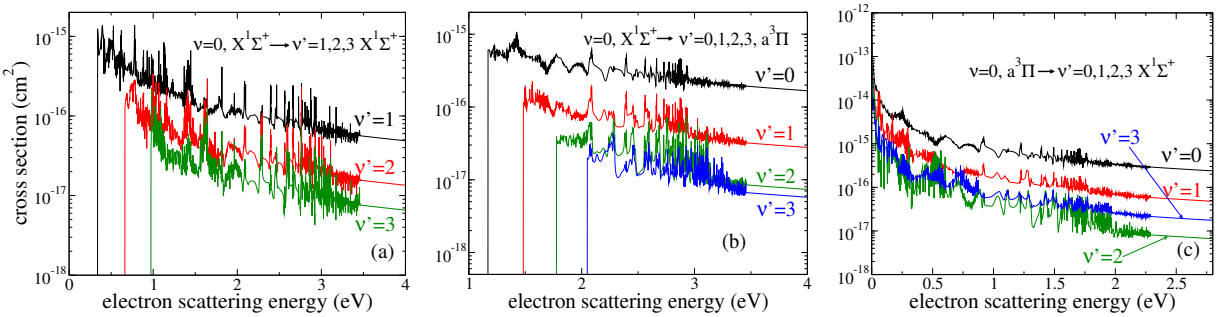

Figure 3.13: Cross sections for vibronic excitations of CH^+ from the ground vibrational level $v = 0$ of the $X^1\Sigma^+$ state to $v = 1,2,3$ of the $X^1\Sigma^+$ state (left panel) , to $v = 0,1,2,3$ of the $a^3\Pi$ state (middle panel), and for vibronic de-excitations from the ground vibrational level $v = 0$ of $a^3\Pi$ to $v = 0,1,2,3$ of the $X^1\Sigma^+$ state (right panel).

have similar shapes near the equilibrium, the largest $X^1\Sigma^+ \rightarrow a^3\Pi$ cross section is expected to be for $\Delta v = 0$, as the present calculation indeed demonstrated. Panel (c) gives cross sections for the de-excitation process $a^3\Pi, v = 0 \rightarrow X^1\Sigma^+, v' = 0-3$.

As pointed out in section 3.2.3 that one has to pay attention that center-of-mass frame should be used in the R-matrix calculations. Since the computed results using center-of-Carbon frame may show big differences, as seen in Fig. 3.14. The cross section for the vibronic excitation from $v = 0$ of the $X^1\Sigma^+$ state to $v = 2$ and $v = 3$ of the $a^3\Pi$ state exhibit more than 20% discrepancies.

Cross sections for vibronic excitations were recently estimated by Chakrabarti *et al.* [111] using an approximated theoretical approach, in which cross sections for electronic excitations computed at the CH^+ equilibrium geometry were multiplied with Franck-Condon overlaps for various combinations of initial and final vibrational levels to obtain the cross sections for vibronic transitions. In that study, electronic differences in vibrational excitation energies were neglected as well as the vibronic Feshbach resonances. The cross sections obtained in Ref. [111] differ significantly – more than an order of magnitude for several transitions – from the present results as shown in Fig. 3.15.

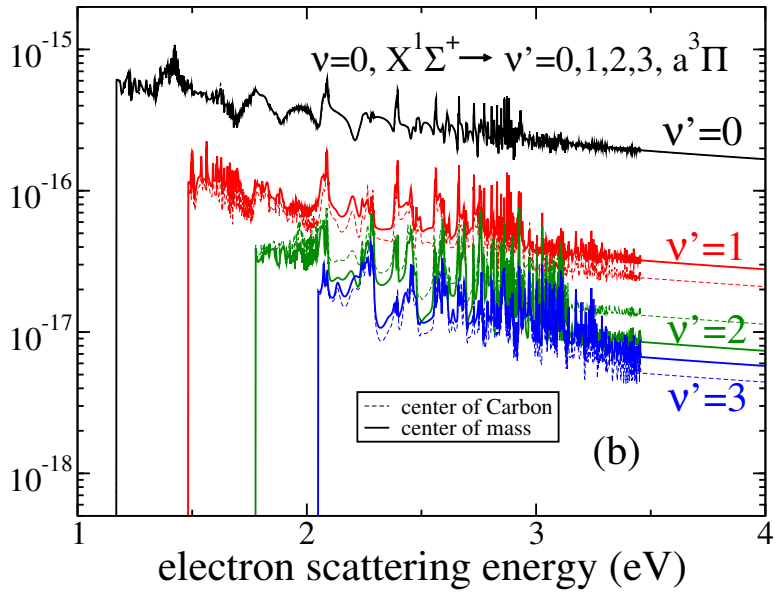

Figure 3.14: Comparision of the computed cross sections by center-of-mass frame (in bold curves) and center-of-Carbon frame (in dashed thin curves). For clarity, Fig. 3.14 only shows the cross sections of the middle panel of Fig. 3.13.

We give the comparison between cross sections of $v = 0$ of the $X^1\Sigma^+$ state to $v = 1, 2, 3$ of the $a^3\Pi$ state obtained by Chakrabarti *et al.* and the computed results using our approach in this thesis. Big difference is clearly observed. The cross sections for the three excitations initiate from an identical electron scattering energy about 1.14 eV. This seems hard to understand physically since thresholds of different vibrational excitations shift (increase or decrease). Furthermore, the shapes of the three cross section curves remain unchanged. This is due to a straightforward multiplying the cross sections for electronic excitation of the $X^1\Sigma^+$ state to the $a^3\Pi$ state with Franck-Condon factors between the considered vibrational states. We attribute the disagreement to the mentioned approximations employed in [111]: (1) neglected differences in vibrational excitation threshold energies, (2) neglected dependence of e^-–CH^+ scattering parameters with the internuclear distance, and (3) the neglected resonances in closed vibronic channels.

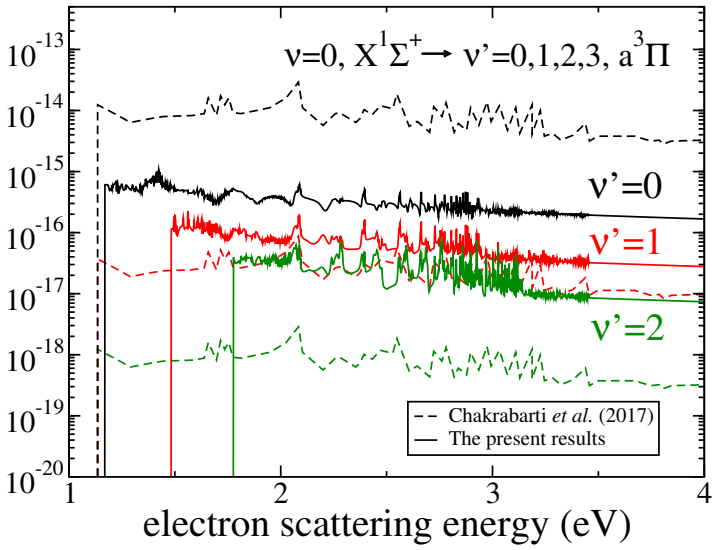

Figure 3.15: Comparision of the cross sections of $v = 0$ of the $X^1\Sigma^+$ state to $v = 1, 2, 3$ of the $a^3\Pi$ state obtained by Chakrabarti *et al.* and the present results.

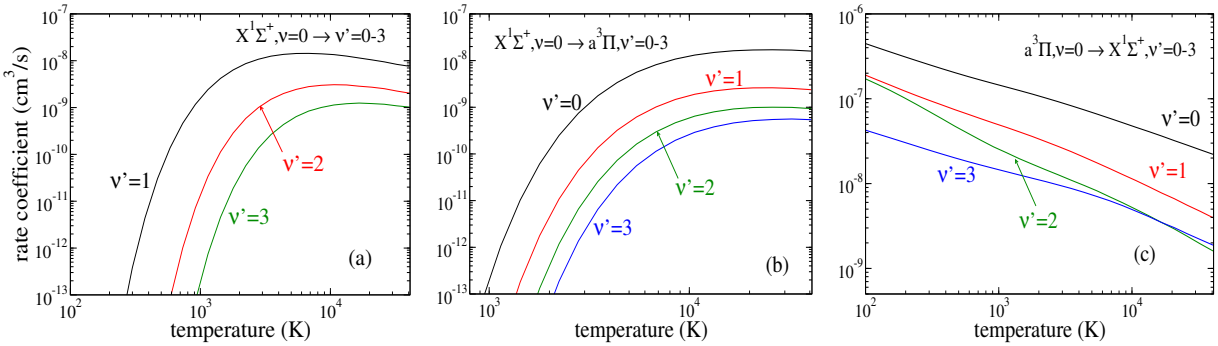

Figure 3.16: Rate coefficients for same vibronic transitions as shown in Fig. 3.13.

Thermally-averaged rate coefficients $\alpha_{v'i',vi}(T)$ of these vibronic (de-) excitations from 10 K to 40000 K are then computed using Eq. (2.75). Figure 3.16 shows computed rate coefficients for the same transitions as the cross sections in Fig. 3.13.

As previous studies [38, 89, 100, 153] and for convenience of use, the computed thermally-averaged

rate coefficients $\alpha_{v'i'\leftarrow vi}$ were fitted using the following analytical formula,

$$\alpha^{fit}_{v'i'\leftarrow vi}(T) = \frac{1}{\sqrt{T}} e^{-\frac{\Delta_{v'i',vi}}{T}} P^{fit}_{v'i',vi}(x) \tag{3.2}$$

where $P^{fit}_{v'i',vi}(x)$ is a quadratic polynomial

$$P^{fit}_{v'i',vi}(x) = a_0 + a_1 x + a_2 x^2 \qquad \text{and} \qquad x = \ln(T) \tag{3.3}$$

with $P^{fit}_{v'i',vi}(x) \approx P^{fit}_{vi,v'i'}(x)$. This quantity could be viewed as the (de-)excitation probability. $\Delta_{v'i',vi}$ in Eq. (3.2) is the threshold energy defined as

$$\Delta_{v'i',vi} = \begin{cases} E_{v'i'} - E_{vi} > 0 & \text{for excitation,} \\ 0 & \text{for de-excitation.} \end{cases} \tag{3.4}$$

Numerically fitted parameters for vibronic transitions are given in Tables A.1-A.6 in the Appendix A. When the parameters given in the tables are used in the fitting formulas of Eqs. (3.2) and (3.3) with T in K, obtained numerical values of rate coefficients will be in units of cm^3/s. In the tables, the electronic states are numerated with index i (or i') with $i = 0$ corresponding to $X^1\Sigma^+$, $i = 1$ to $a^3\Pi$, and $i = 2$ to $A^1\Pi$.

3.6 Uncertainty estimations: choice of basis sets and CAS in the R-matrix method

The scattering matrix is the main uncertainties resource for the resulted cross sections. In section 3.3, we underlined that the selection of the S-matrix is not unique and we could have very close resonance structures reproduced by MQDT elimination procedure as shown in Fig. 3.8. Here we estimate the uncertainties of the results through showing the convergence of the scattering

calculation. The basis set and CAS are varied to test the convergence of the calculations. We performed the calculations in the frame of (1) 4 active electrons are distributed in a fixed number of active orbitals with increased basis sets:`cc-pVDZ`, `DZP`, `cc-pVTZ`, and `cc-pVQZ`, and (2) 4 active electrons are distributed in the increased active orbitals: CAS(4, 5), CAS(4, 6), CAS(4, 7), CAS(4, 9), CAS(4, 10), CAS(4, 12) and CAS(4, 14) with a same basis set, at the fixed equilibrium geometry R_e. The primary step for a scattering calculation is the description of electronic structure for the target ion. Therefore, we need first find out the accurate (close to experimental values) and convergent electronic structure calculation. The CAS and Basis set used in the this calculation are considered for the R-matrix calculations for e^--CH^+ collisional system.

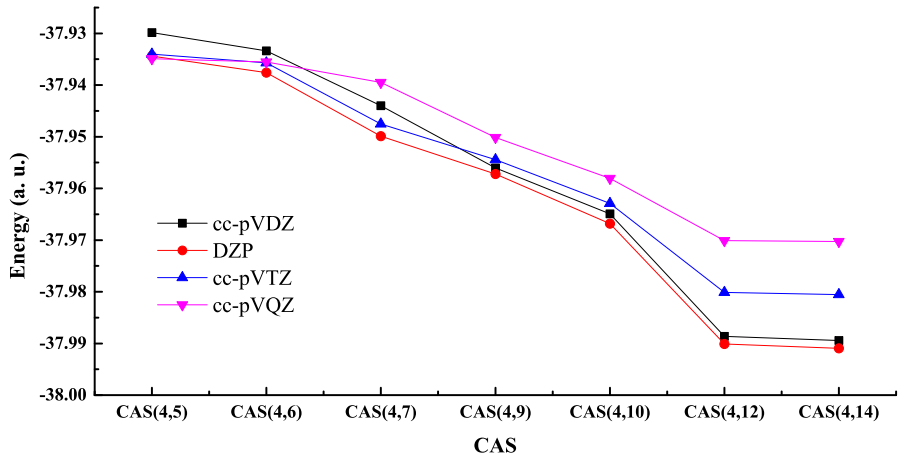

Figure 3.17: Potential energy for the ground electronic state obtained from UK R-matrix calculation at the equilibrium geometry R_e.

As displayed in Fig. 3.17, the potential energy values for the $X^1\Sigma^+$ ground electronic state decreased with the increasing CAS and converged from CAS(4, 12) for all the used basis sets. The dipole moment value of CH^+ has the same behavior that converged from CAS(4, 12) as depicted in Fig. 3.18, suggesting that CAS(4, 12) and CAS(4, 14) are suitable for the final calculation.

Table 3.3: Comparison of the vertical transition energies for the lowest three electronic states obtained by Quantemol. The comparison of the ground state dipole moment at the equilibrium R_e are also shown.

States	cc-pVDZ	DZP	cc-pVTZ	cc-pVQZ	Theory [148]	Exp. [154]
$X^1\Sigma^+$	0.00	0.00	0.00	0.00	0.00	0.00
$a^3\Pi$	1.06 eV	1.05 eV	1.12 eV	1.19 eV	1.20 eV	1.21 eV [155]
$A^1\Pi$	3.23 eV	3.25 eV	3.34 eV	3.42 eV	3.00 eV	3.00 eV
Dipole moment	1.659	1.633	1.607	1.617	1.653 [156]	1.683 [154]

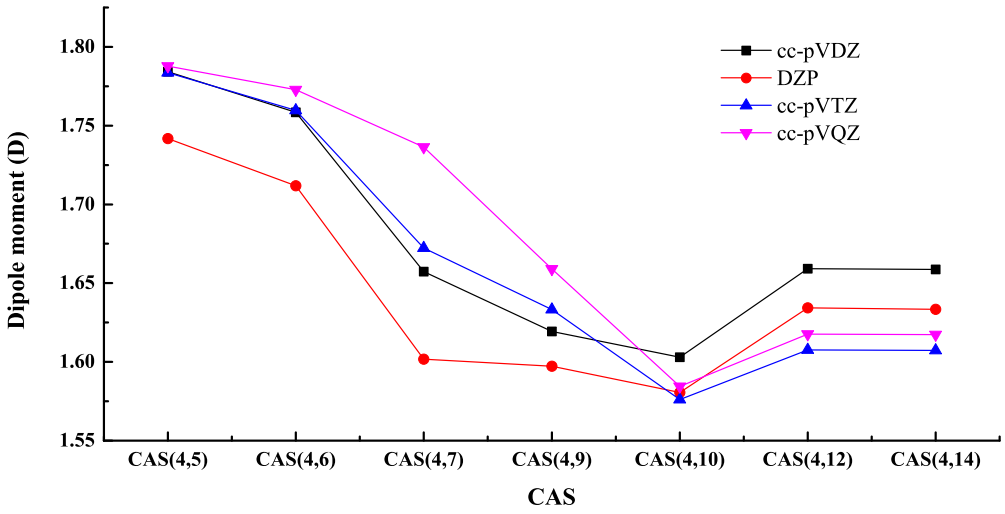

Figure 3.18: Dipole moment of CH^+ obtained with different CAS and basis set at the equilibrium geometry R_e.

We further give the vertical transition energies as seen in the Table 3.3, our results obtained with cc-pVTZ and cc-pVQZ basis sets in CAS(4, 12) are in good agreement with those of Biglari's [148] and experimental data. Considering the dipole moment 1.617 D obtained with cc-pVQZ is closer to the experimental value of 1.683 D, cc-pVQZ and CAS(4, 12) are thus selected for the scattering calculation.

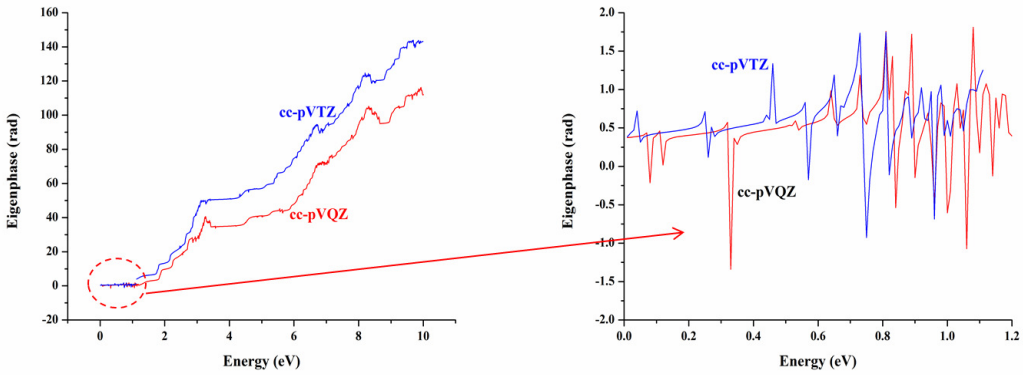

Figure 3.19: Eigenphase sum for $^2A_1$ symmetry of e^--CH^+ system obtained by `cc-pVTZ` and `cc-pVQZ` with the same CAS(4, 12) at R_e (left panel). The resonance structure at the low-energy part is enlarged in the right panel.

Consistence of the resonance position is another demonstration of the stability of the scattering model. Figure 3.19 displayed the eigenphase sum for $^2A_1$ symmetry of e^--CH^+ system in the left panel. Two basis sets `cc-pVTZ` and `cc-pVQZ` with a same CAS(4, 12) are used. The calculations are performed at fixed equilibrium geometry R_e. As we can see in the enlarged picture of the right panel, peaks are on two curves. The density of peaks increases when the electronic scattering energy approaches to the first excited threshold energy.

For the sake of visibility, the resonance positions on the curves were determined by derivative of the eigenphase sum over the scattering energy $\frac{\partial \delta}{\partial E_{el}}$ as shown in Fig. 3.20 for $^2A_1$ symmetry. As outlined by the black dashed line, the positions of the resonance at low energy are generally consistent for the two basis sets. The scattering model with `cc-pVQZ` basis set in CAS(4, 14) was therefore used to produce reliable K-matrix.

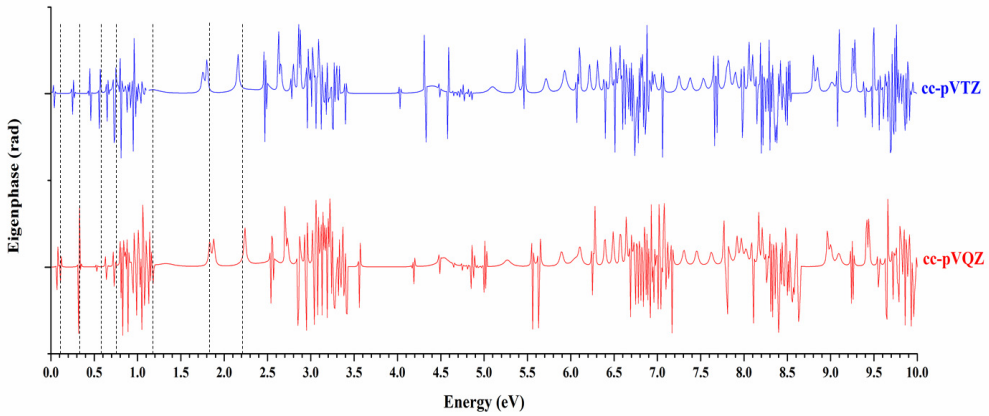

Figure 3.20: Resonance position of $^2A_1$ symmetry at R_e.

3.7 Conclusions

In this chapter, cross sections and rate coefficients for vibronic excitation and de-excitation of CH^+ by electron impact were computed using first principal theoretical approach. The theoretical approach combines the fixed-nuclei scattering matrices obtained for a number of internuclear distances using the UK R-matrix code, the vibronic frame transformation, and the QDT closed-channel elimination procedure. The approach is validated for electronic excitation processes, where calculations were performed for a single fixed internuclear distance of the target, and compared to the results obtained with the UK R-matrix code. The approach could be applied to the ions with low-lying electronic excited states. Such ions were known to be difficult to treat theoretically using previous theoretical methods. There is a large number of radicals that could be, in principle, be considered using the suggested approach. The approach is quite general and can be applied for a number of different processes, taking place in collisions of molecular ions with electrons, including rovibronic excitation, dissociative excitation (DE), photoionization and dissociative recombination (DR).

In this chapter, we took into account only electronic and vibrational structure of the target ion. The rotational structure of each vibrational level was neglected. Therefore, the obtained cross sections and rate coefficients should be viewed as averaged over initial rotational states and summed over final rotational states of the corresponding vibrational states. A better treatment of the vibronic excitation process accounting for the rotational structure is possible and will be considered in a near future. As seen in Eq. (1.1), the cross sections and rate constants for vibronic excitation of CH^+ are the necessary data for the kinetic modeling of the plasma. This is actually the first quantitatively computation of the vibronic excitation of CH^+ by electron impact.

CHAPTER 4: Dissociative recombination of CH^+ by electron impact

4.1 Introduction

As we stated in the introduction of chapter 3, dissociative recombination (DR) competes with vibrational transition and both the processes could be treated in the same MQDT framework that has been described in chapter 3. However, to evaluate the DR cross sections, we have to introduce the outgoing-wave basis functions defined by CAP to account for the dissociation flux in the DR process. The flux lost through the vibrational continua states of the neutral Rydberg state that are associated with the outgoing-wave basis introduced as closed ionization channels. In this chapter, we will present the theoretical approach for low-energy DR of CH^+ in details.

Electron-molecular ion collisional systems in a DR treatment could be theoretically divided into two catalogs, the curve crossing and non-crossing system [157]. In the former case, the potential energy curve (PEC) of the doubly excited neutral molecule crosses the ionic PEC. The direct DR is generally dominant. This is the often case, but one also needs to note that indirect process may play a important role in enhancing the DR with respect to direct pathway. The stepwise MQDT method based on the treatment presented by Giusti-Suzor and Guberman [34, 158] has shown to be the most successful way in description of the DR for such systems, e. g. N_2^+ [31], O_2^+ [116], NO^+ [32, 159], CO^+ [144], BF^+ [160], CF^+ [161], BeH^+ [162, 163], SH^+ [113], OH^+ [164], CH^+ [18, 29, 30, 112]. The least inputs for this approach are PEC of the ionic ground electronic state with vibrational states and the crossed dissociative states of the neutral molecule, electronic couplings between these neutral dissociative states and the Rydberg series converging to the ground ionic state, and R-dependent quantum defects of the considered Rydberg states. For a DR calculation including multiple ionic states, the Rydberg-Rydberg couplings describing the coupling between different ionization channels are also needed. In the later type, the crossing does

not occur where non-Born-Oppenheimer interactions drive the DR through excited states. In such case, the indirect DR is normally dominant. The above mentioned method could not be properly applied due to the failed description in terms of quasi-diabatic states. A convenient Siegert MQDT method was introduced by Hamilton and Greene in 2002 [46] to compute the DR rate for the non-crossing systems based that Siegert pseudostates allow the description of the outgoing flux in predissociation. They applied the method to H_2^+ and accurately reproduced results compared with that of O'Malley [97]. Several years later, they developed an alternative MQDT method with a CAP defining the outgoing-wave vibrational states [107]. Compare with Siegert pseudostate [45], CAP eigenstates obey a simpler orthonormality relationship and work better on preservation of the eigenphases of the MQDT transformed scattering matrix. The methods has also found success in applying on LiH^+ [165], HeH^+ [166], and even triatomic molecular ions H_3^+ [118, 119].

For various molecular ions with low-lying bound excited electronic state that usually belong to the first type, the stepwise MQDT method serves currently as the only available treatment. However, one significant limitation of the treatment is the difficulty in obtaining the electronic couplings. The procedure through diabatization of coupled Rydberg states (i.e. using the quasi-adiabatic states [167]) obtained in *ab initio* calculations, used in the approach, is laborious, not unique, and sometimes not accurate. It becomes even more ambiguous and very complicated for polyatomic ions, such that an extension of the approach to polyatomic ions becomes impractical.

Therefore, we aim to make an attempt to develop a simple approach to compute the DR cross sections of the curve crossing systems in this chapter. In chapter 3, we developed the theoretical approach in the MQDT framework to describe the electron collision with such molecular ions and successfully applied to the study of the vibronic excitations of CH^+. In particular, the neutral doubly excited dissociative state in the electron collision with molecular ions of this type is usually of Rydberg character, especially at a short internuclear distance. This fact suggests that the neutral dissociative state may appear as Rydberg resonances in the electron-ion collisional process.

This kind of resonances could be, as we know, reproduced by MQDT electronic close-channel elimination procedure. The electronic coupling between the initial continuum state of electron-ion collisional system and the neutral dissociative (resonance) state could thus be included in scattering matrix with the help of elimination procedure. In other word, we don't need to explicitly obtain the PECs of neutral dissocitive (resonance) states as the method introduced above for the curve crossing system. Particularly, we applied this approach using the MQDT treatment in conjunction with CAP basis [1] based on our previous study in chapter 3 to the low-energy DR of ground-state CH^+.

The DR process of CH^+ has been repeatedly studied over the years in theory and experiment. It is the main destructive way of CH^+, which serves as a cornerstone in the formation chain of other complex interstellar molecule, especially polyatomic hydrocarbon. On the other hand, a good knowledge of the rate for the process is the key to reconcile the calculated and observed abundance of the interstellar CH^+.

In the early studies, Bardsley and Junker [22] and Krauss and Julienne [23] calculated the adiabatic PECs of CH and CH^+ with different theoretical techniques. They found that the PEC of the repulsive "$^2\Pi(3)$" state of CH (see Fig. 1 of Ref. [22, 23]) intersects the PEC of the ground electronic state of CH^+ near the equilibrium internuclear distance. CH in the "$^2\Pi(3)$" state formed by low-energy e^--CH^+ collision would finally dissociate to $C(^1D)$+$H(^2S)$ through a coupling to "$^2\Pi(2)$" state by the avoided crossing (see Fig. 1 of Ref. [22]). Both groups evaluated a rapid DR occurred with a rate of $> 10^{-7}$ cm^3s^{-1} at 100 K. The conclusion brought the problem that the calculated equilibrium intensity of interstellar CH^+ in the steady-state chemistry model of Smith, Liszt, and Lutz [168] is over 100 times smaller than observed. A few years later, Giusti-Suzor and Lefebre-Brion [24] offered an opposite estimation of a considerably reduced DR rate. They

[1] The outgoing-wave basis functions defined by a CAP

considered Rydberg-type orbitals in the PECs calculations of CH. The resulted PECs showed no cross between "$^2\Pi$" dissociative states and the ionic ground state. A better agreement between the predictions and measurements could be deduced with this small DR rate.

However, the fast DR rate conclusion seems to be supported by the preliminary experimental values of CH^+ DR rate with about 3×10^{-7} cm^3 at 120 K measured by a merged electron-ion beam method [169, 170].

The remained controversy was carefully investigated by Takagi *et al.* in 1991 [29] using self-consistent field and the multi-configuration mixing methods. They pointed out that the Rydberg character basis functions used by Giusti-Suzor and Lefebre-Brion [24] are inadequate to represent the highly excited states around the ionization threshold. Slater-type orbitals (STOs), describing better the diffuse states than the Gaussian, are used in the calculations of the Rydberg series. Diabatic PEC of a neutral anti-bonding state in "$^2\Pi$" symmetry was appointed as the main dissociative channel for CH^+ at low scattering energy. The crossing point with PEC of the ionic ground state is at $R = 1.832$ a_0, within the main Frank-Condon region. The DR rate was for the first time quantitatively computed by a two-step MQDT treatment. The obtained results agree well with the experimental measurements [169]. The calculation of CH^+ DR cross section, however, is limited to the electron scattering energy below 0.30 eV.

With the improved heavy-ion storage-ring technique, a very detailed experimental study on the DR of the fully-relaxed CH^+ was carried out by Amitay *et al.* in 1996 [155]. Branch ratio of the DR fragments was also reported with the help of two-dimensional fragment imaging. The measured DR cross section is in line with previous estimations and of rich resonance. The fast DR rate was attributed to the crossing between the "$2^2\Pi$" dissociative state of CH and the ionic ground state. However, unusual broad resonance structures presented in the DR cross section. Considering the low-lying excited states of CH^+, they tentatively assigned the resonances to the core-excited

Rydberg states.

To identify the observed broad resonances, Carata *et al.* [30] performed an elaborate MQDT calculation of CH^+ DR at low energy. The Rydberg manifolds converging to the $X^1\Sigma^+$ ground electronic state and the next two $a^3\Pi$ and $A^1\Pi$ excited states of the ion core are included in the treatment. They successfully reproduced the prominent structure at low collisional energy (< 4 eV), confirming the assignment of Amitay *et al.* [155]. Whereas the absolute value of the cross section is not reproduced as the interactions of the ionization channels computed with only first order perturbative solution of the Lippman-Schwinger equation. To improve the agreement of DR cross section in magnitude with experimental measurements, Chakrabarti *et al.* [18] recently performed a similar MQDT calculation where the second order solution of the Lippman-Schwinger equation was derived. They obtained quantitatively accurate DR cross section compared with the storage ring data, while the shape is not comparable. One year later, the rotationally resolved DR cross section was considered by the same team [112].

The current chapter is organized in the following way: we first discuss the description of the neutral $2^2\Pi$ dissociative state by the selected energy-independent scattering matrix combined with the MQDT electronic close-channel elimination procedure in section 4.2. Second, the calculation details of the outgoing vibrational basis functions defined by CAP boundary conditions are given in section 4.3. Section 4.4 exhibits the theoretical approach of the DR cross-section calculation using MQDT and the computed results, and section 4.5 conclude the chapter.

4.2 MQDT description of $2^2\Pi$ resonant state

The presently accepted low-energy dissociation pathway for e^--CH^+ system is the $2^2\Pi$ dissociative (resonance) state of neutral CH. This resonance state is started to be labeled as $2^2\Pi$ from the study

of Amitay *et al.* [155] and proved as the dominant dissociation pathway at low energy through analysis of the branch ratio of CH^+ DR fragments. For convenience to follow the discussion in this chapter, we here recall the computed PECs of the electronic states of CH^+ obtained in chapter 3 as shown in Fig. 4.1. The PEC of the $2^2\Pi$ resonance state crosses that of the $X^1\Sigma^+$ ground ionic state near the left turning point of the first excited vibrational state [171], giving rise to a fast DR rate. The PEC of the resonance state below the ionic ground state is obtained through an extrapolation. Here, we plot the 35 vibrational levels for each electronic state involved in the calculation of DR cross section in the figure. The energy values of those vibrational levels are the real part of the eigenenergies obtained using a CAP formalism (see section 2.2.2 and 4.3). These vibrational levels will be used as vibrational ionization thresholds in the MQDT closed-channel elimination procedure (we will discuss in section 4.4).

This curve of the $2^2\Pi$ resonance state shown in Fig. 4.1 is actually the diabatic potential (see Fig.4 of Ref. [29]). In the adiabatic representation, it was divided into two parts due to the avoided crossing. Within the small nuclear distance, i.e. before the avoided crossing point, it is marked as "$3^2\Pi$" state in the Fig.1 of Ref. [23] and "$^2\Pi(3)$" in the Fig.1 of Ref. [22]. In the long-range nuclear distance part, it is "$^2\Pi(2)$" in the Fig.1 of Ref. [22] and "$D^2\Pi$" in the Fig.2 of Ref. [172] and it correlates with the $C(^1D)$+$H(^2S)$ dissociation limit.

The main electronic configuration of the resonance state is $1\sigma^2 2\sigma^2 3\sigma 1\pi 4\sigma$ due to the large distance correlations $3\sigma \rightarrow 1s_H$, $1\pi \rightarrow 2p_C$, $4\sigma \rightarrow 2p_C$. The 4σ orbital has Rydberg character at small nuclear distance. This character is caused by the coupling between the $3\sigma 1\pi(^1\Pi)4\sigma$ and $3\sigma 1\pi(^3\Pi)4\sigma$ of CH, i.e. incident electron in 4σ Rydberg orbital plus the $a^3\Pi$ and $A^1\Pi$ parent states of CH^+. Near and to the left of the crossing of the resonance and ionic ground PEC, the character of the resonance state is mainly the $3\sigma 1\pi(^1\Pi)4\sigma$ (see Fig. 1 of Ref [24]). Therefore, the $2^2\Pi$ resonance state could be included in the MQDT description of e^--CH^+ system if we take the two excited $a^3\Pi$ and $A^1\Pi$ states into consideration in the low-energy scattering calculations.

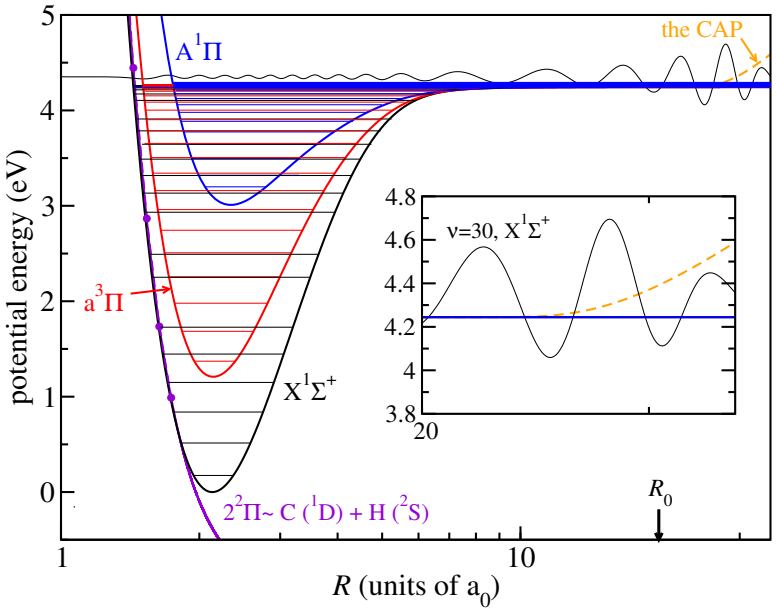

Figure 4.1: Potential energy curves shown are the same in Fig. 3.2. The PEC of the $2^2\Pi$ resonance state (violet dotted curve) is obtained by R-matrix method. An extrapolation is used to plot the PEC of the this state below the ionic ground state (violet solid curve). 35 vibrational levels for each of the three lowest electronic states are shown by horizontal thin lines and of the same color with the corresponding state. The values of the vibrational level energies are the real part of the eigenenergies obtained by the CAP formalism (see see section 2.2.2 and section 4.3). The CAP basis function of $v = 30$, $X^1\Sigma^+$ (black solid curve) is used to illustrate the absorption of the CAP (orange dashed curve). The strength of the CAP is enhanced by a factor of 25 and the position of the CAP state is slightly up displaced for clarity of the illustration. The black bold arrow points to $R_0 = 20\,a_0$ where the CAP begins. The inset shows the enlarged view of the CAP used in the thesis starting from R_0.

The DR of the ground-state CH^+ through $2^2\Pi$ involves a direct process

$$CH^+(vi) + e^-(l\lambda) \rightarrow CH^{**}(2^2\Pi) \rightarrow C(^1D) + H(^2S) \tag{4.1}$$

where the incident electron with partial wave $l\lambda$ in the molecular reference frame is directly captured by ground-state CH^+ into to the $2^2\Pi$ doubly excited neutral dissociative state (see section 2.6.1),

and an indirect process

$$CH^+(vi) + e^-(l\lambda) \rightarrow CH^* \rightarrow CH^{**}(2^2\Pi) \rightarrow C(^1D) + H(^2S) \tag{4.2}$$

where the incident electron is temporarily captured into a vibrational levels of bound Rydberg states CH^* attached to the ionic ground or low-lying excited electronic states (see explanation of IDR in section 2.6.2). i stands for the ion electronic state and v for the vibrational quantum number in the ionic potential. The ground-state CH^+ is in ground vibrational level of the $X^1\Sigma^+$ ground electronic state, i.e. $vi = 00$. The rotational structures are neglected in this study. An alternative type of indirect DR process for CH^+ proceeds through trapping the electron in one of the Rydberg states converging to the low-lying $a^3\Pi$ and $A^1\Pi$ ionic excited states (see Fig. 4.1). Then the predissociation is followed along the coupled neutral $2^2\Pi$ dissociative state. This is actually widely seen in DR of molecular ions with low-lying bound excited electronic states [102–105]. Therefore, three lowest $X^1\Sigma^+$, $a^3\Pi$ and $A^1\Pi$ electronic states should be at least included in the MQDT treatment for an accurate description of the CH^+ DR.

Here, we perform the R-matrix calculations and select the resulted 3×3 energy-independent scattering matrix according to the procedure described in the previous chapter, more details on the calculations could be found in the section 3.2.3. Fig. 4.2 displays the eigenphase of $^2\Pi$ symmetry of e^--CH^+ collisional system obtained at R=1.337, 1.437, and 1.537 bohrs. Different coluors are used to distinguish the three different nuclear distances. The eigenphase below scattering energy of 0.34 eV is zoomed and presented in the inset. We can see a left shift of the eigenphase with the increasing of the internuclear distance. To locate the position and width of the resonance, we evaluate the derivatives of the eigenphase sum of $^2\Pi$ symmetry taken directly from R-matrix calculation at R=1.337, 1.437, and 1.537 bohrs. As we can observe with the solid curves in Fig. 4.3, low-energy resonance is detected. The position of the resonance decreases with the internuclear

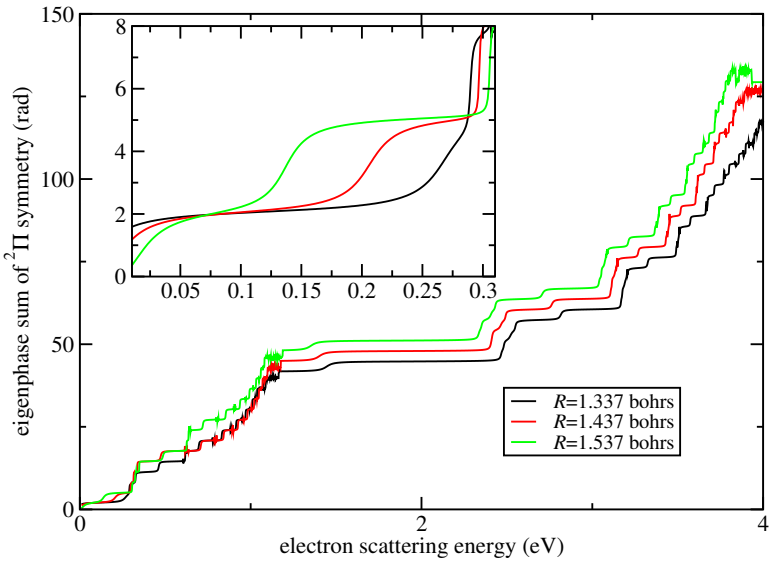

Figure 4.2: Eigenphase of $^2\Pi$ symmetry of e^--CH^+ collisional system obtained at R=1.337 (black), 1.437 (red), and 1.537 bohrs (green). The inset show the enlarged energy range from 0.01 to 0.32 eV. Details of the R-matrix calculations could be found in section 3.2.3.

distance moving far and disappears at R=1.837 bohrs. The resonance is referred as the $2^2\Pi$ state and plotted in the PECs of CH^+ in Fig. 4.1.

The two excited electronic states are closed for the ionization at low scattering energy. The lower-lying (compared with the two excited states as displayed in Fig. 4.1) neutral $2^2\Pi$ resonance state with Rydberg character could be therefore accounted for using the MQDT electronic closed-channel elimination procedure. Similarly to the manner described in section 3.3.2, we performed the elimination procedure using the 3×3 electronic scattering matrices of $^2\Pi$ symmetry selected above the $A^1\Pi$ threshold at R=1.337, 1.437, and 1.537 bohrs. The low-energy resonances are reproduced as shown with dashed curves in Fig. 4.3. For clarity, we listed the positions of these low-energy resonances in Table. 4.1. The position of the resonance is a little left shifted and the width is slightly narrower compared to that of the R-matrix calculation. As pointed out in the preceding chapter, this behaviour was also observed in Fig. 3.7. The shift of the resonance position

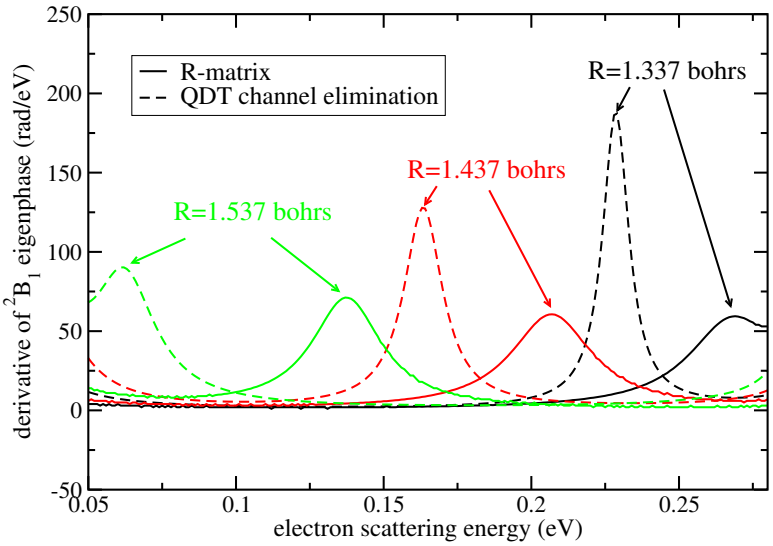

Figure 4.3: The low-energy resonances corresponding to the $2^2\Pi$ resonance state of the e^--CH^+ complex. They are obtained by derivative of the eigenphase sum for $^2\Pi$ symmetry taken directly from R-matrix calculation (solid curves) and MQDT channel elimination (dashed curves). Each color refer to different the resonances obtained at R=1.337 (black), 1.437 (red), and 1.537 bohrs (green). Details of the R-matrix calculations could be found in section 3.2.3.

may be related to the energy point where we selected the scattering matrix.

Table 4.1: Positions of the low-energy resonances (in units of eV) obtained fromthe R-matrix calculation compared to those obtained from channel elimination at different nuclear distance R (in units of bohrs).

R	1.137	1.237	1.337	1.437	1.537	1.637	1.737	1.837
R-matrix	0.388	0.336	0.269	0.207	0.139	0.061	0.42	-
Channel elimination	0.253	0.247	0.230	0.166	0.064	0.036	0.020	-

An important conclusion here is that with the 3×3 energy-independent scattering matrix, the $2^2\Pi$ dissociative state can be described by the MQDT electronic closed-channel elimination procedure. Therefore, the electronic couplings between the initial electronic continuum of e^--CH^+ and the neutral dissociative state (responsible for DDR) are included in the scattering model. The Rydberg-

Rydberg couplings between Rydberg series converging to the three electronic states and the neutral dissociative state (responsible for IDR) are also contained in the selected scattering matrix.

4.3 Outgoing-wave basis functions defined by complex absorbing potential

As we pointed out in section 2.6, the dissociation proceeds through a number of excited Rydberg states, which are bound with respect to dissociation. MQDT treats such a system as a set of coupled vibrational states. To describe the dissociation, the vibrational continuum of the considered PECs should be included in the model. The continua states could be discretized by the outgoing-wave basis defined by the CAP (see section 2.2.2). They were called as CAP basis (states) in Ref. [174]. The introduced basis, on one hand generates a Rydberg series of neutral states, and on the other hand enables the dissociative flux escape if it reaches the boundary. Namely, the DR process is simulated by the absorption of the dissociative flux of the neutral molecule by using the introduced CAP basis.

The artificial complex absorbing potential (CAP) is purely imaginary and added to the adiabatic potentials $V(R)$ using Eq. (2.32). Exponential CAP in the form of Eq. (2.33) is used in the present thesis. L specifies the grid length of the adiabatic potentials of the $X^1\Sigma^+$, $a^3\Pi$ and $A^1\Pi$ electronic states. These PECs are taken from chapter 3 and the calculation details could be found in section 3.2.2. R_0 (as seen in Fig. 4.1) is the starting point of a CAP on the potential. The parameters, i.e. the strength η of Eq. (2.32) and length of Eq. (2.33), of the three lowest $X^1\Sigma^+$, $a^3\Pi$ and $A^1\Pi$ electronic states are appropriately chosen according to Ref. [47]. The CAP should be far away from the main well of the PECs of CH^+. We use $L = 35.0$ bohrs and $R_0 = 20.0$ bohrs for the three electronic states in this thesis. Using Eq. (20) and Table VI of Ref. [47], we compute the CAP strength η with value of 2.835×10^{-4}. This CAP computed by ηW in Eq. (2.32) is drawn in the inset of Fig. 4.1. The absorption of the vibrational dissociative state ($v = 30$, $X^1\Sigma^+$) by the CAP is also

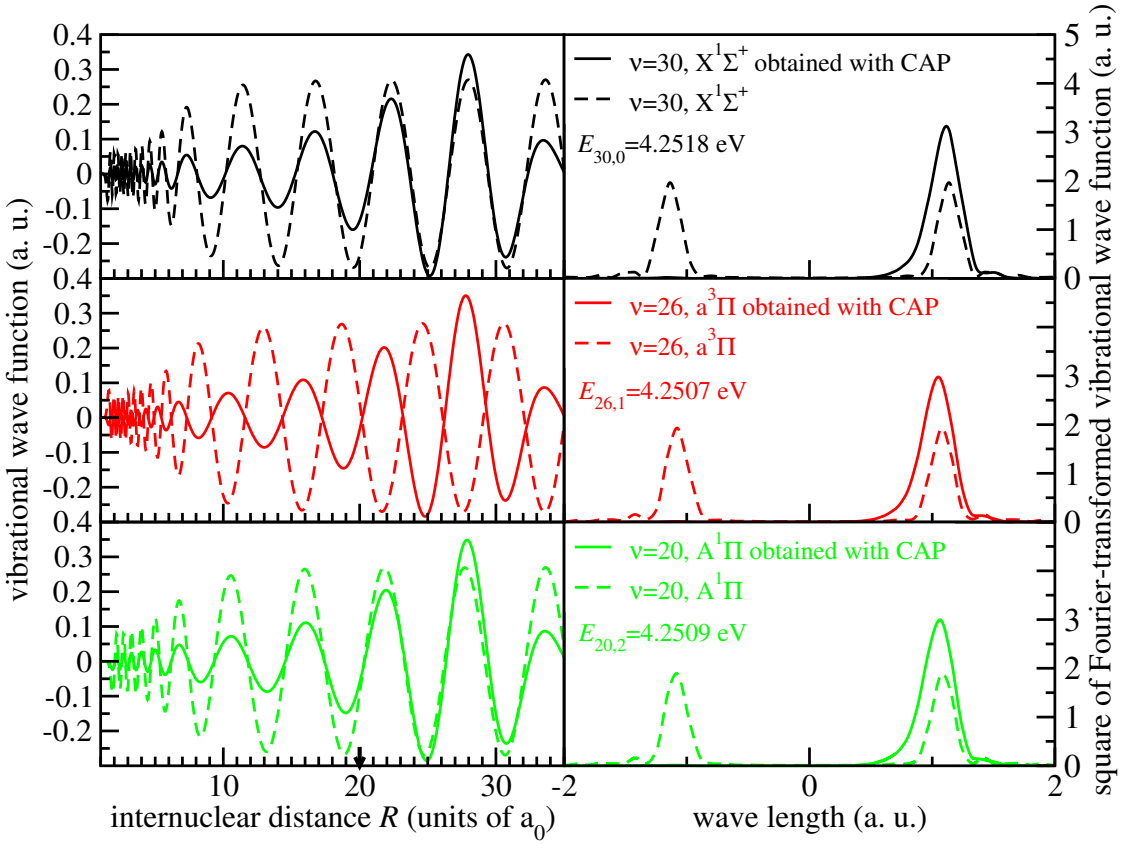

Figure 4.4: Left panel shows the vibrational wavefunction in terms of R for v=30, $X^1\Sigma^+$ (in black), v=26, $a^3\Pi$ (in red), and v=20, $A^1\Pi$ (in green) obtained with (solid curve) and without CAP (dashed curve). While the right panel displays the FT vibrational wavefunctions in momentum k space for the same vibrational states. The arrow in the left panel points to the R_0.

demonstrated in the figure. The complex eigenenergies E_{vi} of Eq. (2.34) and the CAP basis ϕ_{vi} of the Hamiltonian in Eq. (2.32) are obtained by the standard discrete variable representation (DVR) method [43] (see section 2.2.2). The set of obtained vibrational basis $\phi_{vi}(R)$ obey orthonormality relationship of Eq. (2.35). Note that neither the bra nor ket is complex conjugated.

Fourier transformation (FT) technique is used to verify the absorption of the CAP through transferring wavefunctions of vibrational states from R representation to momentum space denoted by k. As seen in the left panel of Fig. 4.4, we plot the wavefunctions of dissociative vibrational states

(vibrational continua states), for instance, v=30, $X^1\Sigma^+$ (black curve), v=26, $a^3\Pi$ (red curve), and v=20, $A^1\Pi$ (green curve) as functions of internuclear distance R. The wavefunctions of the CAP basis are represented by solid curves. These wavefunctions with complex energies asymptotically increasing at large internuclear distance [107] and decrease when they approach the CAP (see Fig. 4.1). They have considerable amplitude in the asymptotic part, whereas small inside the potential-well region. The wavefunctions of the vibrational continua states for the three electronic states of CH^+ obtained without the CAP are in dashed curve. They behaviour nearly as sine function at $R > 20\ a_0$. This means the kinetic energies of the waves are constant, which implies that the CAP could be appropriately placed at $R = 20\ a_0$ and will not perturb the vibrational states in the main well region. The right panel of Fig. 4.4 displays the FT wavefunctions of the vibrational states presented in the left panel. The wavefunctions of the vibrational continua states in momentum k space (dashed curve) present two identical peaks in both positive and negative momentum space. This can be explained by the fact that the wavefunction of a steady state is a linear combination of outgoing/transmitted wave and incoming/reflected wave. As we use the CAP to simulate an infinite grid, it thus results in no reflections, leading to a missing negative component of k. The disappeared peak in the negative k space clarifies the parameters of the CAP are appropriately chosen.

The resulting eigenenergies of vibrational wavefunctions obtained with (curves with star) and without the CAP (curves with circle) for the three electronic states of Fig. 4.1 are shown in Fig. 4.5. As we see in the left panel, The CAP spectrum contains a branch vibrational states whose eigenenergies are below the dissociation limit. They coincides with 23, 19 and 13 bound vibrational states of the $X^1\Sigma^+$, $a^3\Pi$ and $A^1\Pi$ states obtained without CAP, respectively. The added CAP does not affect the positions of the bound states. The states obtained with CAP above the dissociation limits represent the continuum states. Positions and widths of the continuum states depend on the CAP parameters [175]. The right panel shows the enlarged energy region around the dissociation limit. The linear eigenvalues with a slope of 60° corresponds to the converged non-resonant states

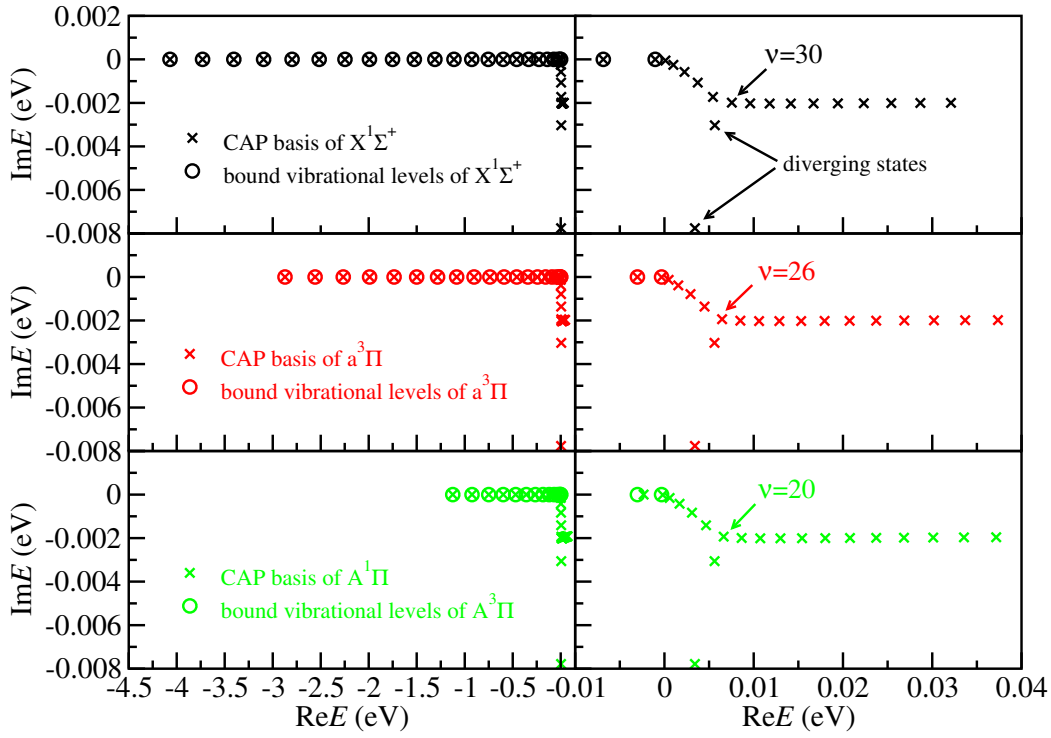

Figure 4.5: Eigenenergies E_{vi} distribution spectrum of the vibrational states of the $X^1\Sigma^+$ (in black), $a^3\Pi$ (in red) and $A^1\Pi$ (in green) states. Stars are used to represent the CAP basis, while circle, square and trangle are used to numerate the bound vibrational states obtained without CAP.

as called in Ref. [176]. The eigenvalues parallel to the horizontal axis are indifferent states as called in Ref. [176]. The three vibrational states $v = 30$, $v = 26$ and $v = 20$ of the three electronic states were singled out and their wavefunctions were analyzed in Fig. 4.4.

Below parallel eigenvalues, we can also see divergent states as called in Ref. [176] due to an incomplete finite grid used in DVR method. The wavefunctions of such states are shown in Fig. 4.6. Their wavefunctions are more localized out of the main potential well which differ from the other CAP basis. The amplitude inside the potential-well region is negligible compared with that in the asymptotic part.

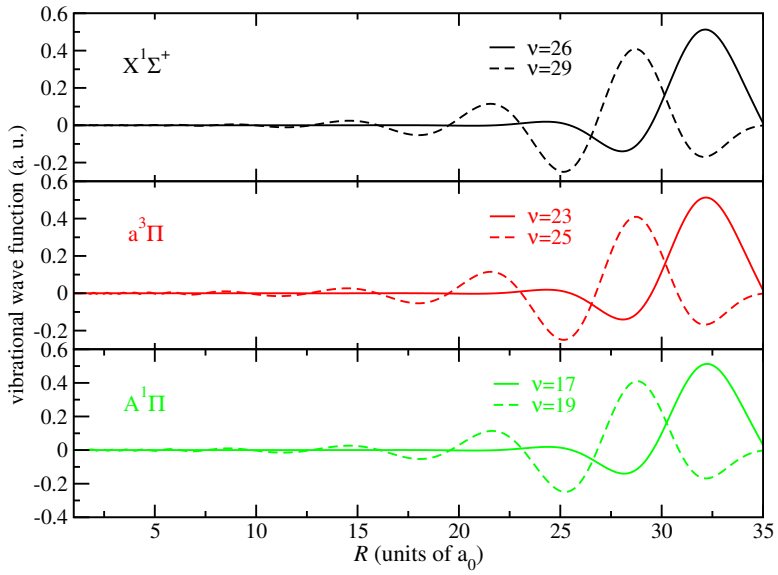

Figure 4.6: The vibrational wavefunctions in terms of R for divergent states $v = 26$ and $v = 29$, $X^1\Sigma^+$ (in black), $v = 23$ and $v = 25$, $a^3\Pi$ (in red), and v=17 and $v = 19$, $A^1\Pi$ (in green) obtained with CAP.

4.4 Theoretical approach and the computed results

Since the neutral $2^2\Pi$ dissociative state is proved to be included in the 3×3 energy-independent electronic scattering matrix $S(E_{\rm el}, R)$ in section 4.2 and the optimal parameters are determined for the CAP in the Section 4.3, the scattering matrix describing the electron collision with the vibrating CH^+ could be constructed using the vibronic frame transformation of Eq. (2.60) in section 2.4.

$$S_{l'\lambda'v'i',l\lambda vi}(E_{\rm el}) = \int \phi_{v'i'}(R) S_{l'\lambda'i,l\lambda i}(E_{\rm el}, R) \phi_{vi}(R) dR \tag{4.3}$$

Here, the CAP basis functions $\phi_{v'i'}$ are not conjugated. $E_{\rm el}$ is the electron scattering energy. The $S_{l'\lambda'v'i',l\lambda vi}(E_{\rm el})$ is obtained by integrating the selected $S_{l'\lambda'i,l\lambda i}(E_{\rm el}, R)$ over the internuclear distance R from 1.137 bohrs to 4.937 bohrs with a interval of 0.1 bohrs. To compromise correct implementation of the above equation in practical calculations in the code, we need to sort the target

states in accordance with the below Table 4.2. Another treatment is averaging the K-matrix over 20 steps right above the threshold (the $A^1\Pi$ electronic state) at different R. This is to alleviate the influence of broad shape resonance situated scattering energy above the $A^1\Pi$ state. The unitarity of the S-matrix are verified to be maintained in the treatments. The averaged scattering matrices are obtained by Eq. (2.52) and selected to be used in the computation of the cross sections.

Table 4.2: The arrangement of the the involved lowest $X^1\Sigma^+$, $a^3\Pi$ and $A^1\Pi$ three electronic states of the target in C_{2v} point group.

Symmetry of the target	
$X^1\Sigma^+$ $(i=0)$	A_1
$a^3\Pi$ $(i=1)$	B_1 B_2
$A^1\Pi$ $(i=2)$	B_2 B_1

Through the transformation, the sets of CAP basis of three electronic states of CH^+ are now incorporated as the ionization channels. Each of the channels associates with the threshold energy of a vibrational level of the ionic electronic states (as seen in Fig. 4.1). The energies E_{vi} for the CAP basis are complex as discussed in the above section (and also see Eq. (2.34) section 2.2.2). They are sorted successively according to the real part of E_{vi} in Fig. 4.1. The electron scattering energy E_{el} in our calculation is restricted within the range of 0.01 eV-3.00 eV as the energy range being of interest is below 4 eV. In the same manner (as we introduced in 3.4), it divides all channels as energetically open when it situated above the corresponding ionization threshold or otherwise closed, termed by "o" or "c". N_o and N_o are used to numerate the number of open and close channels, respectively. The transformed scattering matrix is thus written as submatrices in Eq. (2.71). The physical scattering matrix $S^{phys}(E_{\mathrm{el}})$ restricted to open channels is obtained by MQDT

close-channel elimination procedure

$$S^{phys}(E_{\rm el}) = S^{oo} - S^{oc}\left[S^{cc} - e^{-2i\beta(E_{\rm el})}\right]^{-1} S^{co}, \tag{4.4}$$

where $\beta(E_{\rm el})$ quantities represents the effective quantum numbers as defined in Eq. (2.73) in section 2.5.3). Its form in terms of the vibrational threshold E_{vi} of the ion is

$$\beta(E_{\rm el}) = \frac{\pi}{\sqrt{2(E_{vi} - E_{\rm el})}}\delta_{v'i',vi}. \tag{4.5}$$

They become complex because the higher ionization thresholds E_{vi} are represented in the CAP formalism with complex eigenenergies. This leads to a sub-unitary $S^{phys}(E_{\rm el})$. Physically, the lost flux is associated with the vibrational dissociative states attached to the vibrational closed channels represented by the CAP basis with outgoing-wave characters.

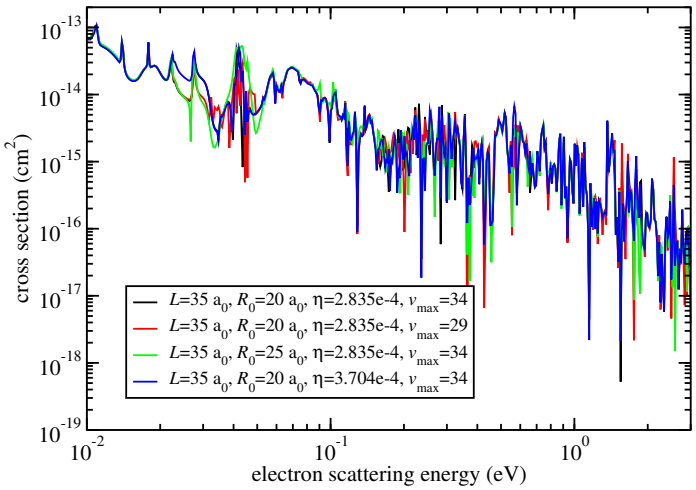

Figure 4.7: Convergence tests of the DR cross section of ground-state CH^+. The results are computed using (1) $L = 35\ a_0$, $R_0 = 20\ a_0$, $\eta = 2.835 \times 10^{-4}$, $v_{max} = 34$ (black) (2) $L = 35\ a_0$, $R_0 = 20\ a_0$, $\eta = 2.835 \times 10^{-4}$, $v_{max} = 29$ (red) (3) $L = 35\ a_0$, $R_0 = 25\ a_0$, $\eta = 2.835 \times 10^{-4}$, $v_{max} = 34$ (green) (4) $L = 35\ a_0$, $R_0 = 20\ a_0$, $\eta = 3.704 \times 10^{-4}$, $v_{max} = 34$ (blue).

To calculate the cross section, we also need the conjugated physical scattering matrix $S^{\dagger phys}(E_{\rm el})$.

It is computed in a same manner with $S^{phys}(E_{\mathrm{el}})$, but with the complex-conjugate scattering matrix element $S^{\dagger}_{l'\lambda',l\lambda}(E_{\mathrm{el}},R)$. The conjugate transformed scattering matrix $S^{\dagger}(E_{\mathrm{el}})$ is obtained through Eq. (2.84). The channel elimination procedure in Eq. (4.5) should also use the complex-conjugate submatrices by Eq. (2.72) As pointed out by Kokoouline [142], the above equation also account for the complex conjugation by changing the sign of the quantity beta.

Once the scattering matrices elements $S^{phys}_{l'\lambda'v'i',l\lambda vi}(E_{\mathrm{el}})$ and $S^{\dagger phys}_{l'\lambda'v'i',l\lambda vi}(E_{\mathrm{el}})$ are determined, the DR cross section for a specific partial wave of the scattering electron is extracted from the unitarity defect of the scattering matrix by using Eq. (2.86). The CH^+ is assumed initially in the ground state which means $v=0$ and $i=0$. The total DR cross section for the ground-state CH^+ is obtained by Eq. (2.87). We include 35 vibrational states for each of the involved electronic state in the DR cross section calculation as seen in Fig. 4.1. The convergence of the computed results are tested by varying the maximum vibrational states (v_{max}), the starting point of the CAP (R_0), the damping strength (η). We used four sets of parameters to compute the cross section as seen in the following Fig. 4.7. A good agreements of these results could be seen in the figure which indicates the convergence of our computed cross section. The results computed with the set of parameters (1) are used for the final cross section calculation of CH^+ in our thesis.

We perform convolution for the computed DR cross sections of CH^+ initially in the lowest vibrational level of the ground electronic state ($vi=00$) with parallel electron energy $E_{\parallel}=0.5$ meV and transverse energy spread $E_{\perp}=17$ meV. The energy values are taken from Ref. [155]. The convolution is performed according Eq. (2) of Ref. [177] written as

$$\sigma(E_{\mathrm{el}}) = \frac{\sigma((\left|\sqrt{2E_{\mathrm{el}}}\right|+u_{\parallel})^2/2+E_{\perp})}{\sqrt{2E_{\mathrm{el}}}} \frac{1}{(2\pi)^{1/2}E_{\perp}\sqrt{\Delta E_{\parallel}}} \int_{-\infty}^{\infty} du_{\parallel} exp(-\frac{u_{\parallel}^2}{2\Delta E_{\parallel}}) \int_{0}^{\infty} dE_{\perp} exp(-\frac{E_{\perp}}{\Delta E_{\parallel}}) \quad (4.6)$$

where $u_{\parallel}$ is defined as velocity that describes the parallel distribution. It represents the deviation of the total velocity ($\left|\sqrt{2E_{\mathrm{el}}}\right|+u_{\parallel}$) from the center of the distribution. The obtained results compared

with experimental and theoretical data as shown in Fig. 4.8. Since our interest is in the low-energy DR as we introduced in the introduction, we thus restricted the energy in our calculations in the range of 0.01-3.0 eV. Numerous Rydberg resonances are seen in the figure. These narrow resonance are usually interpreted as the capture of electron in the vibrationally Rydberg states attached to the ground ionic state. They are partly washed out in the convolution process, and only the prominent resonances survive. The broad ones are tentatively assigned to various bound Rydberg states that converge to the excited ionic states [30, 155]. Overall, the computed results agree well with the experimental data of Amitay *et al*. and decrease as slightly larger than the slope of the experimental curve from a value of 3.55×10^{-13} cm^2 at $E_{el} = 0.01$ eV. Up to $E_{el} = 0.1$ eV, the calculation overestimates the experimental cross section with about a factor of 4. Although some unexpected spikes appear, the shape is well reproduced. We are still seeking for the reasons behind the difference. This may be explained by the heavier resonances recovered by MQDT method as seen in Fig. 3.7, where a higher outgoing flux is provided. Another possibility for the difference is ignorance of the rotational structure in the DR cross sections and this will be confirmed in the further study. The results are clearly close to the experimental values for electron scattering energy above 0.10 eV. They are nearly convoluted along the experimental curve. The prominent resonances detected in experiment centered at, for instance 0.08 eV, 0.20 eV, and 0.50 eV, are all well reproduced. The broad resonance located at $E_{\rm el}$ between 0.7 and 1.2 eV is not well represented, instead three dominant peaks show up in the calculated results. This may be due to a weaker statistics in higher energy range in the experiment. The lower energy resolution prevents the resonance structure appear clearly.

The part in the square brackets of Eq. (2.86) could be regarded as the DR probability $P_{l\lambda 00}$ of the ground-state CH^+ induced by the incident electron with partial wave $l\lambda$

$$P_{l\lambda 00}(E_{\rm el}) = 1 - \sum_{l'\lambda' v' i'} S^{phys}_{l'\lambda' v' i', l\lambda 00}(E_{\rm el}) S^{\dagger phys}_{l\lambda 00, l'\lambda' v' i'}(E_{\rm el}). \tag{4.7}$$

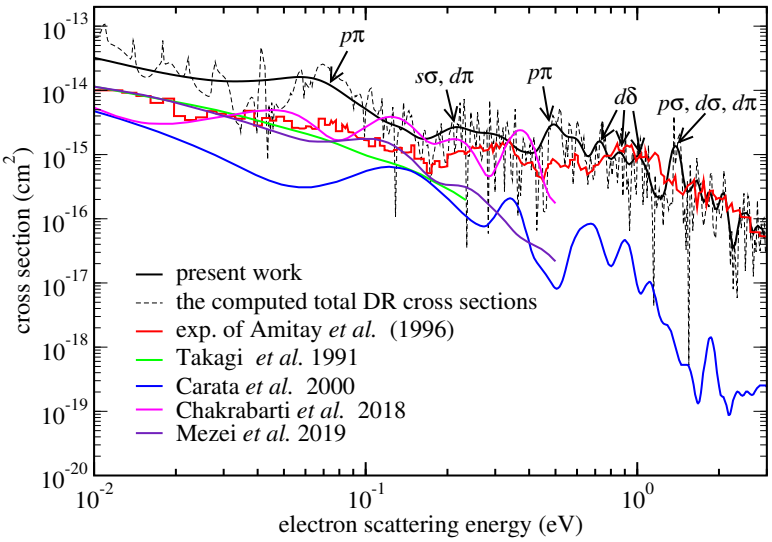

Figure 4.8: Comparison of the DR cross section of the fully relaxed CH^+. The present work in black thin dashed curve and convoluted results in black solid curve compared with experimental measurements of Amitay *et al.* in 1996 (red solid curve), theoretical results of Takagi *et al.* in 1991 (green solid curve), Carata *et al.* in 2000 (blue solid curve) and Chakrabarti *et al.* in 2018 (pink solid curve), and rotationally resolved DR cross section obtained by Mezei *et al.* in 2019 (violet solid curve). Partial waves of the incident electron are assigned to the prominent resonances by arrows pointing to peaks.

Fig. 4.9 displays the partial waves of the incident electron that make dominant contribution to the DR probabilities of ground-state CH^+. Combined target states of CH^+, they could be classified into three type as Takagi did in Ref. [29] (1) σ Rydberg states: $l\lambda = 00$ ($s\sigma$), $l\lambda = 10$ ($p\sigma$) and $l\lambda = 20$ ($d\sigma$) (2) π Rydberg states: $l\lambda = 1-1$ ($p\pi$) and $l\lambda = 2-1$ ($d\pi$), and (3) δ Rydberg state: $l\lambda = 2-2$ ($d\delta$). Note that the partial waves with $\lambda \neq 0$ are double-degenerate. For instance, the $l\lambda = 11$ and $l\lambda = 1-1$ partial waves contribute equally to the DR. As we discussed above, the low-energy neutral dissociative state is of $^2\Pi$ symmetry and dominantly contribute to the CH^+ DR. Therefore, the σ and δ Rydberg states are conjectured to represents the manifolds converging to the $^{1,3}\Pi$ first and second excited electronic states of CH^+. The π Rydberg states are the Rydberg manifolds attached to the ground state of the $^1\Sigma^+$ ground electronic state of CH^+. As we see from

(a)-(d) of Fig. 4.9, dissociation through σ and π Rydberg states below 0.10 eV are dominant. A prominent peak at about 0.08 eV occurs on the $p\pi$ partial wave, which is responsible for the corresponding broad resonance in Fig. 4.8. For the scattering energy within the range of about 0.10 eV to 1.50 eV, all the partial waves presented in the figure contribute to the DR comparably. The prominent resonances located at around 0.20 eV in the DR cross sections are mainly from $s\sigma$ and $d\pi$. The one at about 0.50 eV could be assigned to the spike of $p\pi$ partial wave and another one at about 1.4 eV is consisting of $p\sigma$, $d\sigma$ and $d\pi$ partial waves. The $d\delta$ partial wave contributes considerably to three adjacent resonances located at 0.73 eV, 0.87 eV and 1.04 eV. The $d\sigma$ partial waves dominant the dissociation of CH^+ while the scattering energy is above about 1.50 eV as we see from (c) of Fig. 4.9. The great contribution to the DR cross sections from the $d\delta$ is unexpected since this partial wave was never considered in preceding studies. The big discrepancies between the computed results and experimental measurements observed in the DR cross sections within 0.01-3.00 eV in Ref. [30] might be related the neglect of d-type partial waves, including $d\sigma$, $d\pi$ and $d\delta$.

4.5 Conclusions

In this chapter, we implemented a MQDT method (developed in chapter 3 for vibronic excitation of CH^+ by electron impact) coupled with the CAP formalism to treat the DR process of molecular ions with low-lying excited electronic states. This theoretical approach was applied the method to CH^+ with success. The low-lying bound excited electronic states and the corresponding Rydberg states are also taken into accounted. As we described in chapter 3, the fixed-nuclei R-matrix method is first used to evaluate the multichannel energy-independent electronic scattering matrix. The neutral resonance (dissociative) state is proved to be contained in such scattering matrix in the MQDT description due to the Rydberg character of the resonance state. The CAP basis is

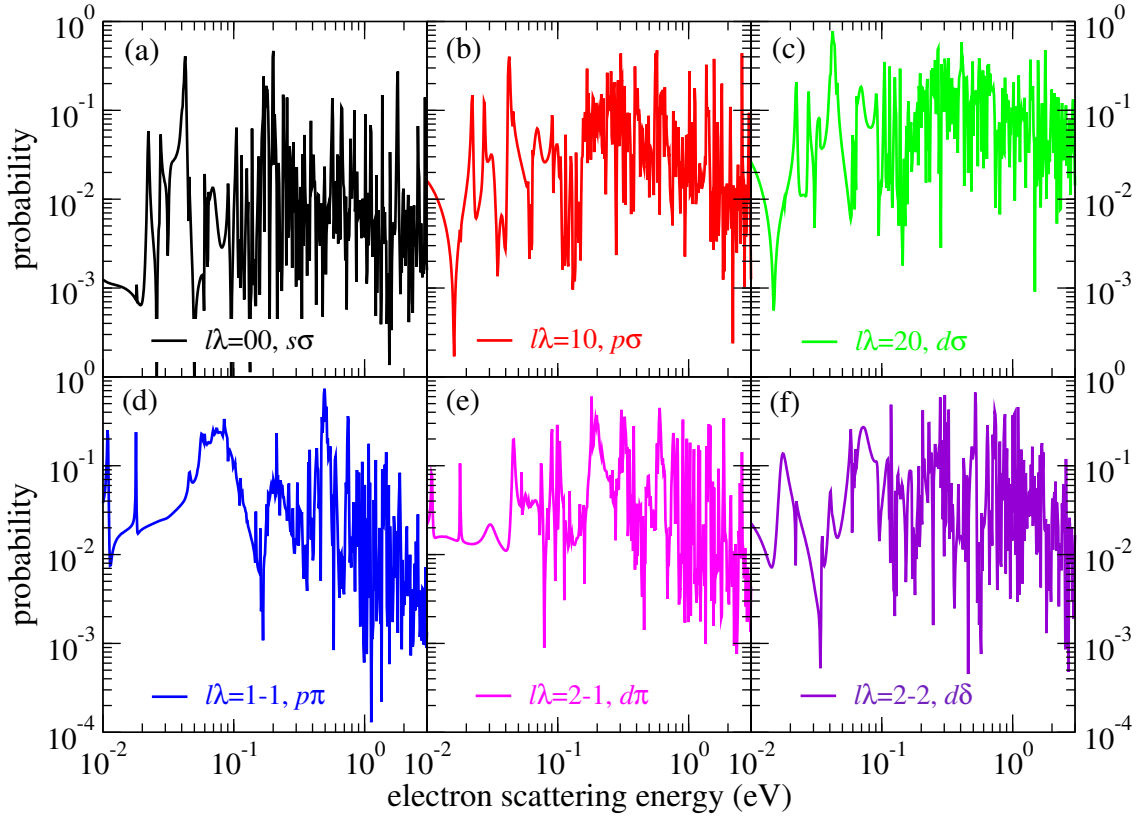

Figure 4.9: DR probabilities of the ground-state CH^+ for six dominant partial waves (a) $l\lambda = 00$, $s\sigma$ (black), (b) $l\lambda = 10$, $p\sigma$ (red), (c) $l\lambda = 20$, $d\sigma$ (green), (d) $l\lambda = 1-1$, $p\pi$ (blue), (f) $l\lambda = 2-1$, $d\pi$ (pink), and (e) $l\lambda = 2-2$, $d\delta$ (violet).

introduced by vibrational frame transformation as the vibrational ionization channel of CH^+. The actual dissociation to the fragments following the electron capture into the Rydberg states are represented by the complex part of the basis. The computed results show a good agreement with the storage-ring experimental measurements. Considering the limitation of the only treatment available for the DR of such molecular ions, we developed an relatively simplified and general theoretical approach in this chapter. Furthermore, this general theoretical approach sheds light on the extension to the treatment for polyatomic ions. However, discrepancies between the computed results and the experimental measurements are observed within electron scattering energy range of 0.01 eV to 0.10 eV. The difference maybe due to neglecting the rotational structure. Therefore, we

include the rotational structure by rotational frame transformation in a further study. The S-matrix needs to be transformed from C_{2v} to $C_{\infty v}$ symmetry point group since complex harmonics should be used in the $C_{\infty v}$ symmetry point group. The transformation was discussed in section 2.1.2. A better treatment of the DR process accounting for the rotational structures could be developed in a further study. The d-type partial waves of the incident electron including $d\sigma$, $d\pi$ and $d\delta$ are found considerably contributing to the DR of CH^+. This may explain the discrepancies observed between theory and experiment in the preceding studies.

CHAPTER 5: Conclusion and perspectives

We successfully developed a simple and efficient theoretical approach to compute the cross sections and rate constants for vibronic excitations of CH^+ by low-energy electron impact. The rotational structure of each vibrational level is neglected in the present approach such that the obtained cross sections and rate coefficients should be viewed as averaged over initial rotational states and summed over final rotational states of the corresponding vibrational level. In this approach, fixed-nuclear R-matrix method is employed to evaluate the Body-fixed scattering matrices. The three lowest $X^1\Sigma^+$, $a^3\Pi$ and $A^1\Pi$ electronic states are included in the scattering calculations. 3×3 electronic scattering matrices above the threshold of $A^1\Pi$ state at different internuclear distance R are selected to compute the vibronic transition amplitudes by vibronic frame transformation. Vibronic Rydberg resonances below the $A^1\Pi$ state are taking into account through the MQDT closed-channel elimination procedure. CH^+ is a typical case among the type of diatomic molecular ions with low-lying bound excited electronic states which are actually of large numbers, such as N_2^+, NH^+, SH^+, OH^+. Previous theoretical methods treating the electron-induced non-adiabatic couplings of such diatomic molecular ions is laborious and impractical to extend to a polyatomic molecular ions. In the approach developed in this thesis, the non-adiabatic couplings are included in the vibronic-frame-transformed 3×3 scattering matrix. The method is quite general and straightforward to implement numerically and to spread over the other diatomic molecular ions with low-lying bound excited electronic states, even polyatomic molecular ions using additional normal mode approximation for the vibrational states of the target molecules.

Furthermore, the approach is promise to describe a number of different processes taking place in the electron collisions with molecular ions. The dissociative recombination of CH^+ is treated with additional CAP formalism based on this approach. Again, taking the 3×3 electronic scattering matrices to include the interaction of electron with the target's $X^1\Sigma^+$, $a^3\Pi$ and $A^1\Pi$ electronic

states. The Rydberg-Rydberg and Rydberg-valence (molecular dissociative state) couplings could be totally represented by the constructed physical scatting matrix by the MQDT closed-channel elimination procedure. This is very different from previous treatments where the quantum defects are used to construct the interaction matrix. Vibronic ionization channels of CH^+ are introduced by a vibronic frame transformation. The outgoing vibrational basis defined by the CAP is used to simulate the dissociation flux in the low-energy e^--CH^+ collisions. The cross sections for dissociative recombination of CH^+ is thus determined and found to agree well with the storage-ring measurements. The combination of the CAP formalism and MQDT treatment was originally developed for non-crossing system (no crossing between the molecular dissociative state and ionic ground state). Applying this method to CH^+ is based the fact that the neutral dissociative state is of Rydberg character, which means the resonance state of CH that crosses with the ionic ground electronic state is essentially a Rydberg state. As we know, a Rydberg state could be recovered by the MQDT electronic closed-channel elimination procedure. The question that whether the molecular dissociative states of the other molecular ions with low-lying bound excited electronic states are also of Rydberg character needs further discuss and explore to be answered. However, the attempt for the dissociative recombination of CH^+ here is effective and significant. Every step of the method is clear because the burdensome computation of the electronic coupling is eliminated. Therefore, it ought to be possible to generalize to polyatomic molecular ions, for instance C_2H^+, which plays an important role in the plasma waste treatment modeling. It will be a revolution of our ability to compute the cross sections for dissociative recombination of molecular ions with low-lying bound excited electronic states.

As pointed out in the manuscript, a better treatment of the vibronic excitation and dissociative recombination processes accounting for rotational resonances is possible. To do this, further development are needed, in particular, transformation of the scattering matrix from C_{2v} to $C_{\infty v}$ symmetry. Besides, inclusion of the rotational structure in the dissociative recombination may

improve the agreement between the computed cross sections and the experimental measurements. The computation of the cross section for dissociative excitation of CH^+ is our another plan since it could be treated within our approach. The storage-ring measurements are available to compare with the computed results. The most challenge work is extending our approach to the polyatomic molecular ions with low-lying bound excited electronic states, since the normal approximation is valid near the equilibrium, i.e. the approximation works at very low vibrational levels and the studies on the vibronic excitations are hardly found so far.

APPENDIX A: The fitting parameters of the rate coefficients for the vibronic excitations of CH^+

Table A.1: Parameters a_0, a_1, and a_2 of the polynomial $P^{fit}_{vi,v'i'}(x)$ of Eq. (3.2) and (3.3) for several pairs of initial and final vibrational levels of the ground electronic state $X^1\Sigma^+$ of CH^+. We specify the threshold energy $\Delta_{v'i',vi}$ for the excitation process in the pair $v'i', vi$ in the second column of each table. For the de-excitation process, $\Delta_{vi,v'i'}$=0.

$v'i' \leftrightarrow vi$	$\Delta_{v'i',vi}$(K)	a_0	a_1	a_2
$10 \leftrightarrow 00$	3934	2.90×10^{-6}	-1.20×10^{-7}	2.30×10^{-9}
$20 \leftrightarrow 00$	7700	1.10×10^{-6}	1.60×10^{-8}	-6.60×10^{-9}
$30 \leftrightarrow 00$	11299	2.90×10^{-7}	5.00×10^{-8}	-5.10×10^{-9}
$20 \leftrightarrow 10$	3766	7.85×10^{-7}	2.17×10^{-7}	-1.22×10^{-8}
$30 \leftrightarrow 10$	7365	4.57×10^{-7}	1.02×10^{-7}	-8.64×10^{-9}
$30 \leftrightarrow 20$	3599	2.39×10^{-6}	2.51×10^{-8}	-5.26×10^{-9}

Table A.2: Same as table A.1 for the electronic state $a^3\Pi$.

$v'i' \leftrightarrow vi$	$\Delta_{v'i',vi}$(K)	a_0	a_1	a_2
$11 \leftrightarrow 01$	3633	5.43×10^{-6}	4.68×10^{-7}	-4.41×10^{-8}
$21 \leftrightarrow 01$	7039	2.01×10^{-6}	5.14×10^{-9}	-3.18×10^{-9}
$31 \leftrightarrow 01$	10216	1.17×10^{-6}	-3.37×10^{-8}	-2.65×10^{-9}
$21 \leftrightarrow 11$	3405	7.53×10^{-6}	6.95×10^{-8}	-2.30×10^{-8}
$31 \leftrightarrow 11$	6583	2.99×10^{-6}	3.58×10^{-8}	-2.48×10^{-9}
$31 \leftrightarrow 21$	3178	6.55×10^{-6}	2.04×10^{-7}	-8.40×10^{-9}

Table A.3: Same as table A.1 for the electronic state $A^1\Pi$.

$v'i' \leftrightarrow vi$	$\Delta_{v'i',vi}$(K)	a_0	a_1	a_2
$12 \leftrightarrow 02$	2290	5.44×10^{-6}	1.74×10^{-7}	-1.09×10^{-8}
$22 \leftrightarrow 02$	4271	2.16×10^{-6}	-1.24×10^{-8}	-6.08×10^{-10}
$32 \leftrightarrow 02$	5971	1.49×10^{-6}	-8.82×10^{-9}	5.33×10^{-10}
$22 \leftrightarrow 12$	1981	1.33×10^{-5}	-1.13×10^{-7}	-3.47×10^{-10}
$32 \leftrightarrow 12$	3680	7.74×10^{-6}	8.39×10^{-9}	-8.35×10^{-10}
$32 \leftrightarrow 22$	1699	3.48×10^{-6}	-1.17×10^{-8}	6.50×10^{-10}

Table A.4: Same as table A.1 for vibronic transitions $vX^1\Sigma^+ \leftrightarrow v'a^3\Pi$.

$v'i' \leftrightarrow vi$	$\Delta_{v'i',vi}$(K)	a_0	a_1	a_2
$01 \leftrightarrow 00$	13572	5.10×10^{-6}	-1.20×10^{-8}	2.30×10^{-9}
$11 \leftrightarrow 00$	17205	3.50×10^{-7}	2.70×10^{-7}	-2.20×10^{-8}
$21 \leftrightarrow 00$	20610	5.00×10^{-7}	3.80×10^{-9}	-3.80×10^{-10}
$31 \leftrightarrow 00$	23788	2.00×10^{-7}	5.70×10^{-8}	-5.70×10^{-9}
$01 \leftrightarrow 10$	9638	4.90×10^{-7}	2.57×10^{-7}	-1.84×10^{-8}
$11 \leftrightarrow 10$	13271	4.30×10^{-6}	5.30×10^{-8}	-2.80×10^{-9}
$21 \leftrightarrow 10$	16677	7.13×10^{-7}	1.72×10^{-8}	-6.09×10^{-10}
$31 \leftrightarrow 10$	19854	6.00×10^{-7}	1.98×10^{-8}	-5.12×10^{-10}
$01 \leftrightarrow 20$	5872	7.06×10^{-7}	1.55×10^{-7}	-1.78×10^{-8}
$11 \leftrightarrow 20$	9505	1.93×10^{-6}	-3.01×10^{-8}	-5.86×10^{-9}
$21 \leftrightarrow 20$	12910	3.97×10^{-6}	-7.95×10^{-8}	6.09×10^{-9}
$31 \leftrightarrow 20$	16088	9.13×10^{-7}	2.49×10^{-8}	-2.09×10^{-9}
$01 \leftrightarrow 30$	2273	3.24×10^{-7}	4.24×10^{-8}	-2.23×10^{-9}
$11 \leftrightarrow 30$	5906	8.23×10^{-7}	1.61×10^{-8}	-3.03×10^{-9}
$21 \leftrightarrow 30$	9311	1.77×10^{-6}	-1.22×10^{-8}	-4.08×10^{-9}
$31 \leftrightarrow 30$	12489	3.31×10^{-6}	-4.24×10^{-8}	3.17×10^{-10}

Table A.5: Same as table A.1 for vibronic transitions $vX^1\Sigma^+ \leftrightarrow v'A^1\Pi$.

$v'i' \leftrightarrow vi$	$\Delta_{v'i',vi}$(K)	a_0	a_1	a_2
$02 \leftrightarrow 00$	34147	3.30×10^{-6}	-2.10×10^{-7}	9.90×10^{-9}
$12 \leftrightarrow 00$	36437	1.70×10^{-6}	-7.70×10^{-8}	2.90×10^{-9}
$22 \leftrightarrow 00$	38418	6.70×10^{-7}	-1.20×10^{-8}	4.70×10^{-10}
$32 \leftrightarrow 00$	40117	3.40×10^{-7}	-2.70×10^{-9}	1.50×10^{-10}
$02 \leftrightarrow 10$	30213	1.21×10^{-6}	4.41×10^{-8}	-3.94×10^{-9}
$12 \leftrightarrow 10$	32503	8.20×10^{-7}	-2.90×10^{-8}	-9.71×10^{-10}
$22 \leftrightarrow 10$	34484	1.01×10^{-6}	2.69×10^{-9}	-3.61×10^{-10}
$32 \leftrightarrow 10$	36183	7.74×10^{-7}	1.83×10^{-8}	-9.69×10^{-10}
$02 \leftrightarrow 20$	26446	4.39×10^{-7}	2.69×10^{-8}	-1.11×10^{-9}
$12 \leftrightarrow 20$	28737	1.17×10^{-6}	-2.14×10^{-8}	7.31×10^{-10}
$22 \leftrightarrow 20$	30718	2.36×10^{-7}	8.67×10^{-10}	-5.88×10^{-11}
$32 \leftrightarrow 20$	32417	3.82×10^{-7}	-5.63×10^{-9}	3.06×10^{-10}
$02 \leftrightarrow 30$	22847	4.27×10^{-7}	-1.51×10^{-8}	-5.84×10^{-11}
$12 \leftrightarrow 30$	25138	1.46×10^{-6}	2.16×10^{-8}	-2.89×10^{-9}
$22 \leftrightarrow 30$	27119	7.21×10^{-7}	1.48×10^{-9}	-3.23×10^{-10}
$32 \leftrightarrow 30$	28818	1.19×10^{-6}	-1.90×10^{-8}	1.04×10^{-9}

Table A.6: Same as table A.1 for vibronic transitions $va^3\Pi \leftrightarrow v'A^1\Pi$.

$v'i' \leftrightarrow vi$	$\Delta_{v'i',vi}$(K)	a_0	a_1	a_2
$02 \leftrightarrow 01$	20575	3.28×10^{-6}	4.81×10^{-8}	-7.56×10^{-9}
$12 \leftrightarrow 01$	22865	7.02×10^{-7}	2.32×10^{-9}	-1.11×10^{-9}
$22 \leftrightarrow 01$	24846	5.83×10^{-7}	-4.73×10^{-9}	-2.56×10^{-11}
$32 \leftrightarrow 01$	26545	4.43×10^{-7}	2.81×10^{-9}	-1.53×10^{-10}
$02 \leftrightarrow 11$	16941	5.03×10^{-6}	2.61×10^{-7}	-1.85×10^{-8}
$12 \leftrightarrow 11$	19232	1.08×10^{-6}	1.17×10^{-8}	-3.14×10^{-9}
$22 \leftrightarrow 11$	21213	1.52×10^{-6}	-4.00×10^{-9}	-3.32×10^{-10}
$32 \leftrightarrow 11$	22912	6.47×10^{-7}	-3.27×10^{-9}	1.69×10^{-10}
$02 \leftrightarrow 21$	13536	1.39×10^{-6}	1.24×10^{-7}	-6.56×10^{-9}
$12 \leftrightarrow 21$	15826	3.69×10^{-6}	-1.94×10^{-8}	9.08×10^{-10}
$22 \leftrightarrow 21$	17807	7.26×10^{-7}	-2.50×10^{-8}	1.19×10^{-9}
$32 \leftrightarrow 21$	19507	5.32×10^{-7}	6.38×10^{-9}	-3.78×10^{-10}
$02 \leftrightarrow 31$	10358	1.30×10^{-6}	-9.89×10^{-8}	2.13×10^{-9}
$12 \leftrightarrow 31$	12649	2.41×10^{-6}	7.13×10^{-8}	-5.00×10^{-9}
$22 \leftrightarrow 31$	14630	1.54×10^{-6}	9.42×10^{-9}	-6.05×10^{-10}
$32 \leftrightarrow 31$	16329	1.08×10^{-6}	-1.35×10^{-9}	4.25×10^{-11}

APPENDIX B: La synthèse

La thèse est consacrée à l'étude des collisions d'électrons à basse énergie avec des molécules d'hydrocarbures et des ions moléculaires (C_xH_y) afin de produire des données importantes et cruciales, notamment des sections transversales et des coefficients de vitesse, qui pourraient être utilisées comme base de données pour la modélisation du traitement des déchets par plasma. Parmi la famille des ions moléculaires d'hydrocarbures, nous avons sélectionné l'ion CH^+ le plus simple présentant un intérêt astrophysique et technologique comme travail de départ. Nous avons développé des traitements théoriques pour calculer les sections transversales pour la (dé)excitation vibronique et la recombinaison dissociative du CH^+ par impact d'électrons à basse énergie. Ces recherches serviront de prototype pour notre future étude sur les ions moléculaires d'hydrocarbures polyatomiques.

Nous étudions la (dés)excitation vibronique et la recombinaison dissociative (DR) de CH^+ produites par la collision d'électrons de faible énergie. Nous développons d'abord une approche théorique de la (dés)excitation vibronique de CH^+ par collision d'électrons. Dans cette approche nous utilisons la méthode de la matrice R à noyaux fixes afin de calculer les matrices de diffusion électron-ion dans l'approximation de Born-Oppenheimer. Nous appliquons ensuite la méthode connue comme « vibronic frame transformation » et la procédure d'élimination des canaux de diffusion fermés dans l'esprit de la théorie des défauts quantiques moléculaires pour construire une matrice de diffusion dépendant de l'énergie qui décrit les interactions entre les canaux vibroniques de l'ion cible induits par l'électron incident. La matrice de diffusion obtenue tient compte de la série de résonances vibroniques de Rydberg dans le spectre de collision. Nous avons calculé les sections efficaces de diffusion pour différentes combinaisons d'états vibroniques initiaux et finaux. Nous avons trouvé un bon accord entre les sections efficaces de diffusion obtenues par la théorie des défauts quantiques et par un calcul direct de la matrice R, ce qui indique que l'approche que

nous avons suivie est un outil fiable pour la détermination des sections efficaces de (dés)excitation vibronique pour des cibles avec des résonances électroniques de faible énergie. L'approche pourrait être appliquée aux ions ayant des états excités électroniques de faible altitude. Ces ions étaient connus pour être difficiles à traiter théoriquement en utilisant les méthodes théoriques précédentes. Il existe un grand nombre de radicaux qui pourraient, en principe, être considérés en utilisant l'approche suggérée. L'approche est assez générale et peut être appliquée à un certain nombre de processus différents, ayant lieu lors de collisions d'ions moléculaires avec des électrons, y compris l'excitation rovibronique, l'excitation dissociative (DE), la photoionisation et la recombinaison dissociative (DR).

Dans le même cadre que celui appliqué aux (dés)excitations vibroniques, nous tentons de développer une approche théorique utilisant ce cadre de traitement MQDT en conjonction avec la base CAP pour calculer la section efficace de diffusion pour la recombinaison dissociative à basse énergie de CH^+ en couplant la fonction de base de l'onde sortante définie par le potentiel d'absorption complexe. Un calcul ab initio utilisant cette approche est appliqué à l'état-sol CH^+. Cela a été fait en prenant en compte la contribution des trois états ioniques $X^1\Sigma^+$, $a^3\Pi$ and $A^1\Pi$ de plus basse énergie et les séries de Rydberg convergeant vers ces états. Les trois états électroniques les plus bas de CH^+ sont inclus dans les calculs de la matrice R. Les couplages Rydberg-Rydberg entre les séries de Rydberg attachées à ces trois états électroniques sont contenus dans la matrice de diffusion 3×3 dépendante de l'énergie de e^--CH^+, contrainte par la procédure d'élimination à canal fermé MQDT. Les sections efficaces de DR que nous avons obtenues sont en bon accord quantitatif avec les résultats des expériences et présentent notamment une résonance analogue à celle qu'on observe dans la courbe de la section efficace de diffusion expérimentale. L'origine des principales résonances que nous avons obtenues est analysée par le calcul des probabilités de DR pour les ondes partielles de l'électron incident. On constate que les ondes partielles de type d, notamment $d\sigma$, $d\pi$ et $d\delta$, contribuent considérablement à la DR de l'état fondamental de CH^+.

Cela peut expliquer les écarts observés entre la théorie et l'expérience dans les études précédentes.

Le développement de cette approche théorique est basé sur un point très critique, à savoir que l'état dissociatif neutre doublement excité dans la collision d'électrons avec des ions moléculaires de ce type est généralement de type Rydberg, surtout à courte distance internucléaire. Ce fait suggère que l'état dissociatif neutre peut apparaître comme des résonances de Rydberg dans le processus de collision électron-ion. Ce type de résonances pourrait être, comme nous le savons, reproduit par la procédure d'élimination électronique à canal fermé MQDT. Le couplage électronique entre l'état continu inital du système de collision électron-ion et l'état dissociatif neutre (résonance) pourrait ainsi être également inclus dans la matrice de diffusion à l'aide de la procédure d'élimination. En d'autres termes, nous n'avons pas besoin d'obtenir explicitement les PEC des états dissociatifs neutres (résonance) comme la méthode introduite ci-dessus pour le système de croisement des courbes. CH^+ est un cas typique parmi les types d'ions moléculaires diatomiques ayant des états électroniques excités liés à faible distance qui sont en fait en grand nombre, comme N_2^+ , NH^+, SH^+, OH^+. Les méthodes théoriques précédentes traitant les couplages non-adiabatiques induits par les électrons de tels ions moléculaires diatomiques sont laborieuses et peu pratiques pour les étendre aux ions moléculaires polyatomiques. Dans l'approche développée dans cette thèse, les couplages non adiabatiques sont inclus dans la matrice de diffusion 3×3 transformée en cadre vibratoire. La méthode est assez générale et simple à mettre en œuvre numériquement et à répartir sur les autres ions moléculaires diatomiques avec des états électroniques excités liés à basse altitude, même les ions moléculaires polyatomiques en utilisant une approximation supplémentaire en mode normal pour les états vibratoires des molécules cibles.

LIST OF REFERENCES

[1] A. Phelps and J. Pack, "Electron collision frequencies in nitrogen and in the lower ionosphere," *Physical Review Letters*, vol. 3, no. 7, p. 340, 1959.

[2] D. L. Huestis, S. W. Bougher, J. L. Fox, M. Galand, R. E. Johnson, J. I. Moses, and J. C. Pickering, "Cross sections and reaction rates for comparative planetary aeronomy," *Space science reviews*, vol. 139, no. 1-4, p. 63, 2008.

[3] A. Luque, U. Ebert, and W. Hundsdorfer, "Interaction of streamer discharges in air and other oxygen-nitrogen mixtures," *Physical review letters*, vol. 101, no. 7, p. 075005, 2008.

[4] W. D. Geppert and M. Larsson, "Dissociative recombination in the interstellar medium and planetary ionospheres," *Molecular Physics*, vol. 106, no. 16-18, pp. 2199–2226, 2008.

[5] B. Boudaiffa, P. Cloutier, D. Hunting, M. A. Huels, and L. Sanche, "Resonant formation of DNA strand breaks by low-energy (3 to 20 eV) electrons," *Science*, vol. 287, no. 5458, pp. 1658–1660, 2000.

[6] A. Karpatne, D. P. Breden, and L. Raja, "Simulations of spark-plug transient plasma breakdown in automotive internal combustion engines," tech. rep., SAE Technical Paper, 2017.

[7] L. J. Kieffer, "A compilation of electron collision cross section data for modeling gas discharge lasers," tech. rep., NATIONAL STANDARD REFERENCE DATA SYSTEM, 1973.

[8] N. J. Wagner, W. W. Gerberich, and J. V. Heberlein, "Thermal plasma chemical vapor deposition of wear-resistant, hard Si-C-N coatings," *Surface and Coatings Technology*, vol. 201, no. 7, pp. 4168–4173, 2006.

[9] D. M. Manos and D. L. Flamm, "Plasma etching: an introduction.(retroactive coverage)," *Academic Press, Inc.(United States), 1989,*, p. 476, 1989.

[10] D. L. Flamm and O. Auciello, *Plasma deposition, treatment, and etching of polymers: the treatment and etching of polymers*. Elsevier, 2012.

[11] D. O'kane and K. Mittal, "Plasma cleaning of metal surfaces," *Journal of Vacuum Science and Technology*, vol. 11, no. 3, pp. 567–569, 1974.

[12] J. Heberlein and A. B. Murphy, "Thermal plasma waste treatment," *Journal of Physics D: Applied Physics*, vol. 41, no. 5, p. 053001, 2008.

[13] G. J. Hedberg and E. E. Knights, "Destruction of hydrocarbon materials," Jan. 16 1996. US Patent 5,484,978.

[14] R. Kalinenko, A. Kuznetsov, A. Levitsky, V. Messerle, Y. A. Mirokhin, L. Polak, Z. Sakipov, and A. Ustimenko, "Pulverized coal plasma gasification," *Plasma Chemistry and Plasma Processing*, vol. 13, no. 1, pp. 141–167, 1993.

[15] L. Mazzoni, R. Ahmed, and I. Janajreh, "Plasma gasification of two waste streams: municipal solid waste and hazardous waste from the oil and gas industry," *Energy Procedia*, vol. 105, pp. 4159–4166, 2017.

[16] E. Gomez, D. A. Rani, C. Cheeseman, D. Deegan, M. Wise, and A. Boccaccini, "Thermal plasma technology for the treatment of wastes: a critical review," *Journal of hazardous materials*, vol. 161, no. 2-3, pp. 614–626, 2009.

[17] M. Capitelli, I. Armenise, E. Bisceglie, D. Bruno, R. Celiberto, G. Colonna, G. D'Ammando, O. De Pascale, F. Esposito, C. Gorse, *et al.*, "Thermodynamics, transport and kinetics of equilibrium and non-equilibrium plasmas: a state-to-state approach," *Plasma Chemistry and Plasma Processing*, vol. 32, no. 3, pp. 427–450, 2012.

[18] K. Chakrabarti, J. Z. Mezei, O. Motapon, A. Faure, O. Dulieu, K. Hassouni, and I. Schneider, "Dissociative recombination of the CH^+ molecular ion at low energy," *Journal of Physics B: Atomic, Molecular and Optical Physics*, vol. 51, no. 10, p. 104002, 2018.

[19] K. Hassouni, F. Silva, and A. Gicquel, "Modelling of diamond deposition microwave cavity generated plasmas," *Journal of Physics D: Applied Physics*, vol. 43, no. 15, p. 153001, 2010.

[20] R. Janev and D. Reiter, "Collision processes of CH_y and CH_y^+ hydrocarbons with plasma electrons and protons," *Physics of Plasmas*, vol. 9, no. 9, pp. 4071–4081, 2002.

[21] D. R. Bates and L. Spitzer Jr, "The density of molecules in interstellar space.," *The Astrophysical Journal*, vol. 113, p. 441, 1951.

[22] J. Bardsley and B. Junker, "Dissociative recombination of CH^+ ions," *The Astrophysical Journal*, vol. 183, p. L135, 1973.

[23] M. Krauss and P. Jlienne, "Dissociative recombination E+ CH^+.," *The Astrophysical Journal*, vol. 183, p. L139, 1973.

[24] A. Giusti-Suzor and H. Lefebvre-Brion, "The dissociative recombination of CH^+ ions," *The Astrophysical Journal*, vol. 214, pp. L101–L103, 1977.

[25] A. Douglas and G. Herzberg, "Note on CH^+ in interstellar space and in the laboratory.," *The Astrophysical Journal*, vol. 94, p. 381, 1941.

[26] W. S. Adams, "Some results with the COUDÉ spectrograph of the mount wilson observatory.," *The Astrophysical Journal*, vol. 93, p. 11, 1941.

[27] https://euro-fusion.org/jet/.

[28] S. Lepp, P. Stancil, and A. Dalgarno, "Atomic and molecular processes in the early universe," *Journal of Physics B: Atomic, Molecular and Optical Physics*, vol. 35, no. 10, p. R57, 2002.

[29] H. Takagi, N. Kosugi, and M. Le Dourneuf, "Dissociative recombination of CH^+," *Journal of Physics B: Atomic, Molecular and Optical Physics*, vol. 24, no. 3, p. 711, 1991.

[30] L. Carata, A. Orel, M. Raoult, I. Schneider, and A. Suzor-Weiner, "Core-excited resonances in the dissociative recombination of CH^+ and CD^+," *Physical Review A*, vol. 62, no. 5, p. 052711, 2000.

[31] D. Little, K. Chakrabarti, J. Z. Mezei, I. Schneider, and J. Tennyson, "Dissociative recombination of N^{2+}: An ab initio study," *Physical Review A*, vol. 90, no. 5, p. 052705, 2014.

[32] I. Schneider, I. Rabadán, L. Carata, L. Andersen, A. Suzor-Weiner, and J. Tennyson, "Dissociative recombination of NO^+: calculations and comparison with experiment," *Journal of Physics B: Atomic, Molecular and Optical Physics*, vol. 33, no. 21, p. 4849, 2000.

[33] C. Lee, "Multichannel dissociative recombination theory," *Physical Review A*, vol. 16, no. 1, p. 109, 1977.

[34] A. Giusti, "A multichannel quantum defect approach to dissociative recombination," *Journal of Physics B: Atomic and Molecular Physics*, vol. 13, no. 19, p. 3867, 1980.

[35] I. N. Levine, D. H. Busch, and H. Shull, *Quantum chemistry*, vol. 6. Pearson Prentice Hall Upper Saddle River, NJ, 2009.

[36] V. Heine, *Group theory in quantum mechanics: an introduction to its present usage*. Courier Corporation, 2007.

[37] http://symmetry.jacobs-university.de/.

[38] M. Khamesian, M. Ayouz, J. Singh, and V. Kokoouline, "Cross sections and rate coefficients for rotational excitation of HeH^+ molecule by electron impact," *Atoms*, vol. 6, no. 3, p. 49, 2018.

[39] T. Lee, "Real harmonic analysis on the special orthogonal group," *arXiv preprint arXiv:1809.10533*, 2018.

[40] http://www.basissetexchange.org.

[41] J. Light, I. Hamilton, and J. Lill, "Generalized discrete variable approximation in quantum mechanics," *The Journal of chemical physics*, vol. 82, no. 3, pp. 1400–1409, 1985.

[42] Z. Bačić, R. Whitnell, D. Brown, and J. Light, "Localized representations for large amplitude molecular vibrations," *Computer physics communications*, vol. 51, no. 1-2, pp. 35–47, 1988.

[43] V. Kokoouline, O. Dulieu, R. Kosloff, and F. Masnou-Seeuws, "Mapped fourier methods for long-range molecules: Application to perturbations in the Rb2(0u+) photoassociation spectrum," *The Journal of chemical physics*, vol. 110, no. 20, pp. 9865–9876, 1999.

[44] C. C. Marston and G. G. Balint-Kurti, "The Fourier grid Hamiltonian method for bound state eigenvalues and eigenfunctions," *The Journal of chemical physics*, vol. 91, no. 6, pp. 3571–3576, 1989.

[45] O. I. Tolstikhin, V. N. Ostrovsky, and H. Nakamura, "Siegert pseudostate formulation of scattering theory: One-channel case," *Physical Review A*, vol. 58, no. 3, p. 2077, 1998.

[46] E. L. Hamilton and C. H. Greene, "Competition among molecular fragmentation channels described with siegert channel pseudostates," *Physical review letters*, vol. 89, no. 26, p. 263003, 2002.

[47] A. Vibok and G. Balint-Kurti, "Parametrization of complex absorbing potentials for time-dependent quantum dynamics," *The Journal of Physical Chemistry*, vol. 96, no. 22, pp. 8712–8719, 1992.

[48] N. Moiseyev, P. Certain, and F. Weinhold, "Resonance properties of complex-rotated hamiltonians," *Molecular Physics*, vol. 36, no. 6, pp. 1613–1630, 1978.

[49] B. Schneider and T. Rescigno, "Complex Kohn variational method: Application to low-energy electron-molecule collisions," *Physical Review A*, vol. 37, no. 10, p. 3749, 1988.

[50] K. Takatsuka and V. McKoy, "Extension of the Schwinger variational principle beyond the static-exchange approximation," *Physical Review A*, vol. 24, no. 5, p. 2473, 1981.

[51] W. Kohn, "Variational methods in nuclear collision problems," *Physical Review*, vol. 74, no. 12, p. 1763, 1948.

[52] T. H. McCurdy and I. G. Morgan, "Tests of the martingale hypothesis for foreign currency futures with time-varying volatility," *International Journal of Forecasting*, vol. 3, no. 1, pp. 131–148, 1987.

[53] N. Douguet, S. F. dos Santos, V. Kokoouline, and A. Orel, "Simplified model to describe the dissociative recombination of linear polyatomic ions of astrophysical interest," in *EPJ Web of Conferences*, vol. 84, p. 07003, EDP Sciences, 2015.

[54] N. Douguet, S. Fonseca dos Santos, M. Raoult, O. Dulieu, A. E. Orel, and V. Kokoouline, "Theoretical study of radiative electron attachment to CN, C_2H, and C_4H radicals," *The Journal of chemical physics*, vol. 142, no. 23, p. 234309, 2015.

[55] J. Schwinger, "A variational principle for scattering problems," in *Physical Review*, vol. 72, pp. 742–742, AMERICAN PHYSICAL SOC ONE PHYSICS ELLIPSE, COLLEGE PK, MD 20740-3844 USA, 1947.

[56] R. F. da Costa, M. T. d. N. Varella, M. H. Bettega, and M. A. Lima, "Recent advances in the application of the schwinger multichannel method with pseudopotentials to electron-molecule collisions," *The European Physical Journal D*, vol. 69, no. 6, p. 159, 2015.

[57] J. Tennyson, "Electron-molecule collision calculations using the R-matrix method," *Physics Reports*, vol. 491, no. 2-3, pp. 29–76, 2010.

[58] P. G. Burke, *R-matrix theory of atomic collisions: Application to atomic, molecular and optical processes*, vol. 61. Springer Science & Business Media, 2011.

[59] E. P. Wigner, "Resonance reactions," *Physical Review*, vol. 70, no. 9-10, p. 606, 1946.

[60] E. P. Wigner and L. Eisenbud, "Higher angular momenta and long range interaction in resonance reactions," *Physical Review*, vol. 72, no. 1, p. 29, 1947.

[61] P. Burke, A. Hibbert, and W. Robb, "Electron scattering by complex atoms," *Journal of Physics B: Atomic and Molecular Physics*, vol. 4, no. 2, p. 153, 1971.

[62] W. Robb, "The use of the R-matrix method in atomic calculations," *Computer Physics Communications*, vol. 4, no. 1, pp. 16–19, 1972.

[63] P. Burke, "The R-matrix method in atomic physics," *Computer Physics Communications*, vol. 6, no. 6, pp. 288–302, 1973.

[64] B. I. Schneider, "R-matrix theory for electron-molecule collisions using analytic basis set expansions. ii. Electron-H_2 scattering in the static-exchange model," *Physical Review A*, vol. 11, no. 6, p. 1957, 1975.

[65] B. Schneider and P. Hay, "Elastic scattering of electrons from F_2: An R-matrix calculation," *Physical Review A*, vol. 13, no. 6, p. 2049, 1976.

[66] P. Burke, "Theory of low energy electron-molecule collisions," in *Advances in Atomic and Molecular Physics*, vol. 15, pp. 471–506, Elsevier, 1979.

[67] P. G. Burke and J. F. Williams, "Electron scattering by atoms and molecules," *Physics Reports*, vol. 34, no. 5, pp. 325–369, 1977.

[68] B. M. Nestmann, K. Pfingst, and S. D. Peyerimhoff, "R-matrix calculation for electron-methane scattering cross sections," *Journal of Physics B: Atomic, Molecular and Optical Physics*, vol. 27, no. 11, p. 2297, 1994.

[69] K. Pfingst, B. M. Nestmann, and S. D. Peyerimhoff, "An R-matrix approach for electron scattering off polyatomic molecules," *Journal of Physics B: Atomic, Molecular and Optical Physics*, vol. 27, no. 11, p. 2283, 1994.

[70] L. Morgan, C. Gillan, J. Tennyson, and X. Chen, "R-matrix calculations for polyatomic molecules: electron scattering by," *Journal of Physics B: Atomic, Molecular and Optical Physics*, vol. 30, no. 18, p. 4087, 1997.

[71] L. A. Morgan, J. Tennyson, and C. J. Gillan, "The UK molecular r-matrix codes," *Computer physics communications*, vol. 114, no. 1-3, pp. 120–128, 1998.

[72] J. Tennyson and L. A. Morgan, "Electron collisions with polyatomic molecules using the R-matrix method," *Philosophical Transactions of the Royal Society of London. Series A: Mathematical, Physical and Engineering Sciences*, vol. 357, no. 1755, pp. 1161–1173, 1999.

[73] P. Burke* and J. Tennyson, "R-matrix theory of electron molecule scattering," *Molecular Physics*, vol. 103, no. 18, pp. 2537–2548, 2005.

[74] P. G. Burke and H. M. Schey, "Elastic scattering of low-energy electrons by atomic hydrogen," *Physical Review*, vol. 126, no. 1, p. 147, 1962.

[75] M. Crees, "Asypck, a program for calculating asymptotic solutions of the coupled equations of electron collision theory," *Computer Physics Communications*, vol. 19, no. 1, pp. 103–137, 1980.

[76] M. Crees, "ASYPCK2, an extended version of ASYPCK," *Computer Physics Communications*, vol. 23, no. 2, pp. 181–198, 1981.

[77] M. Gailitis, "New forms of asymptotic expansions for wavefunctions of charged-particle scattering," *Journal of Physics B: Atomic and Molecular Physics*, vol. 9, no. 5, p. 843, 1976.

[78] K. Baluja, P. Burke, and L. Morgan, "R-matrix propagation program for solving coupled second-order differential equations," *Computer Physics Communications*, vol. 27, no. 3, pp. 299–307, 1982.

[79] L. A. Morgan, "A generalized R-matrix propagation program for solving coupled second-order differential equations," 1984.

[80] G. J. Schulz, "Resonances in electron impact on diatomic molecules," *Reviews of Modern Physics*, vol. 45, no. 3, p. 423, 1973.

[81] H. Feshbach, "Unified theory of nuclear reactions," *Annals of Physics*, vol. 5, no. 4, pp. 357–390, 1958.

[82] H. Feshbach, "A unified theory of nuclear reactions. ii," *Annals of Physics*, vol. 19, no. 2, pp. 287–313, 1962.

[83] M. McCartney, P. Burke, L. Morgan, and C. Gillan, "Resonance effects in low energy electron scattering by HCl," *Journal of Physics B: Atomic, Molecular and Optical Physics*, vol. 23, no. 15, p. L415, 1990.

[84] M. Larsson and A. E. Orel, *Dissociative recombination of molecular ions*. Cambridge University Press, 2008.

[85] E. Chang and U. Fano, "Theory of electron-molecule collisions by frame transformations," *Physical Review A*, vol. 6, no. 1, p. 173, 1972.

[86] N. Lane, "The theory of electron-molecule collisions," *Reviews of Modern Physics*, vol. 52, no. 1, p. 29, 1980.

[87] M. A. Morrison, "The physics of low-energy electron-molecule collisions: a guide for the perplexed and the uninitiated," *Australian journal of physics*, vol. 36, no. 3, pp. 239–286, 1983.

[88] B.-H. Choi and E. Merzbacher, "Angular distribution of fast electrons ejected from k and l shells by proton impact," *Physical Review A*, vol. 1, no. 2, p. 299, 1970.

[89] M. Ayouz and V. Kokoouline, "Cross sections and rate coefficients for rovibrational excitation of HeH^+ isotopologues by electron impact," *Atoms*, vol. 7, no. 3, p. 67, 2019.

[90] M. Seaton, "Quantum defect theory i. general formulation," *Proceedings of the Physical Society*, vol. 88, no. 4, p. 801, 1966.

[91] C. H. Greene and C. Jungen, "Molecular applications of quantum defect theory," in *Advances in atomic and molecular physics*, vol. 21, pp. 51–121, Elsevier, 1985.

[92] M. Seaton, "Quantum defect theory ii. illustrative one-channel and two-channel problems," *Proceedings of the Physical Society*, vol. 88, no. 4, p. 815, 1966.

[93] M. Seaton, "Quantum defect theory," *Reports on Progress in Physics*, vol. 46, no. 2, p. 167, 1983.

[94] M. Aymar, C. H. Greene, and E. Luc-Koenig, "Multichannel rydberg spectroscopy of complex atoms," *Reviews of Modern Physics*, vol. 68, no. 4, p. 1015, 1996.

[95] L. Carata, I. Schneider, and A. Suzor-Weiner, "The role of Rydberg states in dissociative recombination, as revealed by ion storage ring experiments," *Philosophical Transactions of the Royal Society of London. Series A: Mathematical, Physical and Engineering Sciences*, vol. 355, no. 1729, pp. 1677–1691, 1997.

[96] D. Bates, "Dissociative recombination," *Physical Review*, vol. 78, no. 4, p. 492, 1950.

[97] T. F. O'Malley, "Theory of dissociative attachment," *Physical Review*, vol. 150, no. 1, p. 14, 1966.

[98] J. Bardsley and M. Biondi, "Dissociative recomibnation," in *Advances in Atomic and Molecular Physics*, vol. 6, pp. 1–57, Elsevier, 1970.

[99] T. Tanabe, I. Katayama, N. Inoue, K. Chida, Y. Arakaki, T. Watanabe, M. Yoshizawa, S. Ohtani, and K. Noda, "Dissociative recombination of HeH^+ at large center-of-mass energies," *Physical review letters*, vol. 70, no. 4, p. 422, 1993.

[100] M. Ayouz and V. Kokoouline, "Cross sections and rate coefficients for vibrational excitation of heh+ molecule by electron impact," *Atoms*, vol. 4, no. 4, p. 30, 2016.

[101] J. Bardsley, "The theory of dissociative recombination," *Journal of Physics B: Atomic and Molecular Physics*, vol. 1, no. 3, p. 365, 1968.

[102] Z. Amitay, D. Zajfman, P. Forck, T. Heupel, M. Grieser, D. Habs, R. Repnow, D. Schwalm, A. Wolf, and S. L. Guberman, "Dissociative recombination of cold OH^+: Evidence for indirect recombination through excited core rydberg states," *Physical Review A*, vol. 53, no. 2, p. R644, 1996.

[103] S. L. Guberman, "Spectroscopy above the ionization threshold: Dissociative recombination of the ground vibrational level of N_2^+," *The Journal of chemical physics*, vol. 137, no. 7, p. 074309, 2012.

[104] S. L. Guberman, "The vibrational dependence of dissociative recombination: Cross sections for N_2^+," *The Journal of chemical physics*, vol. 139, no. 12, p. 124318, 2013.

[105] S. L. Guberman, "from the physics of electronic and atomic collisions, invited papers for the xix international conference, whistler, canada, july, 1995 new mechanisms for dissociative,"

[106] P. M. Mul, "Dissociative recombination of small molecular ions," 1981.

[107] D. J. Haxton and C. H. Greene, "Ab initio frame-transformation calculations of direct and indirect dissociative recombination rates of $HeH^+ + e^-$," *Physical Review A*, vol. 79, no. 2, p. 022701, 2009.

[108] H. Takagi, "Cross sections of the processes induced by electron collisions with H_2^+, HeH^+, and their isotopes," *Fusion Science and Technology*, vol. 63, no. 3, pp. 406–412, 2013.

[109] V. Laporta, K. Chakrabarti, R. Celiberto, R. Janev, J. Z. Mezei, S. Niyonzima, J. Tennyson, and I. Schneider, "Theoretical resonant electron-impact vibrational excitation, dissociative recombination and dissociative excitation cross sections of ro-vibrationally excited BeH^+ ion," *Plasma Physics and Controlled Fusion*, vol. 59, no. 4, p. 045008, 2017.

[110] N. Pop, Z. Mezei, O. Motapon, S. Niyonzima, K. Chakrabarti, F. Colboc, R. Boată, M. D. E. Epée, and I. F. Schneider, "Reactive collisions of electrons with molecular cations: Application to H_2^+, BeH^+, BF^+," in *AIP Conference Proceedings*, vol. 1796, p. 020014, AIP Publishing LLC, 2017.

[111] K. Chakrabarti, A. Dora, R. Ghosh, B. Choudhury, and J. Tennyson, "R-matrix study of electron impact excitation and dissociation of CH^+ ions," *Journal of Physics B: Atomic, Molecular and Optical Physics*, vol. 50, no. 17, p. 175202, 2017.

[112] Z. J. Mezei, M. D. Epée Epée, O. Motapon, and I. F. Schneider, "Dissociative recombination of CH^+ molecular ion induced by very low energy electrons," *Atoms*, vol. 7, no. 3, p. 82, 2019.

[113] D. Kashinski, D. Talbi, A. Hickman, O. Di Nallo, F. Colboc, K. Chakrabarti, I. Schneider, and J. Z. Mezei, "A theoretical study of the dissociative recombination of SH^+ with electrons

through the 2Π states of SH," *The Journal of chemical physics*, vol. 146, no. 20, p. 204109, 2017.

[114] S. L. Guberman, "Role of excited core rydberg states in dissociative recombination," *The Journal of Physical Chemistry A*, vol. 111, no. 44, pp. 11254–11260, 2007.

[115] M. Fifirig, "Dissociation of $^{14}N_2^+$ ions induced by slow electrons," *Molecular Physics*, vol. 112, no. 14, pp. 1910–1917, 2014.

[116] S. L. Guberman, "Mechanism for the green glow of the upper ionosphere," *Science*, vol. 278, no. 5341, pp. 1276–1278, 1997.

[117] V. Kokoouline, C. H. Greene, and B. Esry, "Mechanism for the destruction of H_3^+ ions by electron impact," *Nature*, vol. 412, no. 6850, pp. 891–894, 2001.

[118] V. Kokoouline and C. H. Greene, "Theory of dissociative recombination of D_{3h} triatomic ions applied to H_3^+," *Physical Review Letters*, vol. 90, no. 13, p. 133201, 2003.

[119] S. F. dos Santos, V. Kokoouline, and C. H. Greene, "Dissociative recombination of H_3^+ in the ground and excited vibrational states," *The Journal of Chemical Physics*, vol. 127, no. 12, p. 124309, 2007.

[120] L. Pagani, C. Vastel, E. Hugo, V. Kokoouline, C. H. Greene, A. Bacmann, E. Bayet, C. Ceccarelli, R. Peng, and S. Schlemmer, "Chemical modeling of L183 (L134N): an estimate of the ortho/para H ratio," *Astronomy & Astrophysics*, vol. 494, no. 2, pp. 623–636, 2009.

[121] C. Jungen and S. Pratt, "Jahn-Teller interactions in the dissociative recombination of H_3^+," *Physical Review Letters*, vol. 102, no. 2, p. 023201, 2009.

[122] N. Douguet, A. E. Orel, C. H. Greene, and V. Kokoouline, "Dissociative recombination of highly symmetric polyatomic ions," *Physical review letters*, vol. 108, no. 2, p. 023202, 2012.

[123] N. Douguet, A. Orel, I. Mikhailov, I. Schneider, C. Greene, and V. Kokoouline, "The role of the Jahn-Teller coupling in dissociative recombination of H_3O^+ and H ions," in *Journal of Physics: Conference Series*, vol. 300, p. 012015, IOP Publishing, 2011.

[124] N. Douguet, V. Kokoouline, and A. E. Orel, "Breaking a tetrahedral molecular ion with electrons: study of NH_4^+," *Journal of Physics B: Atomic, Molecular and Optical Physics*, vol. 45, no. 5, p. 051001, 2012.

[125] I. A. Mikhailov, V. Kokoouline, Å. Larson, S. Tonzani, and C. H. Greene, "Renner-Teller effects in HCO^+ dissociative recombination," *Physical Review A*, vol. 74, no. 3, p. 032707, 2006.

[126] N. Douguet, V. Kokoouline, and C. H. Greene, "Theoretical rate of dissociative recombination of hco+ and DCO^+ ions," *Physical Review A*, vol. 77, no. 6, p. 064703, 2008.

[127] C. Jungen and S. Pratt, "Renner-Teller interactions in the dissociative recombination of HCO^+," *The Journal of chemical physics*, vol. 129, no. 16, p. 164311, 2008.

[128] N. Douguet, V. Kokoouline, and C. H. Greene, "Theory of dissociative recombination of a linear triatomic ion with permanent electric dipole moment: Study of HCO^+," *Physical Review A*, vol. 80, no. 6, p. 062712, 2009.

[129] C. Jungen and S. Pratt, "Low-energy dissociative recombination in small polyatomic molecules," *The Journal of chemical physics*, vol. 133, no. 21, p. 214303, 2010.

[130] V. Kokoouline, N. Douguet, and C. H. Greene, "Breaking bonds with electrons: Dissociative recombination of molecular ions," *Chemical Physics Letters*, vol. 507, no. 1-3, pp. 1–10, 2011.

[131] S. Fonseca dos Santos, N. Douguet, V. Kokoouline, and A. Orel, "Scattering matrix approach to the dissociative recombination of HCO^+ and N_2H^+," *The Journal of chemical physics*, vol. 140, no. 16, p. 164308, 2014.

[132] V. Kokoouline, M. Ayouz, J. Z. Mezei, K. Hassouni, and I. F. Schneider, "Theoretical study of dissociative recombination and vibrational excitation of the ion by an electron impact," *Plasma Sources Science and Technology*, vol. 27, no. 11, p. 115007, 2018.

[133] A. Hickman, R. Miles, C. Hayden, and D. Talbi, "Dissociative recombination of e+$HCNH^+$: Diabatic potential curves and dynamics calculations," *Astronomy & Astrophysics*, vol. 438, no. 1, pp. 31–37, 2005.

[134] V. Ngassam, A. Orel, and A. Suzor-Weiner, "Ab initio study of the dissociative recombination of $HCNH^+$," in *Journal of Physics: Conference Series*, vol. 4, p. 224, IOP Publishing, 2005.

[135] V. Ngassam and A. Orel, "Resonances in low-energy electron scattering from $HCNH^+$," *Physical Review A*, vol. 75, no. 6, p. 062702, 2007.

[136] C. Yuen, M. Ayouz, N. Balucani, C. Ceccarelli, I. Schneider, and V. Kokoouline, "Dissociative recombination of $CH_2NH_2^+$: a crucial link with interstellar methanimine and Titan ammonia," *Monthly Notices of the Royal Astronomical Society*, vol. 484, no. 1, pp. 659–664, 2019.

[137] M. Ayouz, C. Yuen, N. Balucani, C. Ceccarelli, I. Schneider, and V. Kokoouline, "Dissociative electron recombination of NH_2CHOH^+ and implications for interstellar formamide abundance," *Monthly Notices of the Royal Astronomical Society*, vol. 490, no. 1, pp. 1325–1331, 2019.

[138] J. Bardsley, "Configuration interaction in the continuum states of molecules," *Journal of Physics B: Atomic and Molecular Physics*, vol. 1, no. 3, p. 349, 1968.

[139] C. Jungen and O. Atabek, "Rovibronic interactions in the photoabsorption spectrum of molecular hydrogen and deuterium: An application of multichannel quantum defect methods," *The Journal of Chemical Physics*, vol. 66, no. 12, pp. 5584–5609, 1977.

[140] C. Jungen and D. Dill, "Calculation of rotational-vibrational preionization in H_2 by multichannel quantum defect theory," *The Journal of Chemical Physics*, vol. 73, no. 7, pp. 3338–3345, 1980.

[141] A. Giusti-Suzor, J. Bardsley, and C. Derkits, "Dissociative recombination in low-energy e^--H_2^+ collisions," *Physical Review A*, vol. 28, no. 2, p. 682, 1983.

[142] V. Kokoouline and C. H. Greene, "Unified theoretical treatment of dissociative recombination of D_3h triatomic ions: Application to H_3^+ and D_3^+," *Physical Review A*, vol. 68, no. 1, p. 012703, 2003.

[143] O. Motapon, M. Fifirig, A. Florescu, F. W. Tamo, O. Crumeyrolle, G. Varin-Bréant, A. Bultel, P. Vervisch, J. Tennyson, and I. Schneider, "Reactive collisions between electrons and NO^+ ions: rate coefficient computations and relevance for the air plasma kinetics," *Plasma Sources Science and Technology*, vol. 15, no. 1, p. 23, 2005.

[144] J. Z. Mezei, R. Backodissa-Kiminou, D. Tudorache, V. Morel, K. Chakrabarti, O. Motapon, O. Dulieu, J. Robert, W.-Ü. L. Tchang-Brillet, A. Bultel, *et al.*, "Dissociative recombination and vibrational excitation of co+: model calculations and comparison with experiment," *Plasma Sources Science and Technology*, vol. 24, no. 3, p. 035005, 2015.

[145] M. Sommavilla, F. Merkt, J. Z. Mezei, and C. Jungen, "Absorption, autoionization, and predissociation in molecular hydrogen: High-resolution spectroscopy and multichannel quantum defect theory," *The Journal of chemical physics*, vol. 144, no. 8, p. 084303, 2016.

[146] C. H. Greene and C. Jungen, "Molecular applications of quantum defect theory," *Adv. Atom. Molec. Phys*, vol. 21, pp. 51–121, 1985.

[147] M. J. Frisch, G. W. Trucks, H. B. Schlegel, G. E. Scuseria, M. A. Robb, J. R. Cheeseman, G. Scalmani, V. Barone, G. A. Petersson, H. Nakatsuji, X. Li, M. Caricato, A. V. Marenich, J. Bloino, B. G. Janesko, R. Gomperts, B. Mennucci, H. P. Hratchian, J. V. Ortiz, A. F. Izmaylov, J. L. Sonnenberg, D. Williams-Young, F. Ding, F. Lipparini, F. Egidi, J. Goings, B. Peng, A. Petrone, T. Henderson, D. Ranasinghe, V. G. Zakrzewski, J. Gao, N. Rega, G. Zheng, W. Liang, M. Hada, M. Ehara, K. Toyota, R. Fukuda, J. Hasegawa, M. Ishida, T. Nakajima, Y. Honda, O. Kitao, H. Nakai, T. Vreven, K. Throssell, J. A. Montgomery, Jr., J. E. Peralta, F. Ogliaro, M. J. Bearpark, J. J. Heyd, E. N. Brothers, K. N. Kudin, V. N. Staroverov, T. A. Keith, R. Kobayashi, J. Normand, K. Raghavachari, A. P. Rendell, J. C. Burant, S. S. Iyengar, J. Tomasi, M. Cossi, J. M. Millam, M. Klene, C. Adamo, R. Cammi, J. W. Ochterski, R. L. Martin, K. Morokuma, O. Farkas, J. B. Foresman, and D. J. Fox, "Gaussian~16 Revision C.01," 2016. Gaussian Inc. Wallingford CT.

[148] Z. Biglari, A. Shayesteh, and A. Maghari, "Ab initio potential energy curves and transition dipole moments for the low-lying states of CH^+," *Computational and Theoretical Chemistry*, vol. 1047, pp. 22–29, 2014.

[149] H.-J. Werner, P. J. Knowles, G. Knizia, F. R. Manby, *et al.*, "MOLPRO, version 2019.2, a package of ab initio programs," 2019. see.

[150] J. A. Pople, M. Head-Gordon, D. J. Fox, K. Raghavachari, and L. A. Curtiss, "Gaussian-1 theory: A general procedure for prediction of molecular energies," *The Journal of Chemical Physics*, vol. 90, no. 10, pp. 5622–5629, 1989.

[151] J. Tennyson, D. B. Brown, J. J. Munro, I. Rozum, H. N. Varambhia, and N. Vinci, "Quantemol-N: an expert system for performing electron molecule collision calculations

using the R-matrix method," in *Journal of Physics: Conference Series*, vol. 86, p. 012001, IOP Publishing, 2007.

[152] J. Carr, P. Galiatsatos, J. D. Gorfinkiel, A. G. Harvey, M. Lysaght, D. Madden, Z. Mašín, M. Plummer, J. Tennyson, and H. Varambhia, "UKRmol: a low-energy electron-and positron-molecule scattering suite," *The European Physical Journal D*, vol. 66, no. 3, p. 58, 2012.

[153] V. Kokoouline, A. Faure, J. Tennyson, and C. H. Greene, "Calculation of rate constants for vibrational and rotational excitation of the H_3^+ ion by electron impact," *Monthly Notices of the Royal Astronomical Society*, vol. 405, no. 2, pp. 1195–1202, 2010.

[154] R. Hakalla, R. Kępa, W. Szajna, and M. Zachwieja, "New analysis of the Douglas-Herzberg system ($A^1\Pi$-$X^1\Sigma^+$) in the CH^+ ion radical," *The European Physical Journal D-Atomic, Molecular, Optical and Plasma Physics*, vol. 38, no. 3, pp. 481–488, 2006.

[155] Z. Amitay, D. Zajfman, P. Forck, U. Hechtfischer, B. Seidel, M. Grieser, D. Habs, R. Repnow, D. Schwalm, and A. Wolf, "Dissociative recombination of CH^+: Cross section and final states," *Physical Review A*, vol. 54, no. 5, p. 4032, 1996.

[156] K. Kowalski and P. Piecuch, "The active-space equation-of-motion coupled-cluster methods for excited electronic states: Full EOMCCSDt," *The Journal of Chemical Physics*, vol. 115, no. 2, pp. 643–651, 2001.

[157] A. Florescu-Mitchell and J. Mitchell, "Dissociative recombination," *Physics reports*, vol. 430, no. 5-6, pp. 277–374, 2006.

[158] S. L. Guberman and A. Giusti-Suzor, "The generation of O (1 S) from the dissociative recombination of O_2^+," *The Journal of chemical physics*, vol. 95, no. 4, pp. 2602–2613, 1991.

[159] H. Sun and H. Nakamura, "Theoretical study of the dissociative recombination of NO^+ with slow electrons," *The Journal of chemical physics*, vol. 93, no. 9, pp. 6491–6501, 1990.

[160] J. Z. Mezei, F. Colboc, N. Pop, S. Ilie, K. Chakrabarti, S. Niyonzima, M. Lepers, A. Bultel, O. Dulieu, O. Motapon, *et al.*, "Dissociative recombination and vibrational excitation of BF^+ in low energy electron collisions," *Plasma Sources Science and Technology*, vol. 25, no. 5, p. 055022, 2016.

[161] O. Novotnỳ, O. Motapon, M. H. Berg, D. Bing, H. Buhr, H. Fadil, M. Grieser, J. Hoffmann, A. Jaroshevich, B. Jordon-Thaden, *et al.*, "Dissociative recombination of CF^+: Experiment and theory," in *Journal of Physics: Conference Series*, vol. 192, p. 012021, IOP Publishing, 2009.

[162] S. Niyonzima, N. Pop, F. Iacob, Å. Larson, A. Orel, J. Z. Mezei, K. Chakrabarti, V. Laporta, K. Hassouni, D. Benredjem, *et al.*, "Low-energy collisions between electrons and BeD^+," *Plasma Sources Science and Technology*, vol. 27, no. 2, p. 025015, 2018.

[163] S. Niyonzima, S. Ilie, N. Pop, J. Z. Mezei, K. Chakrabarti, V. Morel, B. Peres, D. Little, K. Hassouni, Å. Larson, *et al.*, "Low-energy collisions between electrons and BeH^+: Cross sections and rate coefficients for all the vibrational states of the ion," *Atomic Data and Nuclear Data Tables*, vol. 115, pp. 287–308, 2017.

[164] S. L. Guberman, "The dissociative recombination of OH^+," *The Journal of chemical physics*, vol. 102, no. 4, pp. 1699–1704, 1995.

[165] R. Čurík and C. H. Greene, "Rates for dissociative recombination of LiH^+ ions," in *Journal of Physics: Conference Series*, vol. 115, p. 012016, IOP Publishing, 2008.

[166] R. Čurík and C. H. Greene, "Inelastic low-energy collisions of electrons with HeH^+: Rovibrational excitation and dissociative recombination," *The Journal of chemical physics*, vol. 147, no. 5, p. 054307, 2017.

[167] T. F. O'Malley, "Slow heavy-particle collision theory based on a quasiadiabatic representation of the electronic states of molecules," *Physical Review*, vol. 162, no. 1, p. 98, 1967.

[168] W. H. Smith, L. S. Liszt, and B. L. Lutz, "A reevaluation of the diatomic processes leading to CH and CH^+ formation in the interstellar medium," *The Astrophysical Journal*, vol. 183, pp. 69–80, 1973.

[169] "The dissociative recombination of CH^+ $X^1\Sigma^+$ $(v = 0)$, author=Mitchell, JBA and McGowan, J Wm, journal=The Astrophysical Journal, volume=222, pages=L77, year=1978,"

[170] P. Mul, J. Mitchell, V. D'Angelo, P. Defrance, J. W. McGowan, and H. Froelich, "Merged electron-ion beam experiments. iv. Dissociative recombination for the methane group CH^+,..., CH_5^+," *Journal of Physics B: Atomic and Molecular Physics*, vol. 14, no. 8, p. 1353, 1981.

[171] K. Chakrabarti, R. Ghosh, and B. Choudhury, "R-matrix calculation of bound and continuum states of CH," *Journal of Physics B: Atomic, Molecular and Optical Physics*, vol. 52, no. 10, p. 105205, 2019.

[172] H. Liu and G. Verhaegen, "Electronic states of CH and NH," *The Journal of Chemical Physics*, vol. 53, no. 2, pp. 735–745, 1970.

[173] X. Jiang, C. H. Yuen, P. Cortona, M. Ayouz, and V. Kokoouline, "Cross sections for vibronic excitation of CH^+ by low-energy electron impact," *Physical Review A*, vol. 100, no. 6, p. 062711, 2019.

[174] D. Hvizdoš, C. H. Greene, and R. Čurík, "Energy-dependent frame transformation theory for dissociative recombination," *arXiv preprint arXiv:1910.02631*, 2019.

[175] J. Blandon, V. Kokoouline, and F. Masnou-Seeuws, "Calculation of three-body resonances using slow-variable discretization coupled with a complex absorbing potential," *Physical Review A*, vol. 75, no. 4, p. 042508, 2007.

[176] U. Riss and H.-D. Meyer, "Calculation of resonance energies and widths using the complex absorbing potential method," *Journal of Physics B: Atomic, Molecular and Optical Physics*, vol. 26, no. 23, p. 4503, 1993.

[177] V. Kokoouline and C. H. Greene, "Theoretical study of the H," in *Journal of Physics: Conference Series*, vol. 4, pp. 74–82, 2005.

université PARIS-SACLAY
ÉCOLE DOCTORALE
Interfaces:
matériaux, systèmes, usages

Titre: Bases de données sur les molécules d'hydrocarbures pour les applications de traitement des déchets

Mots clés: Méthode R-matrice, diffusion d'ions électron-CH^+, théorie des défauts quantiques multicanaux, excitation vibronique, recombinaison dissociative, section transversale

Résumé: Dans cette thèse, nous étudions la (dés)excitation vibronique et la recombinaison dissociative (DR) de CH^+ produites par la collision d'électrons de faible énergie. Nous développons d'abord une approche théorique de la (dés)excitation vibronique de CH^+ par collision d'électrons. Dans cette approche nous utilisons la méthode de la matrice R à noyaux fixes afin de calculer les matrices de diffusion électron-ion dans l'approximation de Born-Oppenheimer. Nous appliquons ensuite la méthode connue comme « vibronic frame transformation » et la procédure d'élimination des canaux de diffusion fermés dans l'esprit de la théorie des défauts quantiques moléculaires pour construire une matrice de diffusion dépendant de l'énergie qui décrit les interactions entre les canaux vibroniques de l'ion cible induits par l'électron incident. La matrice de diffusion obtenue tient compte de la série de résonances vibroniques de Rydberg dans le spectre de collision. Nous avons calculé les sections efficaces de diffusion pour différentes combinaisons d'états vibroniques initiaux et finaux. Nous avons trouvé un bon accord entre les sections efficaces de diffusion obtenues par la théorie des défauts quantiques et par un calcul direct de la matrice R, ce qui indique que l'approche que nous avons suivie est un outil fiable pour la détermination des sections efficaces de (dés)excitation vibronique pour des cibles avec des résonances électroniques de faible énergie. De telles cibles étaient difficiles à traiter par voie théorique avec les méthodes précédentes. Dans le même cadre que celui appliqué aux (dés)excitations vibroniques, nous avons calculé la section efficace de diffusion pour la recombinaison dissociative à basse énergie de CH^+ en couplant la fonction de base de l'onde sortante définie par le potentiel d'absorption complexe. Cela a été fait en prenant en compte la contribution des trois états ioniques $X^1\Sigma^+$, $a^3\Pi$ and $A^1\Pi$ de plus basse énergie et les séries de Rydberg convergeant vers ces états. Les sections efficaces de DR que nous avons obtenues sont en bon accord quantitatif avec les résultats des expériences et présentent notamment une résonance analogue à celle qu'on observe dans la courbe de la section efficace de diffusion expérimentale. L'origine des principales résonances que nous avons obtenues est analysée par le calcul des probabilités de DR pour les ondes partielles de l'électron incident. On constate que les ondes partielles de type d, notamment $d\sigma$, $d\pi$ et $d\delta$, contribuent considérablement à la DR de l'état fondamental de CH^+. Cela peut expliquer les écarts observés entre la théorie et l'expérience dans les études précédentes.

Title: Hydrocarbon molecules databases for waste treatment applications

Keywords: R-matrix method, electron-CH^+ scattering, multichannel quantum defect theory, vibronic excitation, dissociative recombination, cross section

Abstract: In this thesis, we investigate the vibronic (de-) excitation and dissociative recombination of CH^+ by low-energy electron impact. We first develop a theoretical approach for the electron-impact vibronic (de-) excitation of CH^+. In this approach, the fixed-nuclear R-matrix method is employed to compute electron-ion scattering matrices in the Born-Oppenheimer approximation. A vibronic frame transformation and the closed-channel elimination procedure in a spirit of molecular quantum defect theory are employed to construct an energy-dependent scattering matrix describing interactions between vibronic channels of the target ion induced by the incident electron. The obtained scattering matrix accounts for Rydberg series of vibronic resonances in the collisional spectrum. Cross sections for vibronic excitation for different combinations of initial and final vibronic states are computed. A good agreement between electronic-excitation cross sections, obtained using the quantum defect theory and in a direct R-matrix calculation, demonstrates that the present approach provides a reliable tool for determination of vibronic (de-) excitation cross sections for targets with low-energy electronic resonances. Such targets were difficult to treat theoretically using earlier methods. Within the same framework applied for the vibronic (de-) excitations, we further compute the cross section for low-energy dissociative recombination of CH^+ by coupling the outgoing-wave basis function defined by complex absorbing potential. The contribution of the three lowest $X^1\Sigma^+$, $a^3\Pi$ and $A^1\Pi$ ionic states and the Rydberg series converging to those states are taken into account. The obtained DR cross sections are quantitatively in good agreement with the experimental measurements and exhibit a resonanc feature analogous to the experimental cross-section curve. The origination of the prominant resonances in the computed results are analyzed through computing the DR probabilities for the partial waves of the incident electron. The d-type partial waves including $d\sigma$, $d\pi$ and $d\delta$ are found considerably contributing to the DR of the ground-state CH^+. This may explain the discrepancies observed between thoery and experiment in the preceeding studies.

Université Paris-Saclay
Espace Technologique / Immeuble Discovery
Route de l'Orme aux Merisiers RD 128 / 91190 Saint-Aubin, France